JUN 1 1957

Journal of Research

of the

National Bureau of Standards

MAY 1957

UNIVERSITY OF MICHIGAN
MAY 27 1957
PHYSICS LIBRARY

VOLUME 58 NUMBER 5

U. S. DEPARTMENT OF COMMERCE
Sinclair Weeks, Secretary
NATIONAL BUREAU OF STANDARDS
A. V. Astin, Director

MAY • 1957
VOLUME • 58
NUMBER • 5

JOURNAL OF RESEARCH

of the

NATIONAL BUREAU OF STANDARDS

PERIODICALS OF THE NATIONAL BUREAU OF STANDARDS

(Published monthly)

The National Bureau of Standards is engaged in fundamental and applied research in physics, chemistry, mathematics, and engineering. Projects are conducted in fifteen fields: electricity and electronics, optics and metrology, heat and power, atomic and radiation physics, chemistry, mechanics, organic and fibrous materials, metallurgy, mineral products, building technology, applied mathematics, data processing systems, cryogenic engineering, radio propagation, and radio standards. The Bureau has custody of the national standards of measurement and conducts research leading to the improvement of scientific and engineering standards and of techniques and methods of measurement. Testing methods and instruments are developed, physical constants and properties of materials are determined, and technical processes are investigated.

JOURNAL OF RESEARCH

The Journal presents research papers by authorities in the specialized fields of physics, mathematics, chemistry, and engineering. Complete details of the work are presented, including laboratory data, experimental procedures, and theoretical and mathematical analyses. Annual subscription: domestic, $4.00; $1.25 additional for foreign mailing.

TECHNICAL NEWS BULLETIN

Summaries of current research at the National Bureau of Standards are published each month in the Technical News Bulletin. The articles are brief, with emphasis on the results of research, chosen on the basis of their scientific or technologic importance. Lists of all Bureau publications during the preceding month are given, including Research Papers, Handbooks, Applied Mathematics Series, Building Materials and Structures Reports, Miscellaneous Publications, and Circulars. Each issue contains 12 or more two-column pages; illustrated. Annual subscription: domestic, $1.00; 35 cents additional for foreign mailing.

BASIC RADIO PROPAGATION PREDICTIONS

The Predictions provide the information necessary for calculating the best frequencies for communication between any two points in the world at any time during the given month. The data are important to all users of long-range radio communications and navigation, including broadcasting, airline, steamship, and wireless services, as well as to investigators of radio propagation and ionosphere. Each issue, covering a period of one month, is released three months in advance and contains 16 large pages, including pertinent charts, drawings, and tables. Annual subscription: domestic, $1.00; 25 cents additional for foreign mailing.

Order all publications from the Superintendent of Documents
U. S. Government Printing Office, Washington 25, D. C.

Use of funds for printing this publication approved by the Director of the Bureau of the Budget (May 4, 1956).

Journal of Research of the National Bureau of Standards Vol. 58, No. 5, May 1957 Research Paper 2755

Frequency Conversion With Nonlinear Reactance

Chester H. Page

A lossless nonlinear impedance subject to an almost periodic voltage (sum of sinusoids) will absorb power at some frequencies and supply power at other frequencies. Necessary and sufficient relations among these powers are found. It is shown that simple cubic capacitors ($Q \propto V^3$) are sufficient for producing any possible conservative modulation or distortion process.

1. General Considerations

Let there be a set of linearly related positive frequencies ω_i, the relations being expressible as

$$\omega_i = \sum_j k_{ij}\omega_j, \tag{1}$$

with the k_{ij} rational numbers. Some of these frequencies (base frequencies) can be independently chosen, and the remaining ones (derived frequencies) expressed by

$$\omega_{di} = \sum_j m_{ij}\omega_{bj}, \tag{2}$$

or, in matrix notation,

$$\Omega_d = \boldsymbol{M}\Omega_b. \tag{3}$$

It is possible to have the ω_i comprise subsets such that

$$\Omega_d^{(j)} = \boldsymbol{M}^{(j)}\Omega_b^{(j)} \qquad j=1 \ldots n, \tag{4}$$

but this represents a highly artificial case in practice.

Let the power absorbed by the nonlinear reactor at frequency ω_i be P_i, and for convenience let $\mathscr{P}_i \equiv P_i/\omega_i$.

Now

$$\sum_i P_i \equiv \sum_i \mathscr{P}_i\omega_i = \sum_i \mathscr{P}_{bi}\omega_{bi} + \sum_i \mathscr{P}_{di}\omega_{di} \tag{5}$$

$$= \mathfrak{P}_b\Omega_b + \mathfrak{P}_d\Omega_d$$

$$= (\mathfrak{P}_b + \mathfrak{P}_d\boldsymbol{M})\Omega_b,$$

and in the case where the ω comprise subsets:

$$\sum_i P_i = \sum_j (\mathfrak{P}_b^{(j)} + \mathfrak{P}_d^{(j)}\boldsymbol{M}^{(j)})\Omega_{bj}. \tag{5'}$$

But for a lossless device, $\sum P_i = 0$ for all choices of the independent (base) frequencies, so

$$(\mathfrak{P}_b^{(j)} + \mathfrak{P}_d^{(j)}\boldsymbol{M}^{(j)})\Omega_{bj} = 0 \qquad \text{all } j \tag{6a}$$

and

$$\mathfrak{P}_b^{(j)} + \mathfrak{P}_d^{(j)}\boldsymbol{M}^{(j)} = 0. \qquad \text{all } j \tag{6b}$$

From (6a), $\sum_i P_i^{(j)} = 0$, so power is conserved for each subset of related frequencies, as well as in toto. Henceforward we shall drop the superscript (j) for convenience, rewriting (6b) as

$$\mathfrak{P}_b + \mathfrak{P}_d\boldsymbol{M} = 0. \tag{7}$$

418835—57——1

Hence the power at each base frequency is determined by the set of powers at the derived frequencies. Ordinarily, the base frequencies are taken as the incommensurate frequencies of the sources; the derived frequencies, those of the sinks. Hence the distribution of power load among the sources is fixed by the power dissipated in the sinks. Expanding (7) into its components:

$$\mathscr{P}_{bj}+\sum_i \mathscr{P}_{di}m_{ij}=0 \qquad \text{all } j. \tag{8}$$

Expressing *all* ω_j in terms of the base frequencies:

$$\omega_i=\sum_j l_{ij}\omega_{bj}, \tag{9}$$

so that the $l_{ij}=m_{ij}$ for ω_i a derived frequency, and $l_{ij}=$

$$\delta_{ij}=\begin{cases}0 & i\neq j\\ 1 & i=j\end{cases}$$

for ω_i a base frequency.

Then $P_{bj}\equiv\sum_i \mathscr{P}_i l_{ij}$ and (8) becomes

$$0=\sum_i \mathscr{P}_i l_{ij}+\sum_i \mathscr{P}_{di}l_{ij}=\sum_i \mathscr{P}_i l_{ij}, \tag{10}$$

or

$$\sum_i P_i l_{ij}/\omega_i=\sum_i\left\{P_i l_{ij}\Big/\sum_n l_{in}\omega_{bn}\right\}=0, \qquad \text{all } j. \tag{11}$$

Because the subscript j refers to base frequencies in the above, there are as many independent relations (11) among the P_i as there are base frequencies. For the particular case of two base frequencies, and the l_{ij} restricted to integers, equations (11) become equations (24) and (25) given by Manley and Rowe.[1] The result, however, is a necessary consequence of conservation of energy in any lossless system, and includes subharmonic combination frequencies.

For further results, it is convenient to re-express the linear dependence among frequencies without reference to the choice of base:

$$\boldsymbol{E}\Omega=0 \tag{12}$$

or

$$\sum_j e_{ij}\omega_j=0 \qquad \text{all } i \tag{12a}$$

with all e_{ij} integers.

If there are B base frequencies, and D derived frequencies, then $\boldsymbol{M}$ (eq(3)) is a $D\times B$ matrix of rational numbers. Let the least common denominator of the first row of $\boldsymbol{M}$ be ϵ_{11}; of the second row, ϵ_{22}; etc., up to ϵ_{DD}. Then, premultiplying (3) by the nonsingular diagonal matrix,

$$\mathfrak{E}_1=\begin{vmatrix}\epsilon_{11} & & \\ & \ddots & \mathbf{0} \\ & & \epsilon_{DD}\end{vmatrix}$$

yields

$$\mathfrak{E}_1\Omega_d=\mathfrak{E}_1\boldsymbol{M}\Omega_b\equiv-\mathfrak{E}_2\Omega_b \tag{13}$$

$$\mathfrak{E}_1\Omega_d+\mathfrak{E}_2\Omega_b=0, \tag{13a}$$

or

$$\mathfrak{E}\Omega=0, \tag{14}$$

[1] J. M. Manley and H. E. Rowe, Some general properties of nonlinear elements. I: General energy relations, Proc. IRE **44**, 904–913 (1956).

where

$$\mathfrak{E}=\begin{array}{c|cc} & D & B \\ D & \mathscr{E}_1 & \mathscr{E}_2 \end{array}$$

$$\Omega=\begin{array}{c|c} & 1 \\ D & \omega_d \\ \hline B & \omega_b \end{array}$$

The matrix $\mathfrak{E}$ just defined is a minimal matrix of the type $\boldsymbol{E}$ in (12); it contains no redundant relations among the ω. We make the notational distinction because later on we shall need an $\boldsymbol{E}$ containing redundancies.

Because $\mathfrak{E}_1$ is nonsingular, (13) can be solved for

$$\boldsymbol{M}=-\mathfrak{E}_1^{-1}\mathfrak{E}_2 \tag{15}$$

and (7) rewritten as

$$\mathfrak{P}_b=\mathfrak{P}_d\mathfrak{E}_1^{-1}\mathfrak{E}_2.$$

Let $\mathfrak{H}\equiv\mathfrak{P}_d\mathfrak{E}_1^{-1}$, a $1\times D$ (row) matrix. Then

$$\mathfrak{P}_d=\mathfrak{H}\mathfrak{E}_1 \tag{16a}$$

$$\mathfrak{P}_b=\mathfrak{H}\mathfrak{E}_2 \tag{16b}$$

$$\mathfrak{P}=\mathfrak{H}\mathfrak{E}, \tag{17}$$

where

$$\mathfrak{P}=\begin{array}{c|cc} & D & B \\ 1 & \mathscr{P}_d & \mathscr{P}_b \end{array}$$

The relation (17) (with $\mathfrak{E}$ defined by (14)) is not only necessary for conservation of power, but it is also sufficient for, by (14),

$$\sum_i P_i\equiv\mathfrak{P}\Omega=\mathfrak{H}\mathfrak{E}\Omega=0.$$

Equation (17) also yields insight into the nature of the frequency mixing process, for (17) is equivalent to

$$P_i=\omega_i\sum_n h_n\epsilon_{ni}, \tag{18}$$

and defining

$$P_{in}\equiv h_n\epsilon_{ni}\omega_i,$$

we have

$$P_i=\sum_n P_{in} \tag{19a}$$

$$\sum_i P_{in}=0, \tag{19b}$$

so that if P_{in} is considered as the power absorbed at ω_i in the nth "mixing process," the total power P_i is the net result of a set of conservative mixing processes. In any particular process, power is absorbed at those frequencies for which h_n and ϵ_{ni} are of the same sign (positive resistance presented to the ith source) and power is delivered at those frequencies for which ϵ_{ni} is of the opposite sign (negative resistance presented).

We also note that if we consider all frequencies involving a given base, the sum of the corresponding powers vanishes. For, from (2), the derived frequencies associated with the jth base are

$$\omega_{di,j}=m_{ij}\omega_{bj}$$

and from (8),

$$\mathscr{P}_{bj}+\sum_i \mathscr{P}_{di}m_{ij}=0,$$

hence

$$0=\mathscr{P}_{bj}\omega_{bj}+\sum_i \mathscr{P}_{di}m_{ij}\omega_{bj} \tag{19c}$$

$$=\mathscr{P}_{bj}\omega_{bj}+\sum_i \mathscr{P}_{di}\omega_{di,j}=P_{bj}+\sum_i P_{di,j}.$$

The equivalent conditions (7) and (17) are not only necessary in the generation of modulation and distortion products by lossless devices, they are also sufficient. That is, for any given $\boldsymbol{M}$ and $\mathscr{P}_d$, a suitable nonlinear network can be found. To prove sufficiency, we first need detailed relations for the behavior of a nonlinear reactor. A capacitor will be used in the analysis, but an inductor would be equivalent with suitable changes of notation.

2. The Mixing Process

Let the voltage

$$V=\sum_1^M a_i \cos(\omega_i t+\theta_i) \tag{20}$$

be impressed on the nonlinear capacitance

$$Q=CV^N, \qquad C>0.$$

Let $\beta_i \equiv \omega_i t+\theta_i$ for convenience.
Then

$$Q=CV^N=C\Big(\sum_1^M a_i \cos\beta_i\Big)^N=C\Big(\sum_1^M a_i(e^{j\beta_i}+e^{-j\beta_i})/2\Big)^N. \tag{21}$$

Applying the polynomial law:

$$Q=C2^{-N}N!\sum_s \prod_{i=1}^M a_i^{s_i}(e^{j\beta_i}+e^{-j\beta_i})^{s_i}/s_i!,$$

where $\sum_s$ indicates the sum over all sets of integers s satisfying

$$s_i\geq 0, \qquad \sum s_i=N.$$

Expanding the binomial yields

$$Q=C2^{-N}N!\sum_s \prod_i a_i^{s_i}\sum_{k_i=0}^{s_i} e^{jk_i\beta_i}e^{-j(s_i-k_i)\beta_i}/k_i!(s_i-k_i)!$$

Let $l_i \equiv 2k_i-s_i$, so that

$$Q=C2^{-N}N!\sum_s \prod_i a_i^{s_i}\sum_{l_i=-s_i}^{s_i} e^{jl_i\beta_i}\Big/\Big(\frac{s_i+l_i}{2}\Big)!\Big(\frac{s_i-l_i}{2}\Big)!, \tag{22}$$

the l_i appearing in $\sum_i$ being those integers between $-s_i$ and $+s_i$ that make s_i+l_i even. For convenience, let

$$[s_i \pm l_i] \equiv \Big(\frac{s_i+l_i}{2}\Big)!\Big(\frac{s_i-l_i}{2}\Big)! \tag{23}$$

Then

$$Q=C2^{-N}N!\sum_s(\prod_j a_j^{s_j})\{\prod_i\sum_{l_i}e^{jl_i\beta_i}/[s_i\pm l_i]\},$$

and the term in braces can be rewritten as

$$\sum_{l_1}\sum_{l_2}\cdots\sum_{l_M}\prod_{i=1}^{M}e^{jl_i\beta_i}/[s_i\pm l_i]=\sum_{l_1}\cdots\sum_{l_M}e^{j\sum l_i\beta_i}\prod_i[s_i\pm l_i]^{-1},$$

making

$$Q=C2^{-N}N!\sum_s\sum_l\prod_i a_i^{s_i}e^{j\sum l_i\beta_i}/[s_i\pm l_i]. \tag{24}$$

Now in summing over l, any set of values $l_1, l_2 \ldots l_M$ may be paired with the set of equal and opposite values. Because $[s_i\pm l_i]$ is even, the odd part of the exponential ($\sin\sum_i l_i\beta_i$) will not contribute to the sum, and we can write

$$Q=C2^{-N}N!\sum_s\sum_l\prod_i a^{s_i}[s_i\pm l_i]^{-1}\cos\left\{\sum_i l_i(\omega_i t+\theta_i\right\}, \tag{25}$$

where $\omega_i t+\theta_i$ has been restored for β_i.

The term of frequency ω_k arises from values of $l_1, l_2, \ldots l_M$ that make $\pm\omega_k=\sum_i l_i\omega_i$, or

$$\sum_{i\neq k}l_i\omega_i+(l_k\pm 1)\omega_k=0. \tag{26}$$

If *all* the integral linear relations among the frequencies are given by the "mixing processes,"

$$\sum_i e_{pi}\omega_i=0 \qquad (\boldsymbol{E}\Omega=0), \tag{27}$$

the ω_k terms arise from

$$l_i=e_{pi}, \qquad i\neq k$$

$$l_k=e_{pk}\pm 1,$$

and

$$Q=C2^{-N}N!\sum_k\sum_s\sum_p\prod_{i\neq k}a_i^{s_i}[s_i\pm e_{pi}]^{-1}\{a_k^{s_k}[s_k\pm(e_{pk}+1)]^{-1}\cos(\omega_k t+\theta_k+\sum_j e_{pj}\theta_j)$$
$$+a_k^{s_k}[s_k\pm(e_{pk}-1)]^{-1}\cos(\omega_k t+\theta_k-\sum_j e_{pj}\theta_j)\}. \tag{28}$$

Expanding the cosines, the expression in the braces becomes

$$a_k^{s_k}\cos(\omega_k t+\theta_k)\cos\left(\sum_j e_{pj}\theta_j\right)\{[s_k\pm(e_{pk}+1)]^{-1}+[s_k\pm(e_{pk}-1)]^{-1}\}$$
$$+a_k^{s_k}\sin(\omega_k t+\theta_k)\sin\left(\sum_j e_{pj}\theta_j\right)\{-[s_k\pm(e_{pk}+1)]^{-1}+[s_k\pm(e_{pk}+1)]^{-1}\}.$$

Recalling the definition (23) of $[s\pm l]$, the coefficients in braces can be simplified, making the final form of Q become

$$Q=C2^{-N}N!\sum_k\sum_s\sum_p\{\prod_{i\neq k}a_i^{s_i}/[s_i\pm e_{pi}]\}a_k^{s_k}[(s_k+1)\pm e_{pk}]^{-1}$$
$$\{(s_k+1)\cos(\omega_k t+\theta_k)\cos(\sum_j e_{pj}\theta_j)+e_{pk}\sin(\omega_k t+\theta_k)\sin\sum_j e_{pj}\theta_j)\}. \tag{29}$$

Differentiating for $I=\dot{Q}$, and writing $a_k^{s_k}=a_k^{s_k+1}/a_k$ for symmetry:

$$I=C2^{-N}N!\sum_k\sum_s\sum_p\omega_k a_k^{-1}\{\prod_{i\neq k}a_i^{s_i}/[s_i\pm e_{pi}]\}a_k^{s_k+1}[(s_k+1)\pm e_{pk}]^{-1}$$
$$\{e_{pk}\cos(\omega_k t+\theta_k)\sin\varphi_p-(s_k+1)\sin(\omega_k t+\theta_k)\cos\varphi_p\}, \tag{30}$$

with $\varphi_p\equiv\sum_j e_{pj}\theta_j$.

If we let

$$s_i'=s_i \qquad i\neq k$$

$$s_k'=s_k+1,$$

the summation $\sum_s$ with $\sum_i s_i=N$ is the same as $\sum_{s'}$ with $\sum_i s_i'=N+1$ and the restriction $s_k'>0$. But if we let $s_k'=0$, the coefficient of $\sin(\omega_k t+\theta_k)$ vanishes, and $[s_k'\pm e_{pk}]^{-1}$ vanishes unless $e_{pk}=0$; but $e_{pk}=0$ eliminates the $\cos(\omega_k t+\theta_k)$ term. Hence $s_k'=0$ contributes nothing, and

$$I=C2^{-N}N!\sum_k\sum_p\sum_{s'}\omega_k a_k^{-1}\{\prod_i a_i^{s_i'}/[s_i'\pm e_{pi}]\}\{e_{pk}\cos(\omega_k t+\theta_k)\sin\varphi_p-s_k'\sin(\omega_k t+\theta_k)\sin\varphi_p\}, \quad (31)$$

with the integers $s_i'\geq 0$, $\sum_i s_i'=N+1$.

Noting that the coefficient of the cosine term can be summed over s' independently of k, we define

$$A_p\equiv\sum_{s'}\prod_i a_i^{s_i'}/[s_i'\pm e_{pi}], \quad (32)$$

the strength of the pth process, and

$$B_{pk}\equiv\sum_{s'}s_k'\prod_i a_i^{s_i'}/[s_i'\pm e_{pi}]=a_k\frac{\partial A_p}{\partial a_k}, \quad (33)$$

making

$$I=C2^{-N}N!\sum_k\sum_p\omega_k a_k^{-1}\{A_p e_{pk}\cos(\omega_k t+\theta_k)\sin\varphi_p-B_{pk}\sin(\omega_k t+\theta_k)\cos\varphi_p\}. \quad (34)$$

The power absorbed at frequency ω_k is

$$P_k=\tfrac{1}{2}C2^{-N}N!\omega_k\sum_p A_p e_{pk}\sin\varphi_p, \quad (35)$$

and if we write $H_p\equiv\frac{CN!}{2^{N+1}}A_p\sin\varphi_p$,

$$P_k/\omega_k=\sum_p H_p e_{pk} \quad (36a)$$

$$\mathfrak{P}=\boldsymbol{HE}. \quad (36b)$$

3. Order of Processes

In eq (32) for A_p, the nonvanishing terms are those for $|e_{pi}|\leq s_i'$, hence $\sum_i|e_{pi}|\leq\sum_i s_i'=N+1$ and we define the order of a process to be $\sum_i|e_{pi}|-1$. A $Q=CV^N$ device gives rise to processes of order N, $N-2$, $N-4$, etc, because e_{pi} must be of the same parity as s_i'.

The result of a process of given order can be produced by the superposition of processes of other orders, introducing new frequencies for which $P_i=0$. That is, high-order processes can be indirectly yielded by low-order devices by cascaded modulation, if suitable reactance loads are added to the circuit and d-c bias to obtain even-order processes from odd. By introducing dummy frequencies involving only reactive power, the result of any desired set of processes can be achieved using only simple nonlinear devices of the form $Q=CV^3$. A constructive demonstration of this will constitute our proof of sufficiency.

4. Redundancies

The relation (36b) represents the net effect of all mixing processes, both the minimal set and the redundant ones. Partitioning into

$$\mathfrak{P}_a=\boldsymbol{HE}_1 \quad (37a)$$

$$\mathfrak{P}_b=\boldsymbol{HE}_2 \quad (37b)$$

leaves redundancies in $\boldsymbol{E}_1$, making it singular, so that $\boldsymbol{H}$ cannot be found from the given $\mathfrak{P}_d$. In certain special cases, the frequencies are such that there are no redundant relations, and $\boldsymbol{E} \equiv \mathfrak{E}$, so that $\boldsymbol{H} = \mathfrak{H} = \mathfrak{P}_d \mathfrak{E}_1^{-1}$, if the processes of $\mathfrak{E}$ are all of order N. Then the amplitudes a_i can be chosen arbitrarily and the A_p computed (one process for each derived frequency). The sin φ_p are then known, and a sufficiently large choice of C will make the φ_p real.

Because

$$\Phi = \boldsymbol{E}\Theta = \boldsymbol{E}_1\Theta_d + \boldsymbol{E}_2\Theta_b, \tag{38}$$

the phases at base frequencies can be assigned, and the remainder are determined by

$$\Theta_d = \boldsymbol{E}_1^{-1}(\Phi - \boldsymbol{E}_2\Theta_b) = \boldsymbol{E}_1^{-1}\Phi + \boldsymbol{M}\Theta_b. \tag{39}$$

Equation (34) yields both current components, so the sink impedances are readily computed.

In the general case of mixed-order $\mathfrak{E}$, the introduction of additional derived frequencies with corresponding null components of $\mathfrak{P}_d$ can convert (17) into

$$\mathfrak{P}' = \boldsymbol{H}'\boldsymbol{E}', \tag{40}$$

with $\boldsymbol{E}'$ of (say) third order, but the set of frequencies will usually allow redundant processes. Our plan of attack is to express the given $\mathfrak{E}$ in terms of third-order processes alone, and to subdivide the resulting set of frequencies into subsets not possessing third-order redundancies. Then for these subsets, each complete $\boldsymbol{E}$ is also a minimal $\mathfrak{E}$, and the subsets of mixing processes can be carried out by separate cubic capacitors, using common base-frequency sources.

The only first-order process that is possible is the identity $\omega_i = \omega_i$, because the ω were defined to be positive and distinct. Because a third-order device can produce only first- and third-order processes, the problem of enumerating producible processes among a set of frequencies is relatively straightforward. Although a second-order device has the same simplicity, using $Q = CV^3$ in the sufficiency proof automatically extends the sufficiency to (a) symmetrical devices and (b) devices with positive slope throughout.

5. Minimal Third-Order Processes

Instead of choosing the source frequencies as bases, we take suitable subharmonics of the sources, so that all derived frequencies will be integral harmonics and combinations. We start by expressing harmonics of ω in terms of minimal third-order processes, i. e., third-order processes defining a set of frequencies not possessing any redundant processes of third order.

For generating an odd harmonic, $O_1\omega$, we take a sequence of odd harmonics $O_n\omega$ generated by

$$O_{n+1} = O_n/3 \tag{41}$$

if integral, and otherwise

$$O_{n+1} = (O_n \pm 1)/2,$$

using the sign that makes O_{n+1} odd. This procedure yields a sequence that can be generated from ω by third-order processes in one and only one way.

For an even harmonic, we again divide by 3 if possible, and repeat until we have an even term not containing 3 as a factor. We then start an odd series with

$$O_1 = \frac{E \pm 1}{3}, \qquad O_2 = E - O_1$$

and continue down from O_2 to ω as before, but add zero (d-c) to the sequence. In reverse, we find that O_1 and E are generated by

$$2O_1=O_2\pm 1$$

$$E=O_1+O_2+(\text{zero}).$$

For combination tones, $A\omega_a+B\omega_b+\ \ldots$, we partition the sum into a sum of three combination tones, then repartition these in the same way, etc. A partial sum of two terms can be partitioned by using the artifice $A\omega_a+B\omega_b=A\omega_a+B\omega_b+0$, as was done for even harmonics. The original combination tone can thus be reduced to nonredundant third-order processes that use harmonics of the base frequencies for starting points. These harmonics can then be reduced as before.

6. Choice of Base Frequencies

Our procedure for expressing various frequencies by minimal processes was based on those frequencies being integral harmonics. In terms of the original arbitrary base frequencies, we had

$$\omega_{di}=\sum_j m_{ij}\omega_{bj}, \tag{2}$$

where m_{ij} are rational fractions. For each j, let the L.C.D. of the m_{ij} be D_{jj}; then

$$\omega_{di}=\sum_j r_{ij}\omega_{bj}/D_{jj}, \tag{43}$$

where r_{ij} are integers. Let the new bases be $\omega_{Bj}\equiv\omega_{bj}/D_{jj}$ so that

$$\Omega_d=\boldsymbol{R}\Omega_B,\ \Omega_b=\boldsymbol{D}\Omega_B. \tag{44}$$

Some of the frequencies of ω_B are new frequencies (associated with zero power) and some may be members of the old sets ω_d and ω_b. All remaining members of ω_d and ω_b comprise the components of a new ω_D:

$$\Omega_D=\mathfrak{M}\Omega_B. \tag{45}$$

By the minimal process procedure of the previous section, the frequencies in ω_D may be associated in sets

$$\Omega_{Dl}=\mathfrak{M}_l\Omega_B, \tag{46}$$

where m_{lij} are integers, so that the corresponding $\mathfrak{E}_l$ as determined by the procedure leading to (13) and (14) is

$$\mathfrak{E}_l=\boxed{I\ \big|\ -\mathscr{M}_l} \tag{47}$$

A given frequency may appear in several vectors ω_{Dl}.

Let the voltages at frequencies appearing in ω_{Dl} be impressed on the lth cubic capacitor, $Q=C_lV^3$. For each of these capacitors, the relation (16a) becomes

$$\mathfrak{H}_l=\mathfrak{P}_{Dl}$$

and all components are known. Assigning arbitrary nonzero amplitudes to all voltages, the A_{li} are readily computed. The phases of the base frequencies can be assigned; for convenience we let each $\theta_{Bli}=0$. Then (39) and (35) yield

$$\Theta_{Dl}=\Phi_l$$

$$\theta_{Dli}=\sin^{-1}2^4\mathscr{P}_{Dli}/3!C_lA_{li}.$$

Using zero-impedance generators at all frequencies involved, their interconnections with the l capacitors is a trivial problem.

It has been demonstrated that any modulation-distortion operation that satisfies the necessary conditions for lossless devices can be produced with nonlinear capacitors, and in particular, with cubic capacitors. The demonstration of sufficiency, however, utilized perfect generators. It would be more satisfying to demonstrate the operation using generators at only those frequencies at which the net power input is positive, and using passive linear impedances at all sink and null-power frequencies. This can be done for any *given* set of base frequencies; variation of frequencies may lead to variation of the strengths of the several mixing processes, depending on the reactance-versus-frequency behavior of the elements and the particular circuit configuration used.

The discussion is simplest when there is only one base frequency; all sinks are rational harmonics of a given source. The procedure we have used for generating minimal processes was such that if any base harmonic was common to two minimal processes, all lower frequencies involved were also common. (Except for the d-c bias needed in some processes, which can be handled by connecting individual bias batteries immediately adjacent to the capacitors.) Thus an ordered tree of generators can be assembled, with various capacitors connected at appropriate points on the "trunk" or upright "limbs." Equation (34) gives both components of current at each frequency (for arbitrary assigned voltages), so impedances can be calculated for replacing all generators except the power source. The impedances for the null-power dummy frequencies will be purely reactive; those for sink frequencies will have positive resistance. By associating each sink with one capacitor only, all common impedances are purely reactive. The necessary reactances are computed from the base of the trunk upward, leaving the "terminal twigs" for sink loads and independent reactance adjustments. Such adjustments can be made for any *given* base frequency, but cannot be guaranteed for frequency variations.

Because the general combination tones are sums and differences of harmonics of the bases, the harmonic-generating trees are to be interconnected with combination-tone sinks and their associated capacitors. In the case of harmonics that are both sink frequencies and steps in the development of combination tones, extra branches can be added to the harmonic-generating trees, so that the harmonic sink loads do not carry the harmonic current used in generating combination tones. Thus *all* mutual impedances can be made purely reactive, and *all* loads isolated. Thus the necessary relations among frequencies and powers are also sufficient for realization with cubic capacitors, at any set of incommensurate spot frequencies.

7. Regeneration and Stability

It is apparent from eq (19b) that in a given process power is absorbed by the capacitor at some frequencies and delivered at other frequencies, or that in each mixing process the capacitor presents positive and negative resistance components at various frequencies. At a given frequency, some processes may absorb energy, and some may deliver energy. At a frequency associated with passive impedance (no generator), any power dissipated in the impedance is the net power delivered at this frequency by the capacitor. The total effective resistance of the circuit at this frequency is zero. The impressed voltage at this frequency is zero and the current is uniquely determined by the processes; the circuit is stable.

On the other hand, if for some processes the capacitor delivers power at the frequency of one of the generators, we call it a regenerative process; it presents negative resistance to the generator. If the total resistance so presented is zero or negative, the circuit is sometimes said to be unstable.[2] If a circuit is unstable in this sense, i. e., if it can supply power to an

[2] Manley & Rowe, op. cit., p. 908.

external generator, then there is current at this frequency even in the absence of the generator. Hence the unstable frequency is merely any one of the frequencies generated by the network. If this frequency is a rational harmonic or combination tone of the other generators, the effect is entirely expected. But the unstable frequency may be incommensurate with all the source frequencies. In this case the network is said to oscillate. This condition occurs when the set of frequencies involved in mixing processes is such that the number of base frequencies exceeds the number of independent sources. Then by (19c) at least one frequency involving the excess base is associated with negative power (unless *all* such frequencies are associated with zero power, in which case the extra base is not needed).

This type of oscillation can occur in systems that are ordinarily considered stable, i. e., one that exhibits bounded responses to all bounded driving forces, and possesses no free oscillations. The presence of such oscillations is, however, dependent on threshold values of generator voltages, because for sufficiently small generator voltages, only integral harmonics and combination tones can appear.[3]

WASHINGTON, October 3, 1956.

[3] Unpublished work, to appear in J. Wash. Acad. Sci.

Journal of Research of the National Bureau of Standards Vol. 58, No. 5, May 1957 Research Paper 2756

Amplitude and Phase of the Low-Frequency Ground Wave Near a Coastline

James R. Wait

A theoretical analysis is given for the amplitude and the phase change of the ground wave, originating from a distant transmitter on land, as it crosses a coastline. The land and sea are assumed to be smooth, and homogeneous with a sharp boundary of separation. Attention is focused on the effects that take place near the coastline when it is not permissible to employ arguments based on the principle of stationary phase. A limited comparison is made with the recent experimental work of Pressey, Ashwell, and Fowler.

1. Introduction

With the increased use of low-frequency radio navigational systems, it has become important to understand the mechanism of ground-wave propagation over inhomogeneously conducting terrain. Theoretical treatments of this problem usually employ an idealized two-part media having a sharp boundary separating homogeneous media. The extension of these analyses to three or more media is straightforward, although tedious. In most of the previous work,[1] the numerical values of the fields are only valid for distances from the boundary greater than a wavelength or so, as a consequence of the approximations employed. It is the purpose of the present note to investigate the field near the boundary by a refinement of the stationary phase method.

2. Theoretical Development

In an earlier paper (see footnote 1), analysis and computations were presented for the propagation of ground waves over a mixed path on a flat earth. The boundary separating the two media of contrasting conductivity was assumed to be straight and approximately normal to the propagation path. A relation was derived for the mutual impedance Z' between the terminals of the transmitting and the receiving antennas, both of which are represented by dipoles. The conductivity of the earth to the left of the boundary is denoted by σ and that to the right by σ_1. It is convenient to let

$$Z'=Z+\Delta Z, \tag{1}$$

where Z is the mutual impedance for the two antennas, A and B, corresponding to an earth that is all homogeneous with conductivity σ and ΔZ is the increment to account for the portion of the path to the right of the boundary with conductivity σ_1. From the early work it follows that

$$Z=-\frac{h_a h_b i\mu\omega}{2\pi(r_0+R_0)}\, e^{-i\beta(r_0+R_0)} F(r_0+R_0,\eta)\left[1+\frac{1}{i\beta(r_0+R_0)}-\frac{1}{\beta^2(r_0+R_0)^2}\right], \tag{2}$$

where $\beta=2\pi/$free-space wavelength, and h_a and h_b are the effective heights of the antennas at A and B, $\mu=4\pi\times10^{-7}$, $\omega=$angular frequency, $\eta=(i\mu\omega/\sigma)^{1/2}$. $F(r_0+R_0,\eta)$ is a slowly varying Sommerfeld attenuation function defined previously (see footnote 1), and is a function of the separation distance r_0+R_0 and surface impedance η.

[1] J. R. Wait, Mixed path ground wave propagation; 1. Short distances, J. Research NBS 57, 1 (1956) RP2687. References to the work of Millington, Clemmow, Bremmer, Furutsu, and others are given here.

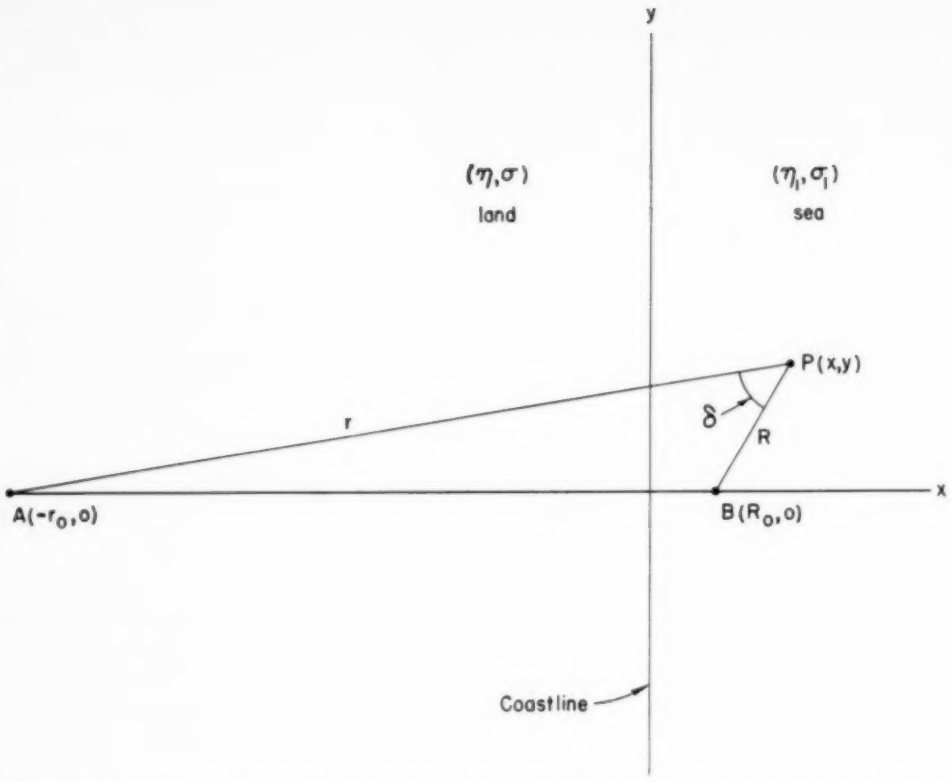

FIGURE 1. *Schematic representation of a land-sea boundary with a transmitter at* A *and a receiver at* B.

The corresponding expression for the increment ΔZ is an integration over the media to the right of the boundary, which, in figure 1, corresponds to positive values of x;

$$\Delta Z=\frac{(\eta_1-\eta)\beta^2 h_a h_b}{4\pi^2}\int_{x=0}^{\infty}\int_{y=-\infty}^{+\infty}\frac{e^{-\beta(r+R)}}{rR}F(r,\eta)F'(R,\eta,\eta_1)\left(1+\frac{1}{i\beta R}\right)\left(1+\frac{1}{i\beta r}\right)\cos\delta\,dxdy, \qquad (3)$$

where r and R are the distances from the variable point P to A and B, respectively, and δ is the angle between unit vectors at P in the direction of increasing r and R. The attenuation function $F(r,\eta)$ is of the same form as that in eq (2); however, $F'(R,\eta,\eta_1)$ is some unknown slowly varying function that depends on R, η, and $\eta_1[=(i\mu\omega/\sigma_1)^{1/2}]$. By utilizing a stationary phase principle, the area integration can be reduced to a line integral from $x=0$ to R_0, enabling a solution to be carried out. To this approximation, $F'(R,\eta,\eta_1)$ could be replaced by $F(R,\eta_1)$. It was admitted that this procedure leads to a result that is not valid near the boundary. As a further consequence of this stationary phase argument, the reflected wave from the boundary is neglected. In the present instance, R_0 is considered small compared with r_0. It then can be anticipated that the important contribution of the integration will be confined to a region where x and y are small compared with r_0. In this region it is permissible to assume:

$$F(r,\eta)\simeq F(r_0,\eta)\simeq F(r_0+R_0,\,\eta),$$

$$F'(R,\eta,\eta_1)\simeq 1, \qquad \text{(subject to } \sigma_1>>\sigma)$$

$$1/r\simeq 1/r_0, \qquad \cos\delta\simeq(x-R_0)/R, \qquad \beta(r+R)\simeq\beta(r_0+x+R).$$

In other words, the boundary is in the Fraunhofer field of the source at A. Then it follows that

$$\Delta Z\simeq(\eta_1-\eta)\frac{\beta^2 h_a h_b}{4\pi^2 r_0}e^{-i\beta r_0}F(r_0,\eta) \qquad (4)$$

$$\cdot\int_{x=0}^{\infty} e^{-i\beta x}\int_{y=-\infty}^{+\infty}\frac{e^{-i\beta R}}{R}\frac{(x-R_0)}{R}\left(1+\frac{1}{i\beta r}\right)dydx, \tag{5}$$

where

$$R\cong[(x-R_0)^2+y^2]^{1/2}.$$

It is now noted that

$$\int_0^{\infty}\frac{e^{-i\beta R}}{R}\,dy=-\frac{\pi i}{2}H_0^{(2)}[\beta|x-R_0|], \tag{6}$$

which is a consequence of Campbell and Fosters [2] pair No. 917, which requires β to have a finite negative imaginary part. $H_0^{(2)}$ is the Hankel function of the second kind. Using this result, it follows that

$$\Delta Z=\frac{(\eta_1-\eta)i\beta h_a h_b}{2\pi^2 r_0}e^{-i\beta r_0}F(r_0,\eta)I, \tag{7}$$

where

$$I=-\frac{\pi i}{2}\int_{x=0}^{\infty}e^{-i\beta x}\frac{d}{dx}H_0^{(2)}[\beta|x-R_0|]\,dx. \tag{8}$$

Integrating by parts and changing the integration variable leads to

$$I=\frac{\pi i}{2}\left\{H_0^{(2)}(\beta R_0)-ie^{-i\beta R_0}\left[\int_0^{\beta R_0}H_0^{(2)}(z)e^{+iz}dz+\int_0^{\infty-i\epsilon}H_0^{(2)}(z)e^{-iz}dz\right]\right\} \tag{9}$$

for $R_0>0$, and

$$I=\frac{\pi i}{2}\left\{H_0^{(2)}(-\beta R_0)-ie^{-i\beta R_0}\int_{-\beta R_0}^{\infty-i\epsilon}H_0^{(2)}(z)e^{-iz}dz\right\} \tag{10}$$

for $R_0<0$, where ϵ is any arbitrarily small real number.[3]

Now it can be readily verified that

$$\frac{\partial}{\partial z}\{ze^{\pm iz}[H_0^{(2)}(z)\mp iH_1^{(2)}(z)]\}=e^{\pm iz}H_0^{(2)}(z), \tag{11}$$

so the integrations can be carried to yield

$$I=i\frac{\pi}{2}[(1-i\beta R_0)H_0^{(2)}(\beta R_0)-\beta R_0 H_1^{(2)}(\beta R_0)] \tag{12}$$

for $R_0>0$, and

$$I=i\frac{\pi}{2}(1-i\beta R_0)H_0^{2)}(-\beta R_0)+\beta R_0 H_1^{(2)}(-\beta R_0)] \tag{13}$$

for $R_0<0$. After a little substitution and cancellation, it is easy to show that

$$\frac{Z'}{Z}=1+\frac{\Delta Z}{Z}$$

$$=1+qe^{\frac{3i\pi}{4}}e^{i\alpha}[(1-i\alpha)H_0^{(2)}(\alpha)-\alpha H_1^{(2)}(\alpha)] \tag{14}$$

---

[2] A. N. Campbell and R. Foster, Fourier integrals (D. Van Nostrand Co., Inc., New York, N. Y., 1948).

[3] The finite value of ϵ insures that the integrals converge in the Riemann sense. After carrying out the evaluation, ϵ can be set equal to zero.

with $\alpha=\beta R_0>0$, and

$$\frac{Z'}{Z}=1+qe^{\frac{3i\pi}{4}}e^{-i\alpha}[(1+i\alpha)H_0^{(2)}(\alpha)-\alpha H_1^{(2)}(\alpha)] \tag{15}$$

with $\alpha=\beta R_0>0$. In the above

$$q=\frac{\eta-\eta_1}{\eta}\left|\frac{\eta}{\eta_0}\right|\cong 0.0075\left(1-\sqrt{\frac{\sigma}{\sigma_1}}\right)(f_{mc}/\sigma)^{1/2}, \tag{16}$$

where f_{mc} is the frequency in megacycles per second; q is a measure of the conductivity contrast between the two media and is a positive or negative real number if displacement currents in the ground can be neglected. Also, as a consequence of the approximate boundary conditions, $|\eta|<<\eta_0=120\pi$, and therefore $|\Delta Z/Z|$ is restricted to values small compared with unity.

3. Discussion of Results

It is instructive, at this stage, to discuss the behavior of the ratio Z'/Z for large α (i. e., large electrical distances from the boundary). The asymptotic developments for the Hankel function can then be employed, to yield

$$1+\frac{\Delta Z}{Z}\cong 1+iq\left(\frac{2\alpha}{\pi}\right)^{1/2}\left[1+i\,\frac{3}{8\alpha}-\frac{5}{128\alpha^2}+\ldots\right] \tag{17}$$

when $R_0>0$, and

$$1+\frac{\Delta Z}{Z}\cong 1-q\left(\frac{1}{2\pi\alpha}\right)^{1/2}e^{-2i\alpha}\left[1-\frac{i}{24\alpha}+\ldots\right] \tag{18}$$

when $R_0<0$. It is most significant to note that the right-hand side of eq (17), when the square-bracket term is replaced by unity, corresponds to the first term of a development in higher powers of $\sqrt{\alpha}(\eta_1/\eta_0)$ obtainable from the earlier paper (see appendix). That is, the formulas derived by the stationary phase methods are probably only valid if $\alpha\gg 1$ corresponding to R_0 large compared to the wavelength. On the other hand, the stationary phase development would yield a value of unity for the right-hand side of eq (18). This would also be valid at large distances, in wavelengths, from the boundary. The departure from unity can be interpreted as a reflected wave from the boundary that forms, with the incident wave, a standing wave pattern on the transmitter side of the boundary. A more detailed view of the situation is illustrated in figures 2 and 3, where the amplitude and phase of $(1+\Delta Z/Z)$ are shown plotted as a function of R_0/λ for various values of q. It is interesting to note that very near the boundary the field has a logarithmic singularity because of the behavior of the zero-order Hankel function as its argument approaches zero. It is believed that the solution is not strictly valid for very small values of α because the approximate boundary condition introduced in the earlier paper is not applicable at or close to a discontinuity in the surface impedance.[4]

The appropriate values of the amplitude and phase $1+\Delta Z/Z$ derivable by stationary phase methods are also shown in figures 2 and 3 and indicated by dotted curves. There are significant differences between the two methods of calculations for regions within a few wavelengths of the boundary. However, the phase curves on the seaside of the boundary are almost identical to stationary-phase evaluated case, except for regions very close to the boundary.

It is interesting to compare these results with some phase measurements made very recently by Pressey, Ashwell, and Fowler.[5] They confirmed the presence of the phase recovery effect that is experienced by a wave passing from land to sea. They also observed systematic variations, about the median recovery effect, whose magnitudes are of the order of 5° very

[4] The approximate boundary conditions are not valid for R_0/λ less than about $|\eta/\eta_0|$ or a small fraction of a wavelength for well-conducting ground.

[5] B. G. Pressey, G. E. Ashwell, and C. S. Fowler, Change of phase of a low frequency ground wave propagated across a coast line, Proc. Inst. Elec. Engrs. [B] **103,** 527 (1956).

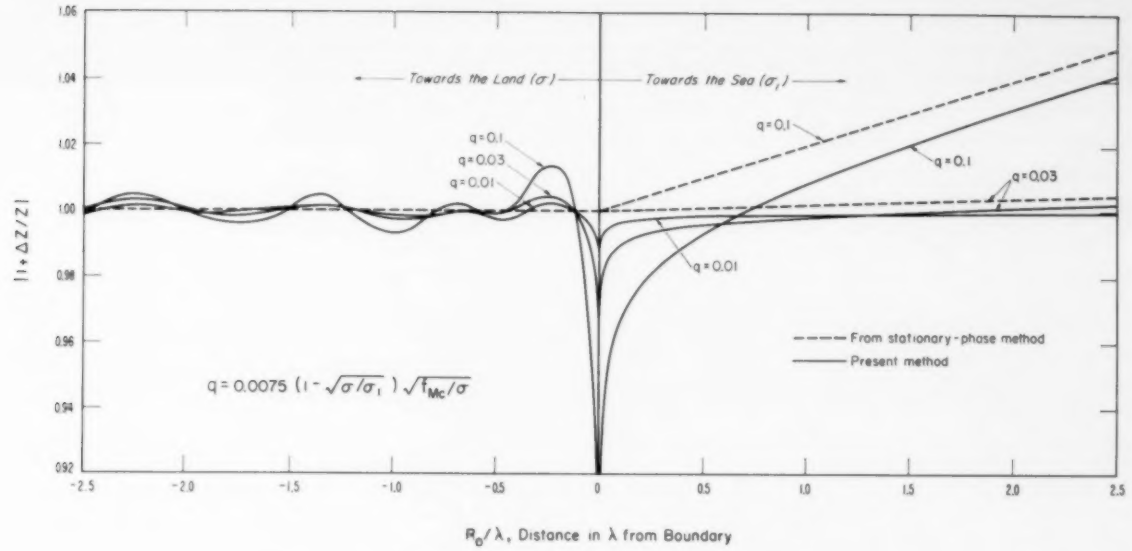

FIGURE 2. *Relative amplitude of the field near the coastline.*
The ordinate is the relative amplitude of the field at B for a distant transmitter at A on the land (fig. 1).

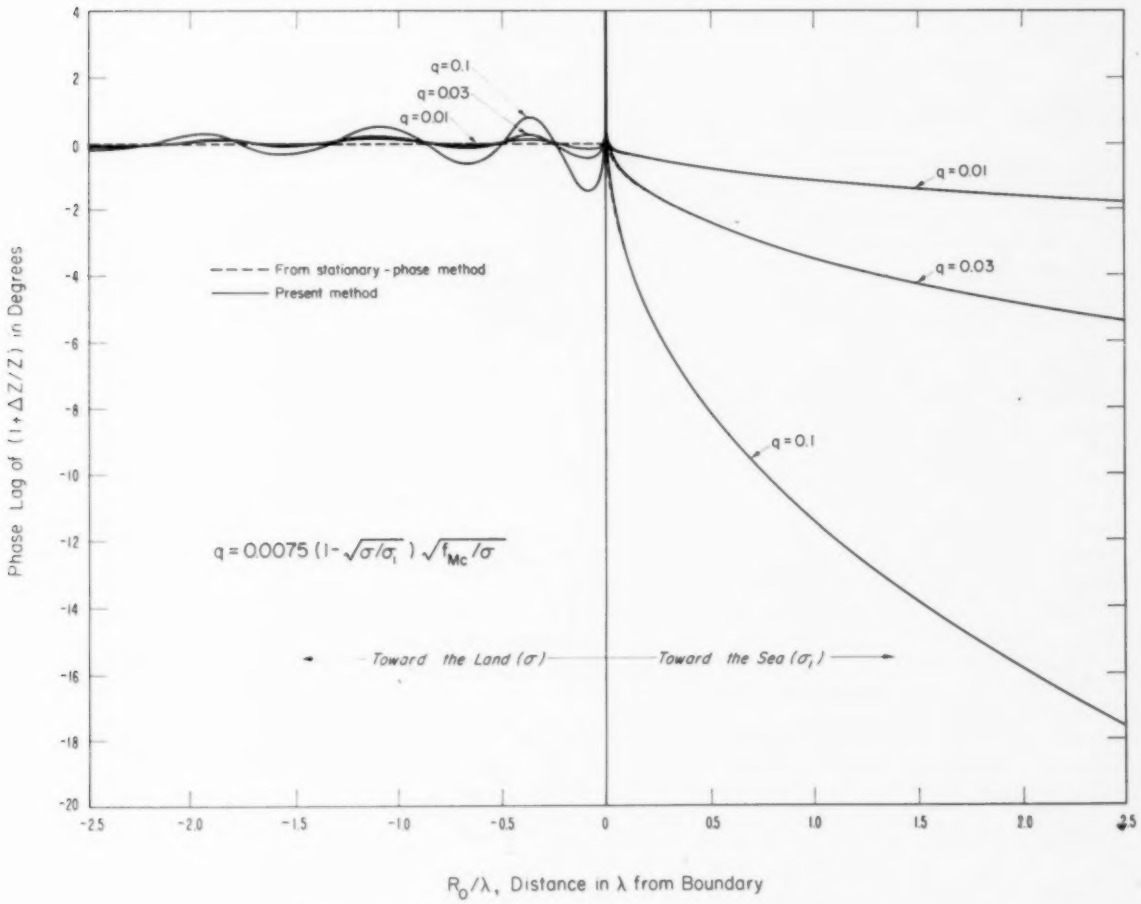
q = 0.1
q = 0.03
q = 0.01
q = 0.01
q = 0.03
q = 0.1
From stationary-phase method
Present method
q = 0.0075 (1 - √σ/σ1) √fMc/σ
Toward the Land (σ)
Toward the Sea (σ1)
Phase Lag of (1 + ΔZ/Z) in Degrees
R0/λ, Distance in λ from Boundary

FIGURE 3. *Relative phase of the field near the coastline.*
The ordinate is the relative phase of the field at B (fig. 1).

near the coast and decay to a negligible value within a few wavelengths from the boundary toward the sea. These variations, which are not predicted by the present theory, are of a form that varied from path to path and seemed to be dependent on the topography of the coastline. In practically all cases, however, they observed a large and rather *sudden increase of phase lag* very near the boundary, which is in qualitative agreement with figure 3. There was also some evidence from Pressey, Ashwell, and Fowler's work that a standing wave does exist on the transmitter side of the boundary, although the data here is rather meager.

4. Appendix

The stationary phase approach gives (see footnote 1)

$$F'(r_0+R_0,\eta,\eta_1)=F(r_0+R_0,\eta)-i\epsilon\omega(\eta-\eta_1)\left(\frac{d}{2\pi i\beta}\right)^{1/2}\int_0^{R_0}\frac{F(r_0+x,\eta)F(R_0-x,\eta_1)}{[(r_0+x)(R_0-x)]^{1/2}}\,dx,$$

where

$$F(x,\eta)=1-i2\rho^{1/2}\int_{i\rho^{1/2}}^{\infty}e^{-s^2}ds e^{-\rho}$$

and

$$\rho=-\frac{i\beta x}{2}\left(\frac{\eta}{\eta_0}\right)^2.$$

If r_0 is large compared to R_0, it is permissible to use the approximation

$$\frac{F(r_0+x,\eta)}{(r_0+x)^{1/2}}\cong\frac{F(r_0)}{r_0^{1/2}}$$

and the power series expansion of the function $F\,(R_0-x,\,\eta_1)$ to yield

$$\frac{F'}{F}\cong\frac{Z'}{Z}\cong 1-\frac{2i\left(1-\sqrt{\frac{\sigma_1}{\sigma}}\right)}{\sqrt{\pi}}\left[\rho_1^{1/2}-\frac{i\sqrt{\pi}\rho_1}{2}-\frac{2\rho_1^{3/2}}{3}+\cdots\right],$$

where

$$\rho_1=-\frac{i\beta R_0}{2}\left(\frac{\eta_1}{\eta_0}\right)^2=\frac{\alpha}{2}\left|\frac{\eta_1}{\eta_0}\right|^2.$$

Boulder, Colo., October 25, 1956.

Journal of Research of the National Bureau of Standards Vol. 58, No. 5, May 1957 Research Paper 2757

Vessels for the Storage and Transport of Liquid Hydrogen [1]

B. W. Birmingham, E. H. Brown, C. R. Class,[2] and A. F. Schmidt

The design and construction of a large-scale hydrogen liquefier by the National Bureau of Standards required a concurrent development of large, transportable liquid-hydrogen containers. These containers, known as Dewar vessels after the inventor, James Dewar, had to be capable of road and air transport, which implied ruggedness and light weight. This article reports on large-scale liquid-hydrogen Dewar development conducted by the NBS Cryogenic Engineering Laboratory. A 440-liter and an 840-liter Dewar are discussed. Every effort has been made to design Dewars with very low hydrogen-loss rates within the limitations of the transport requirement.

1. Dewar Configuration

The optimum Dewar configuration is spherical, because the sphere has the smallest area-to-volume ratio of any shape. In practice, however, such theoretical configurations must be tempered by the commercial availability of variously shaped metal heads. The shape of each of the NBS Dewars [1] [3] was governed by different considerations. The 440-liter Dewar was designed around readily available commercial heads. The 840-liter Dewar was designed to fit a specific space and required special tooling for head fabrication. Figures 1 and 2 show Dewar cross sections; figures 3 and 4 show the completed Dewars.

2. Insulation Methods

Only two methods of Dewar insulation appeared feasible at the time of the design: the use of powder insulation, such as silica aerogel, at a moderate vacuum, and the use of an unfilled space at a high vacuum. Although the moderate vacuum associated with powder insulation brings many advantages—such as reducing the importance of very minute leaks and making the achievement of a static vacuum easier—the insulation value when used in moderate thickness does not appear to be as great as that of an unfilled space at a high vacuum (up to about 0.01-μ Hg pressure) with surfaces having a high reflectivity (low emissivity). As one of the primary goals was the achievement of a low hydrogen loss without making the Dewar too bulky, high vacuum rather than evacuated powder was chosen for the Dewar insulation.

With high-vacuum insulation, heat energy flows to the inner surfaces by three mechanisms: thermal radiation, residual gas conduction, and solid conduction through piping and insulating supports.

Without any shielding, thermal radiation from room temperature directly to the liquid-hydrogen container would be excessive and would make it difficult to develop a low-loss hydrogen Dewar. In order to reduce this thermal radiation, a liquid-nitrogen-cooled radiation shield was planned. This shield completely surrounds the liquid-hydrogen container and intercepts all ambient temperature radiation from the outer shell. Thermal radiation to the liquid-hydrogen container is then reduced by a factor of at least 200 and becomes of the same order of magnitude as the residual gas conduction and the solid conduction.

When considering heat transfer to the nitrogen-cooled shield, residual gas conduction for a vacuum of the order of 0.01-μ Hg is relatively unimportant compared with thermal radiation. A low heat leak to the nitrogen-cooled shield therefore requires highly reflecting surfaces. Throughout the NBS Dewar development program high insulating vacuums and surfaces of high reflectivity were emphasized.

3. Materials of Construction

Several factors must be considered in varying degrees in regard to the materials of construction of Dewar vessels. Mechanical properties, thermal conductivity, surface reflectivity, out-gassing rates, and diffusion properties are some of the more important factors. For equipment designed for transport, another factor—weight—is also of considerable importance.

Among the various mechanical properties of metals, brittleness or notch sensitivity is one of the most important in cryogenic work, because many metals—notably the ferritic steels—become very brittle just below room temperature. Some of the common engineering metals whose impact strengths (as measured by Charpy or Izod notch tests) are satisfactory down to liquid-hydrogen temperatures, are austenitic steels (such as the stainless types, 304, 316, 321, and 347), copper, many copper alloys, and aluminum.

For piping, good strength and low thermal conductivity are necessary. Of the more common materials, stainless steel and Monel have these characteristics. Of these two, Monel not only has a thermal conductivity approximately twice that of stainless steel, but it is also more expensive. Thus, in the absence of any other compelling factors, stainless steel is ordinarily used for all internal piping.

The choice of shell materials is more difficult because a greater number of factors are involved. For low weight, aluminum is indicated. For high reflectivity, both copper and aluminum are good, but aluminum probably maintains its reflectivity better

[1] Work supported by the U. S. Atomic Energy Commission and the U. S. Air Force.
[2] Now with Beech Aircraft Corp.
[3] Figures in brackets indicate the literature references at the end of this paper.

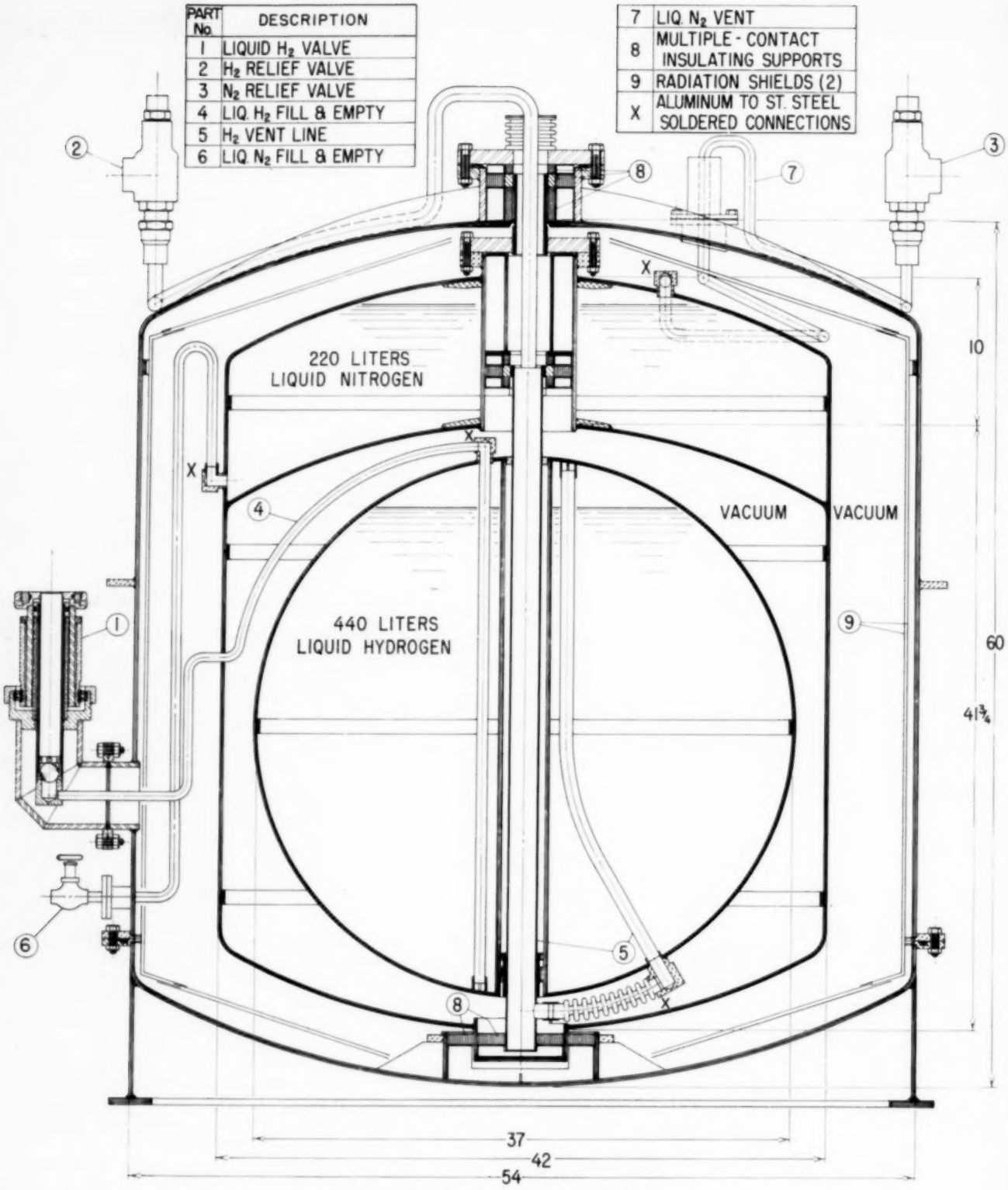

FIGURE 1. *440-liter liquid hydrogen Dewar.*

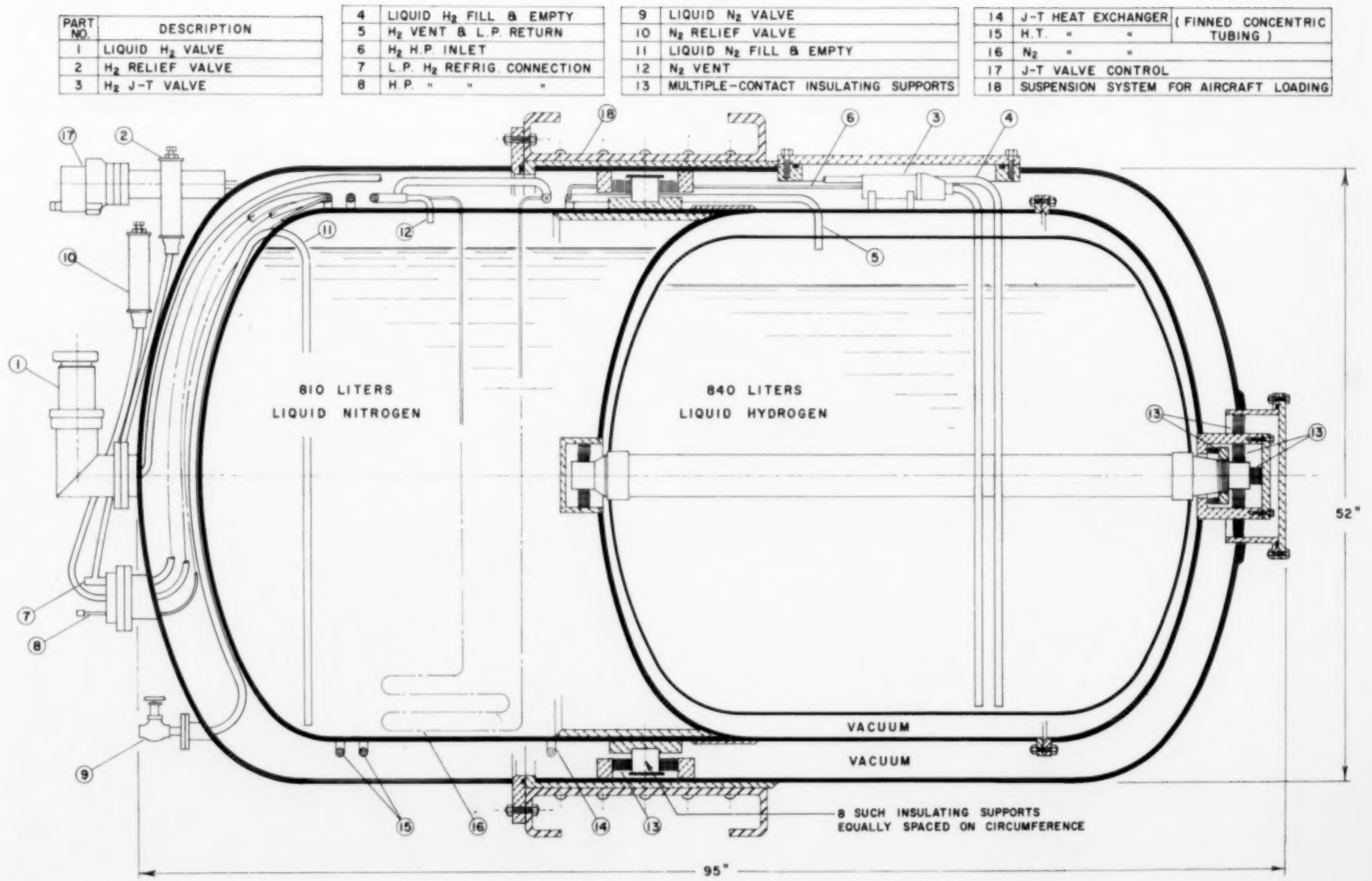
PART NO. | DESCRIPTION
1 | LIQUID H_2 VALVE
2 | H_2 RELIEF VALVE
3 | H_2 J-T VALVE
4 | LIQUID H_2 FILL & EMPTY
5 | H_2 VENT & L.P. RETURN
6 | H_2 H.P. INLET
7 | L.P. H_2 REFRIG. CONNECTION
8 | H.P. " " "
9 | LIQUID N_2 VALVE
10 | N_2 RELIEF VALVE
11 | LIQUID N_2 FILL & EMPTY
12 | N_2 VENT
13 | MULTIPLE-CONTACT INSULATING SUPPORTS
14 | J-T HEAT EXCHANGER (FINNED CONCENTRIC TUBING)
15 | H.T. " "
16 | N_2 " "
17 | J-T VALVE CONTROL
18 | SUSPENSION SYSTEM FOR AIRCRAFT LOADING
810 LITERS LIQUID NITROGEN
840 LITERS LIQUID HYDROGEN
VACUUM
VACUUM
8 SUCH INSULATING SUPPORTS EQUALLY SPACED ON CIRCUMFERENCE
52"
95"

FIGURE 2. *840-liter liquid hydrogen Dewar.*

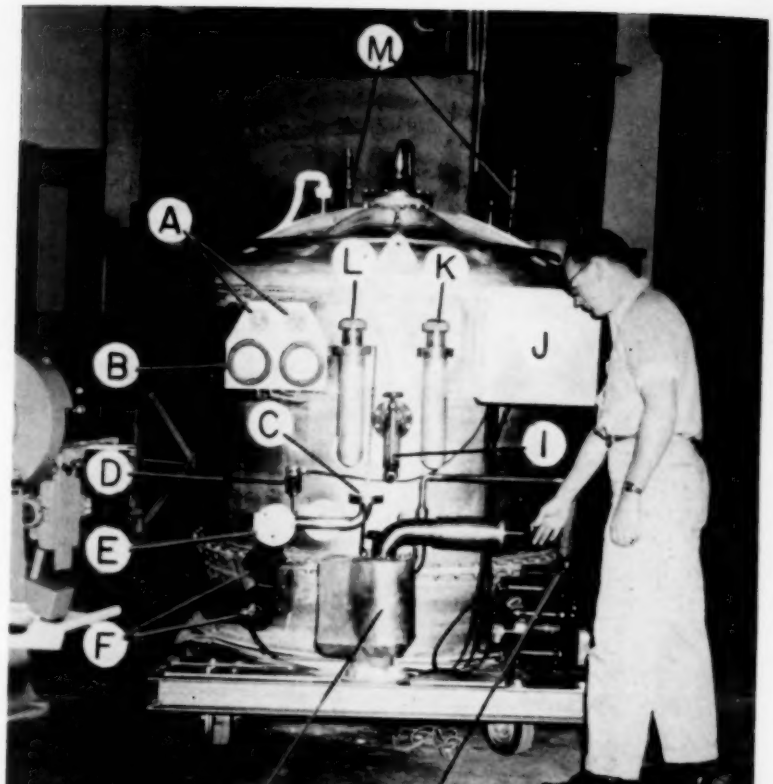

FIGURE 3. *440-liter liquid hydrogen Dewar.*

A, Liquid-level gages (N_2 and H_2); B, pressure gages (N_2 and H_2); C, weight-loaded relief valve; D, insulating vacuum gage; E, auxiliary vacuum pump connection; F, blowers; G, shielded air-cooled diffusion pump; H, mechanical vacuum pump; I, liquid N_2 fill-and-discharge valve; J, electrical system switch panel and vacuum gage control unit; K, liquid H_2 discharge valve; L, liquid H_2 fill valve; M, relief valves (H_2 and N_2).

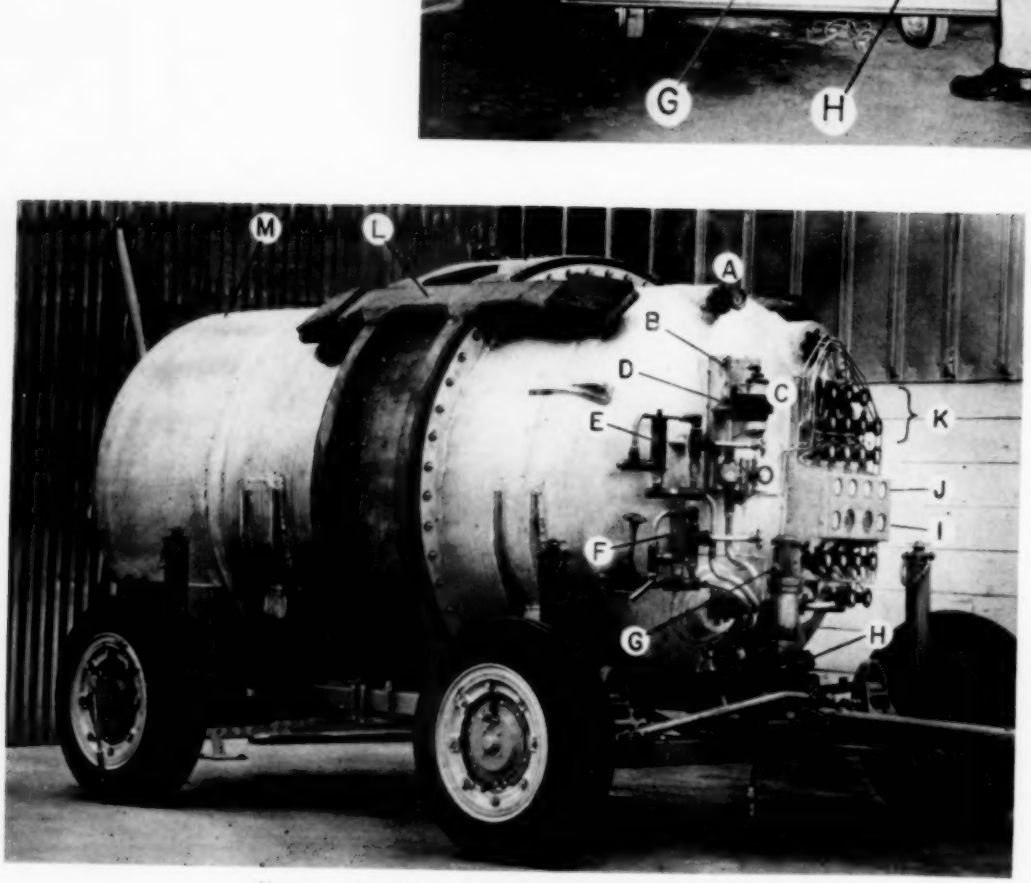

FIGURE 4. *840-liter liquid hydrogen Dewar.*

A, J-T valve control; B, H. P. H_2 refrigerator connection; C, H. P. H_2 line filter; D, L. P. H_2 refrigerator connection; E, N_2 relief valve; F, H_2 relief valve; G, liquid H_2 fill and discharge valve; H, liquid N_2 fill and discharge valve; I, liquid level and pressure gages (H_2 and N_2); J, pressure gages for monitoring refrigeration process; K, refrigerator heat exchanger warmup connections; L, suspension system for aircraft loading; M, vacuum pumping system enclosure.

than copper. It is possible to use stainless steel covered with aluminum foil to obtain a high reflectivity. For high thermal conductivity, which is desirable in some places, either copper or aluminum can be used. Finally, because the solubility of hydrogen in aluminum is much less than that in stainless steel [2], aluminum should be a very good material with respect to hydrogen diffusion.

For the outer shell, where low weight and high reflectivity are important, aluminum would appear to be the ideal material. For the liquid-nitrogen-cooled radiation shield, low weight, high reflectivity, and high thermal conductivity are desirable. The latter factor—high thermal conductivity—is important because the liquid nitrogen is in contact with only a restricted area of the shield, which means that thermal energy reaching the remainder of the shield must flow to the liquid nitrogen by solid conduction. This combination of requirements again indicates aluminum.

For the liquid-hydrogen container, high reflectivity, low hydrogen diffusion, and, again, high thermal conductivity are the important factors. Liquid hydrogen when kept in a shell of relatively low conductivity, i. e., stainless steel, supports a temperature gradient that is undesirable when the vessel is sealed to allow pressure buildup. The top layer of the liquid may be as much as 1 to 1½ deg C warmer than the bottom layer, and the vapor pressure in the vapor space above the liquid is correspondingly high. This pressure buildup is undesirable in a sealed-off container because it causes the safety valves to relieve the vessel prematurely, and in a refrigerated vessel causes the refrigerator to cycle more frequently. In stainless or other poorly conducting shells, this stratification can be overcome by thermal equilibrators—vertical copper or aluminum sheets or rods which conduct heat from the top to the bottom of the liquid—but it is simpler, if possible, to accomplish this by use of a good thermal-conductivity material in the shell itself, e. g., aluminum or copper.

Because of the above combination of reasons it was decided to fabricate most of the Dewar shells from aluminum. The particular type of aluminum chosen was the weldable alloy 52S, which in liquid oxygen equipment had been found to be even less susceptible than 61S to cracking in the welds at low temperatures. Although aluminum had been used extensively in liquid-oxygen plants and Dewars, as mentioned by Gillette [3], this appears to be the first time its use was considered both for liquid-hydrogen temperatures and for high-vacuum vessels. The solution of the one foreseeable problem that arose because of this choice, transition joints between aluminum shells and stainless steel tubing, is discussed below.

4. Insulating Supports

Acceleration, shock, and vibration conditions can be quite severe in equipment subject to road and air transport. For instance, the following mechanical service conditions were imposed as 840-liter Dewar design objectives:

(1) *Acceleration:*

(a) Vertical accelerations from −3 g to +5 g, including acceleration of gravity.

(b) Horizontal accelerations from −4 g to +4 g.

Accelerations are continuously applied for periods not exceeding 1 sec.

(2) *Shock:*

Shocks of 5 g applied in either direction along three mutually perpendicular axes, with each shock being from 10 to 15 msec duration.

(3) *Vibration:*

(a) 0.05-in. double amplitude (total excursion) from 5 to 10 cps.

(b) 0.036-in. double amplitude from 10 to 75 cps.

Vibration continuous in any one or all of three mutually perpendicular planes.

Thus it is readily seen that a Dewar capable of road and air transport requires a sturdy suspension system (i. e., a system for supporting one shell from another). This suspension system must also be a good thermal insulator in order to minimize conduction heat leak to the cold shells. From a mechanical viewpoint it is desirable to have the suspension system rigid to eliminate the possibility of internal resonances that could be caused by vibration during transport, and from an assembly viewpoint the suspension system should be simple.

For the suspension system used on the NBS Dewars, there appeared to be a choice between either stainless-steel cables or rods, or multiple-contact thermal insulators which have been developed by the NBS Cryogenic Engineering Laboratory. Stainless-steel cables have been employed very successfully, from a thermal point of view, in liquid-hydrogen transport Dewars. However, their use has resulted in two major difficulties. First, getting the proper distribution of tension on all support cables causes a very difficult assembly problem. Second, experience has shown that such cables may be stretched considerably under repeated loading and thermal cycling. This stretching lowers the natural frequency of the suspension system and makes it difficult for the Dewar to meet acceleration and shock specifications.

Some remarks on the development of multiple-contact thermal insulators by the Bureau might be of interest. During various experiments it has been observed that difficulty is experienced in transferring heat across metal surfaces clamped together in supposedly good contact in a vacuum. The surfaces may appear quite smooth and yet, due to microscopic irregularities, may present only a small area of metal-to-metal contact; thus, the net area for solid conduction is quite small. This area depends on load and metal hardness. When one multiplies this effect by lamination, rigid members that are also good thermal insulators can be readily devised. Preliminary experiments by the NBS Cryogenic Engineering Laboratory have indicated that the apparent thermal conductivity of a laminated stainless steel or Monel insulating support under high unit loads (1,000 psi) would be about one-fiftieth that of the metal itself [4]. Further experiments [5] indicate that, by proper

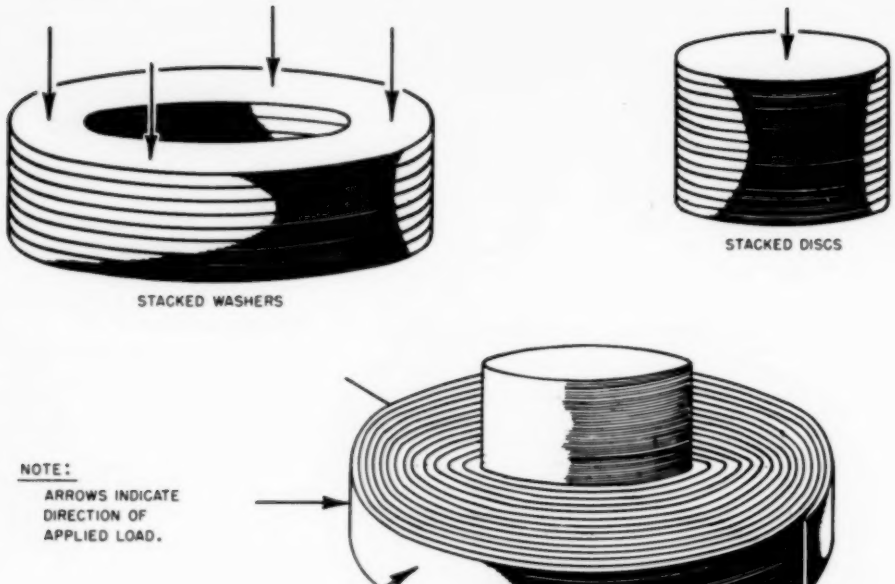

FIGURE 5. *Insulating supports.*

design (dusted surfaces and moderate unit loads), ratios as low as one two-hundredth of the base metal can be achieved.

The insulating supports developed for the NBS Dewars were rigid laminae formed from thin stainless steel (0.002 to 0.005 in. thick). Washers and disks were used to support axial loads, and tightly wound coils were used to support loads that were radial (with respect to the coil) (see fig. 5).

5. Joining Aluminum to Stainless Steel

To use metallic tubing of low thermal conductivity such as stainless steel in Dewars of aluminum-alloy shell construction, it is necessary to make aluminum-to-stainless-steel tubing joints that will remain vacuum-tight over a possible range of +130° to −420° F. Because the coefficient of thermal expansion of aluminum and most of the common aluminum alloys is approximately 50 percent greater than that of stainless steel, the joint must be sufficiently ductile to withstand all stresses imposed upon it by thermal expansion and contraction. In addition, the joint must be designed to accommodate an amount of vibration and shock loading commensurate with specified service requirements. Finally, the simplicity and ease of actually making the joint is a desirable and almost essential feature, as some form of field repair work may prove necessary upon occasion.

Four basic methods of joining aluminum to stainless steel have been successfully used, each of which employs soft solder as the filler material. (For a survey of methods of joining aluminum to stainless steel, see [6].) In all cases, the aluminum and stainless-steel tubing were initially of the same nominal size; however, prior to the joining operation, the aluminum tube was swaged out at one end for a length of approximately 1 in. so that it would fit easily over the outside diameter of the stainless-steel tube, thus forming a tubular lap joint (see fig. 6). In an aluminum-to-stainless-steel connection such as is described here, it is of definite value to utilize the aluminum as the outer member, because in cooling from the soldering temperature to room temperature, and eventually from room temperature to −420° F, the joint tends to close up and become even tighter than when fabricated, due to the greater contraction taking place in the aluminum as compared with the stainless steel.

In brief, the four joining methods are as follows: (1) To eliminate the usual amount of difficulty involved in effectively tinning aluminum, the portion of aluminum to be used is first copperplated in an approved manner, thus providing an excellent soft solder base. Subsequent tinning of the copperplated area and the stainless-steel member provides the basis for a satisfactory joint. (2) An alternative method to that described above concerns the use of ultrasonic soldering equipment, which removes the troublesome aluminum oxide layer by cavitation, thereby permitting the oxide-free aluminum alloy to be tinned directly. (3) When it is found necessary to make, or repair, an aluminum-to-stainless-steel connection without benefit of copperplating or ultrasonic equipment, such as in the field, friction tinning can be of value. In this method, molten solder is applied to the aluminum working surface

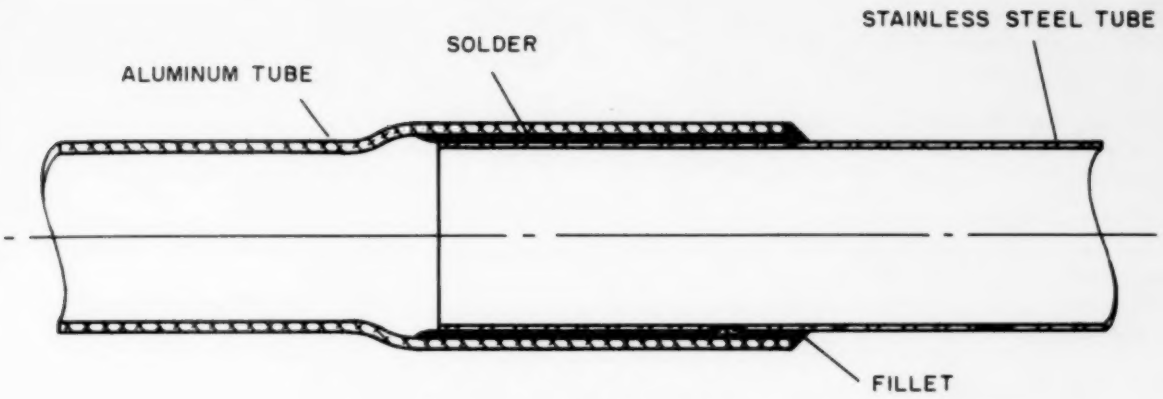

FIGURE 6. *Tubular lap joint.*

and a sharp implement is used to rub the surface free of oxide beneath the solder, again permitting the oxide-free aluminum alloy to be tinned directly. (4) In order to avoid the annoying and ever-present possibility of oxidizing the stainless steel when making the joint, it is often beneficial to use a copper transition, or intermediate member in the connection. The copper sleeve may be joined either to the inner or outer surface of the stainless steel by suitable silver brazing technique, and the free end is tinned with soft solder. The joint is made after treating the aluminum portion as in (1), (2), or (3) above.

A number of other methods have been tried for this type of work, some of which have been erratic in reproducibility and others of which have met with little or no success.

Possibly one of the more desirable methods of making a bimetallic joint involves the molecular bonding of aluminum and its alloys to steel. In this process, the aluminum is cast by any of the standard casting methods, against a specially prepared, clean, ferrous surface. In this manner, any practicable aluminum form can be incorporated into the joint design. Tests on a preliminary batch of 5 such bimetallic joints indicated that 4 remained vacuum-tight between room temperature and −320° F, and 1 leaked at any temperature. A very poor intermetallic bond was observed on the one failure that occurred, but the remaining four appeared good.

It appears that the best method of joining aluminum and stainless steel depends greatly upon the application involved as well as the availability and suitability of equipment to do the particular job. Although it is not necessary to employ an expert to fabricate connections of this type, a certain amount of skill and care is of considerable value in doing good work.

6. Auxiliary Design Features

The transfer of liquid hydrogen from these large vessels is usually accomplished by increasing the gas pressure in the free space above the liquid until it is sufficient to force the liquid through an insulated transfer line to the receiving vessel at a lower pressure. A simple, convenient method for pressurizing has been developed at the Bureau. It consists of a circulating pump, which withdraws cold hydrogen gas from the Dewar through a copper warmup tube and then returns the gas to the space above the liquid in the Dewar. In such a system, for every standard cubic foot of hydrogen gas circulated, about 2.5 whr is available to cause evaporation. This raises the pressure over the liquid. If pressurized quickly enough, only the top layer of liquid hydrogen will come to equilibrium with the vapor. This technique makes possible the transfer of subcooled liquid hydrogen and results in smaller losses than when transferring liquid hydrogen at saturation temperature.

The pump used with the 440-liter Dewar is a ⅓-hp oilless diaphragm paint-sprayer compressor with a 5.8-cfm free gas displacement. The pump is small and compact enough to be permanently mounted on the Dewar. The time required to pressurize the full Dewar from 1 to 15 psig is about 3 min. The time required to pressurize the Dewar when half-full or nearly empty is somewhat longer. Transfer rates of over 2,000 liters/hr have been accomplished with this pressurizing technique.

One of the predominantly experimental features of the 440-liter Dewar is centered around the use of two liquid-hydrogen lines, one at the top, the other at the bottom of the hydrogen container. Prior to fabrication, various theories existed as to the desirability of filling the liquid-hydrogen container from the top rather than from the bottom, and vice versa. If the filling takes place from the top, a great deal of splashing occurs, and an additional line at the bottom is required to empty the Dewar. If, on the other hand, the filling takes place from the bottom, flash vapor from the transfer operation bubbles through the liquid as it collects in the container, possibly entraining liquid and carrying it out the vent line. However, the vessel may be emptied through the same line. Contrary to speculation, no difference was noted between top and bottom ports in the filling operation, so it appears advisable to use a single valve and line leading to the bottom of the hydrogen container for both filling and emptying.

The insulating vacuum of each Dewar was provided by an air-cooled oil-diffusion pump having a rated speed of 260 liters/sec, together with associated forepump, valves, and safety features. The 840-liter Dewar was required to operate at ambient temperatures up to 130° F, at which temperature considerable backstreaming of oil vapor from the diffusion pump was found in laboratory tests. To prevent the oil from condensing on the cold good-reflective surfaces in the Dewar and thereby raising the emissivities, a baffle cooled by metallic contact with the liquid-nitrogen-cooled shield was installed in the pumping line to the Dewar vacuum space.

7. Thermal Calculations

Preliminary heat-transfer studies were carried out on various support and insulation methods in order to obtain predicted values for the heat flow into the liquid-nitrogen-cooled shield and the liquid-hydrogen container of each Dewar. As mentioned above, the heat flow to each of these shells can be broken down into three mechanisms: (1) Thermal radiation, (2) residual gas conduction, and (3) heat flow through piping and insulating supports.

For heat-transfer calculations the Dewars may be considered as two separate units. The first unit consists of a liquid-nitrogen container at 77° K surrounded by the outer shell at 300° K; the second, a hydrogen container at 20° K surrounded by the liquid-nitrogen-cooled shield at 77° K. Each of these units is considered separately in calculations because the two important figures in the results are the evaporative loss rates of liquid nitrogen and liquid hydrogen.

7.1. Radiation

Radiant energy transfer may be calculated from the Stefan-Boltzmann equation,

$$\dot{Q}=\sigma\epsilon A_1(T_2^4-T_1^4),$$

where

$\dot{Q}$ = watts,
$\sigma=0.0037\times10^{-8}$ w in.$^{-2}$ deg K^{-1},
ϵ = emissivity factor,
T_1 = temperature of inner surface in degrees K,
T_2 = temperature of outer surface in degrees K,
A_1 = area of inner surface in square inches.

The emissivity factor used in the above equation is obtained from a correction formula developed by Christiansen [7] for concentric spheres and cylinders:

$$\frac{1}{\epsilon}=\frac{1}{\epsilon_1}+\frac{A_1}{A_2}\left(\frac{1}{\epsilon_2}-1\right),$$

where the subscripts 1 and 2 refer to the inner and outer surfaces, respectively. A value of 0.04 for ϵ_1 and ϵ_2 was used in the radiation calculations, although at the time there were no experimental data for the particular alloy used to substantiate this value. Subsequent experiments resulted in a value of 0.03 for these surfaces. However, irregularities due to piping and supports would increase the effective emissivity so that 0.04 appears to be a reasonable value.

7.2. Residual Gas Conduction

The residual gas conduction was calculated from an equation derived by S. S. Kistler [8]. In slightly modified form this equation can be written,

$$\dot{q}=0.374C_v\sqrt{\frac{M}{T_m}}\frac{T_2-T_1}{\frac{L}{l_1}+\left(\frac{2}{\alpha}-1\right)\frac{1}{P}},$$

where

$\dot{q}$ = watts per square inch of inner surface,
C_v = specific heat of the residual gas at constant volume in joules per gram per degree K,
$T_m=(T_1+T_2)/2$ = mean temperature of the gas in degrees K,
T_1 = temperature of the inner surface in degrees K,
T_2 = temperature of the outer surface in degrees K,
L = perpendicular distance between inner and outer surface in inches,
l_1 = mean free path of the gas in inches at T_m and a pressure of 1 mm Hg,
P = pressure of the gas in mm Hg,
α = accommodation coefficient factor of the surfaces,
M = molecular weight of gas.

It should be noted that $\dot{q}$, the rate of energy flow per unit of area, is used directly, because at low pressures the concept of specific conductivity for the gas is meaningless. If the residual gas is air the value of l_1 will be $l_1=6.56\times10^{-6}\ T_m$ in., whereas if the residual gas should be hydrogen, the value of l_1 would be $l_1=12.2\times10^{-6}T_m$ in. As in the radiation calculations, a correction for the Dewar configuration must be applied. It seems reasonable to use a Christiansen-type correction factor to define an effective accommodation coefficient, α.

$$\frac{1}{\alpha}=\frac{1}{\alpha_1}+\frac{A_1}{A_2}\left(\frac{1}{\alpha_2}-1\right).$$

A_1 and A_2 are the areas of the inner and outer surfaces, respectively, and α_1 and α_2 are the accommodation coefficients of the surfaces for the residual gas molecules.

7.3. Piping and Insulating Support Conduction

Heat flow through the piping was computed by use of the standard heat-conduction equations and values of thermal conductivity available in the literature [9]. Calculations on insulating support conduction were made at a time when limited data were available on thermal contact resistance (see section 4). An informal communication contained the only data available at that time. A figure of approximately 0.75 mw/cm °C was given for the equivalent thermal conductivity of a Monel coil. Because stainless steel provides better insulation than Monel, and because the thermal conductivity decreases with decreasing temperature a value of k=0.5 mw/cm °C was arbitrarily chosen for the calculations.

8. Thermal Performance

8.1. The 440-Liter Dewar

The average total heat leak by piping, residual gas and support conduction, and thermal radiation for the 440-liter Dewar, during a period of time exceeding 1½ years of actual Dewar operation, is shown in table 1.

8.2. The 840-Liter Dewar

A representative set of performance data for the 840-liter Dewar, over an operational period of 6 months, is given in table 2.

Thus it is seen that under comparable conditions—10^{-5} mm Hg insulating vacuum and 50° to 60° F ambient temperature—the hydrogen capacity, hydrogen heat leak, and nitrogen heat leak of the 840-liter Dewar is approximately twice that of the 440-liter Dewar. The daily evaporation of liquid hydrogen expressed as a percentage of the total capacity is nearly the same for both vessels. With similar design objectives some improvement percentagewise should be expected in the performance of the larger vessel. In this case, however, more stringent mechanical service conditions resulted in more heat flow through insulating supports and nullified such improvement.

9. Refrigeration

It is frequently desirable to store liquid hydrogen without loss. For short periods this may be accomplished by sealing the hydrogen container and allowing a moderate pressure rise. In Dewars of the type discussed here, storage durations of 1 week or more result in a pressure increase of about 1 atm within the hydrogen system when the hydrogen container is initially about 90 percent full of liquid.

TABLE 2. *Performance data for 840-liter Dewar*

Residual pressure	Outer shell temperature	Liquid hydrogen		Liquid nitrogen	
		Heat leak	Daily evaporation (percentage of total capacity)	Heat leak	Daily evaporation
mm Hg	° *F*	*w*	%	*w*	*Liters*
10^{-5}	52	2.5	0.80	118.0	63.2

To keep hydrogen without loss indefinitely, it is necessary to periodically refrigerate the hydrogen to prevent excessive pressure rise in the hydrogen shell. Several refrigeration schemes have been proposed and developed, which operate on the principle of recondensing the vapor formed from the liquid hydrogen evaporation by circulating a colder gas, used as a refrigerant, through a closed condensing coil. The Bureau has developed a refrigerator that utilizes the principle of reliquefying the vapor formed from evaporation of liquid hydrogen by circulating the hydrogen vapor in a simple Joule-Thomson-type hydrogen liquefier. A high refrigeration efficiency is achieved. The components of this refrigeration system include the usual compression, purification, purging, and control equipment, along with the necessary heat exchangers and expansion valve.

The 840-liter Dewar is capable of being refrigerated by equipment using this new application of the Joule-Thomson process. The only components operating at low temperatures, and thus requiring insulation, are the heat exchangers and expansion valve. These were mounted in the Dewar insulating vacuum space. The remainder of the refrigeration

TABLE 1. *Average total heat leak*

Residual pressure [a]	Outer shell temperature	Liquid hydrogen		Liquid nitrogen			
		Heat leak	Daily evaporation (percentage of total capacity)	Without additional shields		With additional shields	
				Heat leak	Daily evaporation	Heat leak [c]	Daily evaporation
mm Hg	° F	*w*	%	*w*	*Liters*	*w*	*Liters*
10^{-4}	60	3.7	2.29	----------	----------	---------	----------
5×10^{-5}	60	2.0	1.24	----------	----------	---------	----------
10^{-5}	60	[b] 1.3 (1.4)	[b] 0.81 (0.89)	[b] (63.8)	[b] (34.2)	---------	----------
10^{-6}	60	[b] 0.9 (0.8)	[b] .56 (0.46)	[b] 62.5 (61.1)	[b] 33.5 (32.7)	52.0	27.8

[a] For the purpose of studying the effect of a variable insulating vacuum, the tabulated data for pressures above 10^{-6} mm Hg were obtained by introducing a small leak to the system, because a vacuum between 10^{-6} and 10^{-7} mm Hg was usually maintained during normal operation.

[b] Numbers in parentheses represent design calculations.

[c] It will be noted that the addition of two rigidly supported aluminum radiation shields [9, fig. 1] between the outer shell and the liquid-nitrogen-cooled radiation shield reduced the actual heat leak to the liquid nitrogen shield approximately 16 percent.

equipment is mounted on a dolly, which can be brought easily to the Dewar and connected. Construction of the refrigerator in this manner has resulted in maximum efficiency and simplicity because all connections are warm and the Dewar insulating vacuum is utilized to insulate all low-temperature components of the refrigeration cycle.

A detailed description of this reliquefying hydrogen refrigerator is planned for a subsequent report.

10. Conclusions

The National Bureau of Standards has developed rugged, lightweight vessels for storing and transporting liquid hydrogen. These vessels have a very low loss rate. Techniques employed in this development include vacuum-tight aluminum welding, joining aluminum to stainless steel, the use of novel insulating supports, and methods for improving the reflectivity of metallic surfaces. It appears entirely feasible, by further refinements in producing surfaces of high reflectivity and employing mechanical designs with less support conduction, to effect a still further improvement, making possible the low-loss transportation of liquid helium.

11. References

[1] Government erects $3,500,000 low temperature laboratory, Refrig. Eng. p. 1082 (1953).
[2] Donald P. Smith, Hydrogen in metals (Univ. Chicago Press, 1948).
[3] H. W. Gillette, The behavior of engineering metals, p. 353 (John Wiley & Sons, Inc., New York, N. Y., 1951).
[4] Russell B. Scott (private communication).
[5] R. P. Mikesell and R. B. Scott, Heat conduction through insulating supports in very low temperature equipment, J. Research NBS **57,** 371 (1956) RP2726.
[6] Morton C. Smith and David D. Rabb (private communication).
[7] Max M. Jakob and G. A. Hawkins, Elements of heat transfer, 1st ed., p. 125 (John Wiley & Sons, Inc., New York, N. Y., 1942).
[8] S. S. Kistler, The relation between heat conductivity and structure in Silica Aerogel, J. Phys. Chem. **39,** 79 (1935).
[9] Robert L. Powell and William L. Blanpied, Thermal conductivity of metals and alloys at low temperatures, NBS Circ. 556 (1954).

12. An Improved Vessel

A. F. Schmidt and B. W. Birmingham

Subsequent to the work reported in the preceding sections, the 440-liter liquid-hydrogen Dewar was converted in capacity and design to a 500-liter Dewar with several predominant modifications and improvements. A comparison of figures 1 and 7 will service to illustrate these changes. In brief, the aluminum 440-liter spherical container was replaced with a 500-liter stainless-steel dish-ended cylindrical tank, externally silver-sprayed in order to increase the surface reflectivity. The vertical stainless-steel center support tube was decreased in wall thickness to 0.016 in. (one-fifth of its former value), and lateral motion of the inner container with respect to its radiation shield was nullified by 2 sets of 3 stainless-steel aircraft cables, $\frac{3}{32}$ in. in diameter, which replaced the stainless-steel coil strips previously used; $\frac{1}{8}$-in. aircraft cables also replaced the entire bottom coil assembly. The rigidly supported double set of "floating radiation shields" was exchanged for a single "floating shield" attached to the outer shell by 3 long stainless-steel tubes, and Teflon bumpers spaced the shield from the nitrogen shell at the top. In order to reduce the over-all height of the assembly, vent lines and valves were brought through the side of the Dewar.

The thermal performance of this 500-liter Dewar over a 1-month period is given in table 3.

TABLE 3.—*Thermal performance of 500-liter Dewar*

Residual pressure	Outer shell termperature	Liquid hydrogen		Liquid nitrogen	
		Heat leak	Daily evaporation (percentage of total capacity)	Heat leak	Daily evaporation
mm Hg 10^{-6}	° *F* 96	*w* 0.47	% 0.26	*w* 29.5	*Liters* 15.8

A note of interest may be inserted here relative to one aspect of safety involved in the use of this vessel. Users have been concerned about the consequences of sudden loss of insulating vacuum for containers of this type. A dangerous rise of pressure was feared. In this container a 1-in.-diameter hole was suddenly opened in the outer wall of the Dewar vacuum space, resulting in the entire contents—both hydrogen and nitrogen—evaporating and being vented through the respective $\frac{3}{4}$-in. vent lines. The pressure rise resulting from the rapid evaporation did no damage.

In conclusion, these changes confirm that application of design modifications recommended in section 10 were justified. A liquefied-gas-storage vessel has been developed with a daily hydrogen evaporation rate of approximately $\frac{1}{4}$ percent of the total capacity in the 500-liter size range. It is planned to evaluate this vessel as a liquid-helium-storage Dewar.

PART NO.	DESCRIPTION
1	LIQUID H_2 VALVE
2	H_2 RELIEF VALVE
3	N_2 RELIEF VALVE
4	LIQUID H_2 FILL & EMPTY
5	H_2 VENT LINE
6	LIQUID N_2 FILL & EMPTY

7	N_2 VENT LINE
8	MULTIPLE-CONTACT INSULATING SUPPORTS
9	RADIATION SHIELD
10	TEFLON BUMPER
X	ALUMINUM TO STAINLESS SOLDERED CONNECTIONS

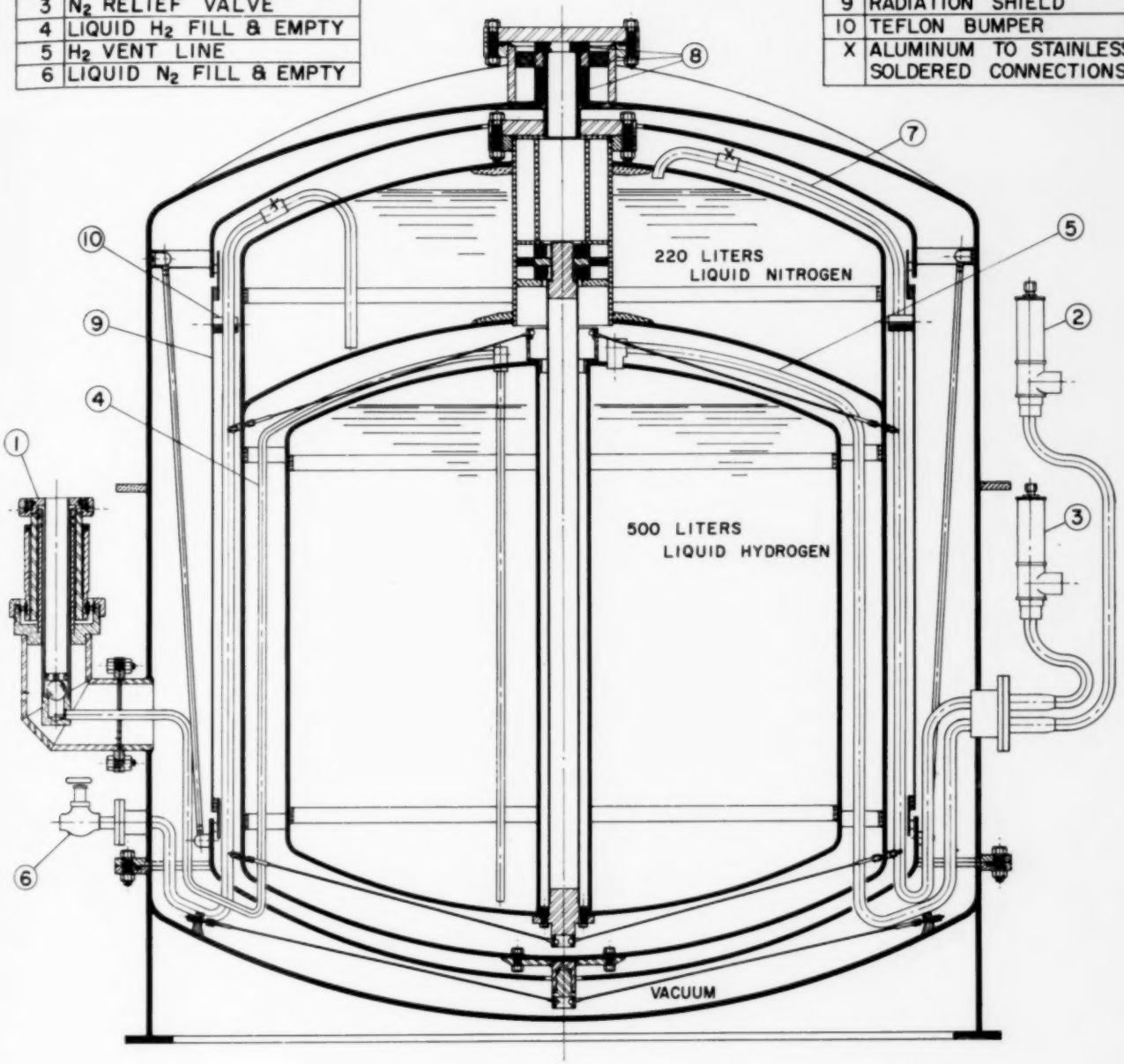

FIGURE 7. *500-liter liquid hydrogen Dewar.*

BOULDER, COLO., October 27, 1955.

Journal of Research of the National Bureau of Standards Vol. 58, No. 5, May 1957 Research Paper 2758

Infrared Spectra of Polychlorobenzenes

Earle K. Plyler, Harry C. Allen, Jr., and E. D. Tidwell

The infrared spectra of 12 chlorinated benzenes have been measured from 2 to 38 microns. In addition, the spectra of benzene, monofluorobenzene, monobromobenzene, and monoiodobenzene have been included. An assignment of the fundamental bands of the monosubstituted benzenes has been made. Some of the frequencies of the other compounds have also been assigned.

The spectrum of each compound is shown in the figures, and a table containing all the observed bands is included.

1. Introduction

There is now available the complete group of substituted chlorobenzenes, from monochlorobenzene to hexachlorobenzene. These have been purified by the Hooker Electrochemical Co. and have been made available through R. H. Kimball. A measurement of the infrared spectra of these chlorinated benzenes will serve two purposes. First, it will serve as a catalog of the spectra of these compounds, which will be useful for identification and for intercomparison with other substituted benzenes. Second, some of the typical vibrations can be traced from one substituted molecule to another, thus showing the effect of position of the chlorine atoms in the molecules on the vibrational frequencies.

It would be a gigantic task to try to assign all the observed bands for 12 chlorinated benzenes. This has not been undertaken, but a study of some of the types of vibrations has been made and the classifications listed.

In addition to the spectra of the chlorobenzenes, there have been included the spectra of monofluorobenzene, monobromobenzene, and monoiodobenzene. These vibrational bands of monosubstituted benzenes have been classified and the wave numbers compared with those of monofluorobenzene.

2. Experimental Methods and Results

The spectra were measured on a prism spectrometer. Prisms of NaCl, KBr, and KRS-5 were used for the measurements from 2 to 38 μ. Cell thicknesses from 0.05 to 1.6 mm were used in different parts of the spectrum. The cell thickness was varied in regions of strong absorption so that the position of band center could be adequately determined. Where a thinner cell was used, the results are placed on the graphs as an insert curve. Several of the chlorinated benzenes are normally solids and have been measured in solution. Carbon tetrachloride was used for the solvent from 2 to 8 μ, carbon disulfide from 8 to 22 μ, and benzene or methylcyclohexane from 22 to 38 μ. In some regions the absorption of several of the liquids was so intense that the spectrum was determined in solution. The bands measured under these conditions are designated on the figures. Carbon tetrachloride has an absorption band of medium intensity in the region of 6.4 μ, and bands of the solutes in this region could be determined only approximately. The absorption spectrum of the compounds in the CCl_4 solution show the CCl_4 band at 6.4 μ plus any absorption of the solute.

The observed spectra of the chlorinated benzenes are shown in nine figures. The absorption spectra of benzene, fluorobenzene, chlorobenzene, bromobenzene, and iodobenzene are shown from 2 to 38 μ in figures 1 and 2. Figures 3 and 4 include the spectra of *o*-dichlorobenzene, *m*-dichlorobenzene, and *p*-dichlorobenzene. The *p*-dichlorobenzene was measured in solution. The spectra of the three trichlorobenzenes are shown in figures 5 and 6, and the spectra of the tetrachlorobenzenes are included in figures 8 and 9. The spectra of pentachlorobenzene and hexachlorobenzene from 2 to 15 μ are shown in figure 7 and from 15 to 38 μ in figure 9.

In the region from 23 to 38 μ the spectrum of hexachlorobenzene is represented by a broken line. In this case, and other spectral regions of the compounds, the broken line indicates that the spectrum is less accurately determined than for the regions of the solid line. The uncertainty arises either from atmospheric absorption or some absorption present in the solvent. Bands of low intensity in the regions of solvent absorption are probably not observed.

Table 1 is a list of the observed bands of all the compounds. The wavelength, wave number, and intensity are listed for the bands of each substance. Bands of low intensity are not included. The intensity is given in terms of percentage of transmission, and is included primarily for identification purposes. No correction has been applied for radiation loss at the cell windows, nor has the percentage of transmission been reduced to a uniform cell thickness, but sufficient data are given so that a quantitative comparison of intensities can be made. It is estimated that the wavelengths are correct to ± 0.03 μ in the region from 2 to 15 μ and to ± 0.06 μ from 15 to 38 μ.

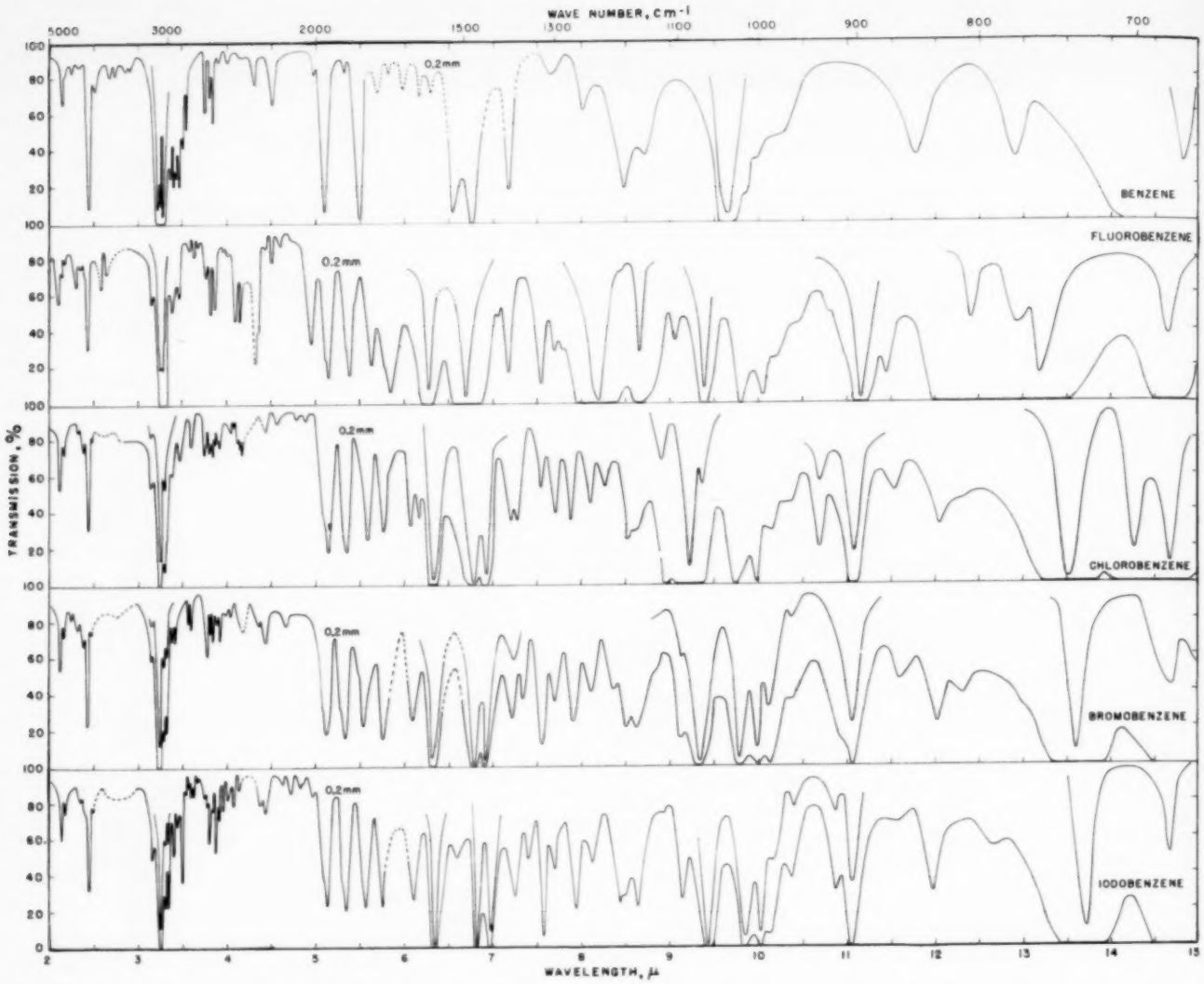

FIGURE 1. *Infrared absorption spectra of benzene, fluorobenzene, chlorobenzene, bromobenzene, and iodobenzene from 2 to 15 microns.*

Dotted sections represent regions of atmospheric interference.

3. Discussion of Results

Any complete assignment of the vibrational frequencies as determined from liquids or solutions is very difficult because the distinctive band shapes arising from the rotational fine structure are washed out. In the present case the difficulty is aggravated because the spectra beyond 38 μ were not obtained. Thus many of the important low-lying fundamentals were not observed. However, with the help of the excellent work of Randle and Whiffen,[1] some of the bands have been assigned. Some help was also obtained from the calculations of Garg.[2]

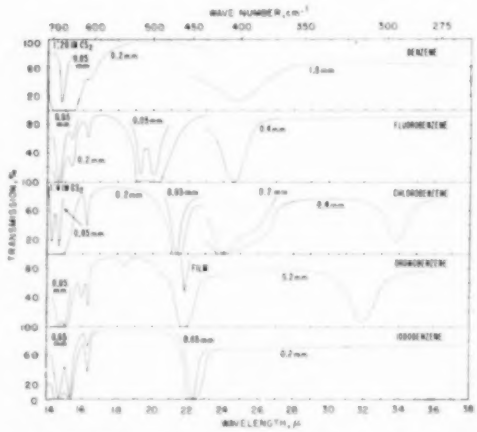

FIGURE 2. *Continuation of the spectra of the compounds of figure 1 in the region from 14 to 38 microns.*

[1] R. R. Randle and D. H. Whiffen, Molecular Spectroscopy Rept. of Conf. Hydrocarbon Research Group, Inst. Petroleum (Oct. 1954).
[2] S. N. Garg, Current Sci. **22**, 298 (1953).

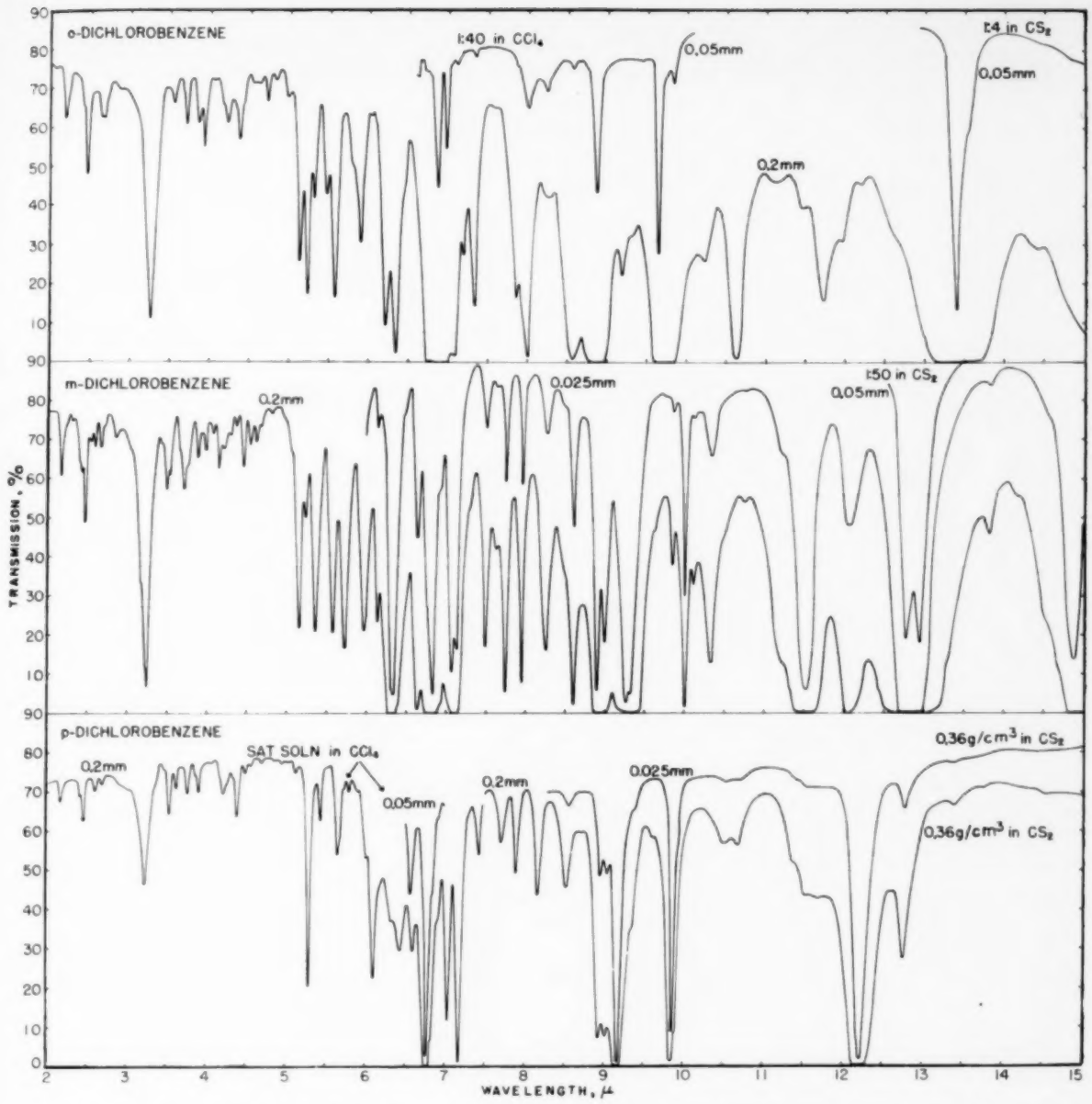

FIGURE 3. *Infrared spectra of orthodichlorobenzene, metadichlorobenzene, and paradichlorobenzene from 2 to 15 microns.*

The insert curves are for thinner cells or solutions in CCl_4 or CS_2.

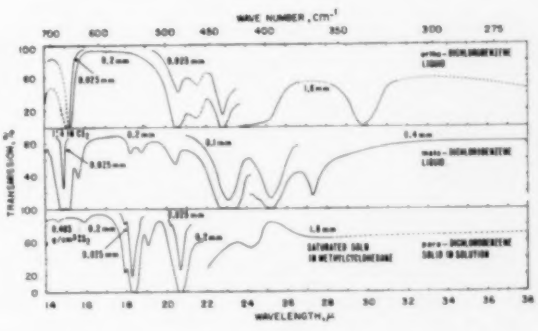

FIGURE 4. *Continuation of the spectra of figure 3 in the region from 14 to 38 microns.*

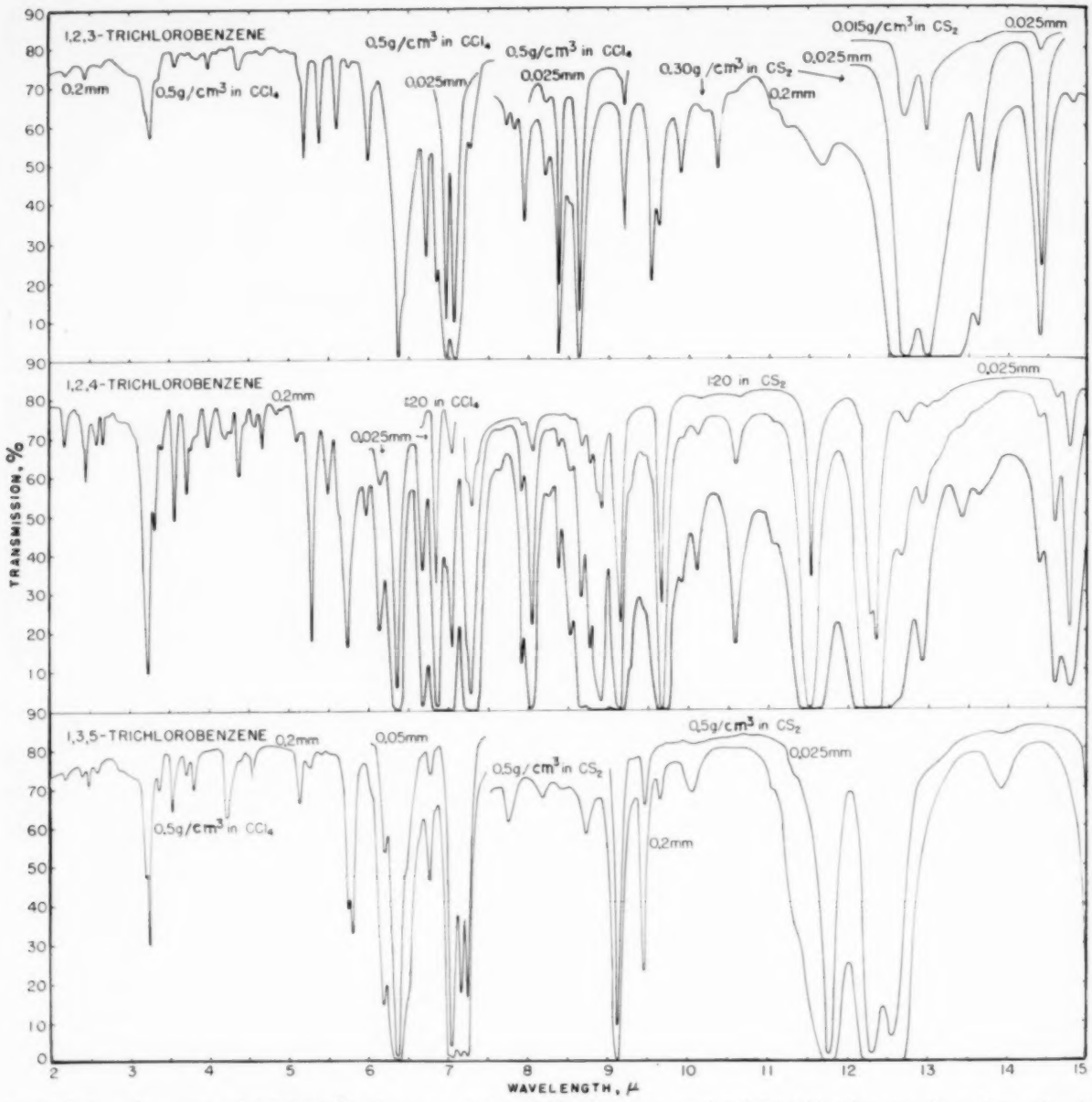

FIGURE 5. *Infrared spectra of 1,2,3-trichlorobenzene, 1,2,4-trichlorobenzene, and 1,3,5-trichlorobenzene from 2 to 15 microns.*

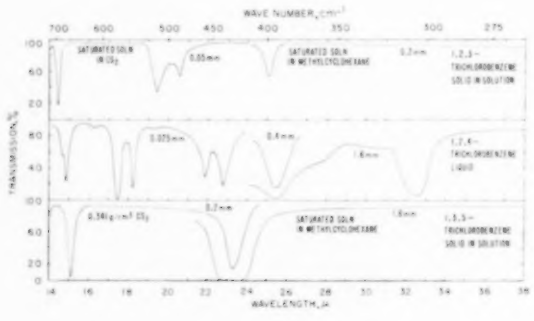

FIGURE 6. *Continuation of the spectra of the trichlorobenzenes from 14 to 38 microns.*

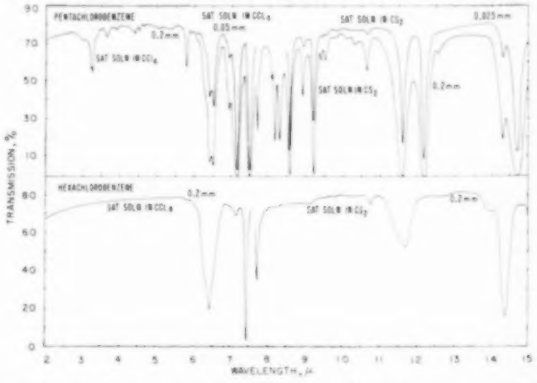

FIGURE 7. *Infrared spectra of pentachlorobenzene and hexachlorobenzene from 2 to 15 microns.*

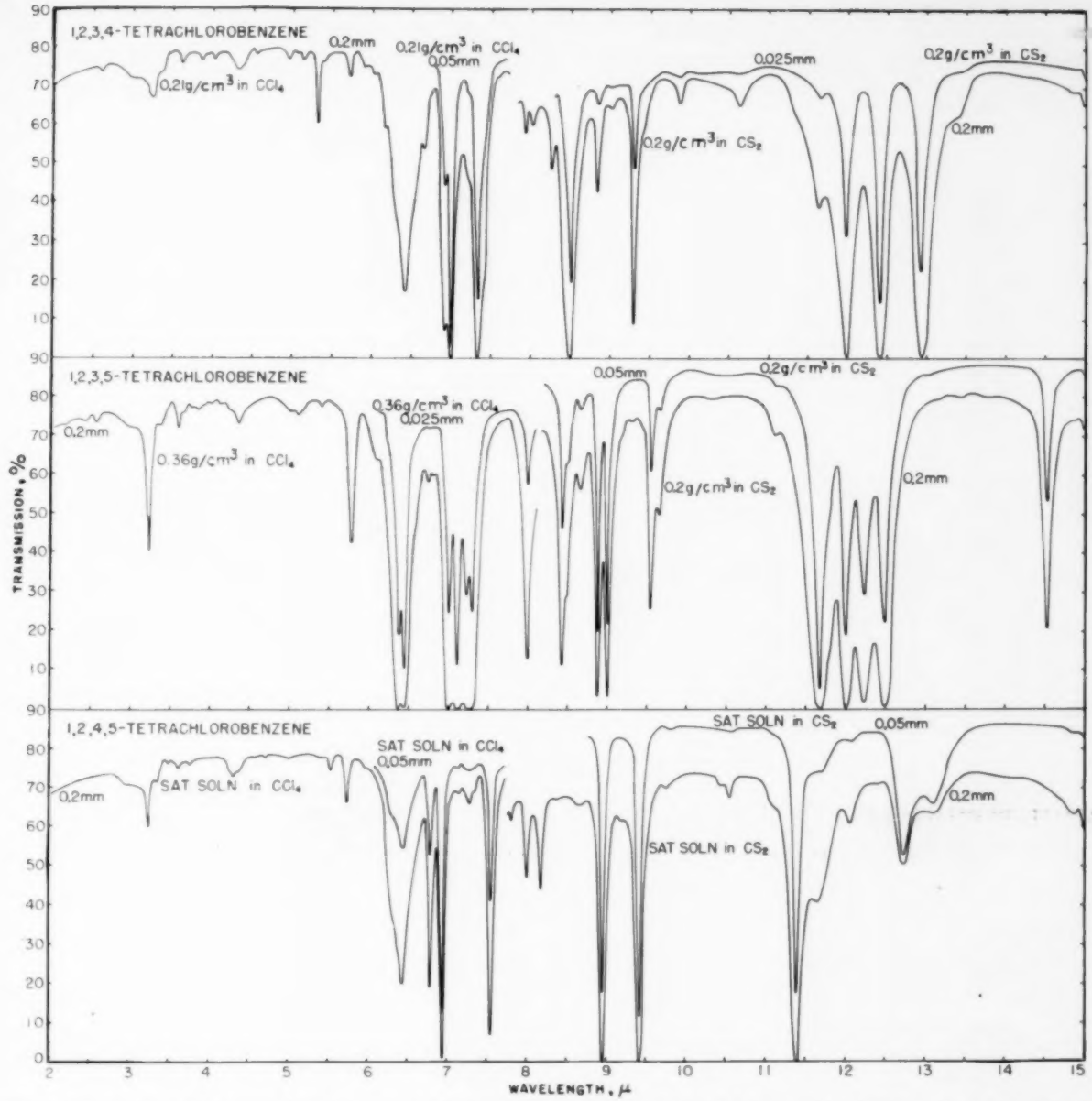

FIGURE 8. *Spectra of 1,2,3,4-tetrachlorobenzene, 1,2,3,5-tetrachlorobenzene, and 1,2,4,5-tetrachlorobenzene from 2 to 15 microns.*

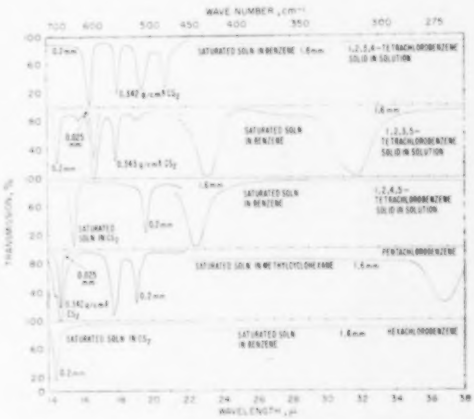

FIGURE 9. *Infrared spectra of the tetachlorobenzenes, pentachlorobenzene, and hexachlorobenzene from 14 to 38 microns.*

The dotted lines indicate that no bands of medium or strong intensity are present in that part of the spectrum.

TABLE 1. *Observed bands*

Observed wavelength	Wave number	Intensity [a]	Observed wavelength	Wave number	Intensity [a]
Benzene					
μ	cm^{-1}	$\frac{cm^{-1}}{cm^{-1}}$	μ	cm^{-1}	$\frac{cm^{-1}}{cm^{-1}}$
2.12	4,716	35	4.98	2,008	20
2.15	4,651	20	5.11	1,957	94
2.22	4,505	20	5.33	1,876	20
2.31	4,329	15	5.50	1,818	96
2.42	4,132	90	5.70	1,754	35
2.48	4,032	30	5.83	1,715	20
2.65	3,774	20	5.99	1,669	30
2.71	3,690	20	6.17	1,621	35
2.83	3,534	15	6.20	1,500	35
2.88	3,472	15	6.55	1,527	95
3.21	3,115	[b] 92	6.77	1,477	100
3.23	3,096	[b] 90	7.18	1,393	80
3.26	3,067	[b] 95	7.64	1,309	20
3.36	2,976	75	8.01	1,248	40
3.39	2,950	80	8.48	1,179	80
3.42	2,924	75	8.71	1,148	65
3.45	2,899	80	9.65	1,036	[b] 95
3.49	2,865	60	9.86	1,014	85
3.52	2,841	50	9.97	1,003	65
3.74	2,674	40	10.27	974	55
3.79	2,639	30	11.77	850	65
3.82	2,618	45	12.88	776	65
3.89	2,571	10	14.81	675	100
4.01	2,494	10	16.26	615	60
4.31	2,320	25	24.79	403	[d] 90
4.52	2,212	35			
Fluorobenzene					
2.08	4,808	45	5.39	1,855	85
2.10	4,762	30	5.44	1,838	45
2.15	4,651	20	5.63	1,776	80
2.27	4,405	35	5.78	1,730	80
2.32	4,310	25	5.85	1,709	90
2.40	4,167	70	6.28	1,592	[b] 90
2.56	3,906	35	6.69	1,495	[b] 95
2.62	3,817	30	7.07	1,414	50
3.14	3,185	45	7.18	1,393	80
3.22	3,106	[b] 75	7.54	1,326	90
3.24	3,086	[b] 80	7.70	1,299	70
3.26	3,067	[b] 80	7.79	1,284	70
3.27	3,058	[b] 70	8.15	1,227	[b] 95
3.37	2,967	50	8.20	1,220	[b] 100
3.45	2,899	45	8.66	1,155	[b] 70
3.55	2,817	15	9.07	1,103	65
3.57	2,801	15	9.40	1,064	[b] 90
3.62	2,762	20	9.81	1,019	100
3.66	2,732	15	10.06	994	80
3.75	2,667	30	10.11	989	75
3.80	2,632	50	------	------	------
3.85	2,597	45	------	------	------
3.95	2,532	15	------	------	------
4.00	2,500	15	11.16	896	[b] 95
4.09	2,445	55	11.46	873	80
4.11	2,433	55	12.39	807	[b] 55
4.16	2,404	55	12.45	803	[b] 40
4.33	2,309	80	12.93	773	[b] 55
4.35	2,299	60	13.18	759	[b] 85
4.44	2,252	15	14.64	683	[b] 95
4.52	2,212	25	15.53	644	[b] 40
4.61	2,169	15	16.28	614	40
4.95	2,020	65	19.26	519	[b] 90
5.11	1,957	75	20.00	500	[b] 90
5.15	1,942	85	24.56	407	[c] 100
5.34	1,873	70			
Chlorobenzene					
2.08	4,808	50	4.11	2,433	25
2.13	4,695	30	4.14	2,416	30
2.28	4,386	15	4.17	2,398	30
2.35	4,255	25	4.44	2,252	20
2.41	4,149	70	4.56	2,193	15
2.45	4,082	20	4.78	2,092	10
3.12	3,205	45	4.89	2,045	10
3.24	3,086	100	5.14	1,946	80
3.28	3,049	95	5.35	1,869	80
3.36	2,976	40	5.59	1,789	75
3.45	2,899	30	5.76	1,736	70
3.58	2,793	25	6.07	1,647	70
3.72	2,688	30	6.16	1,623	65
3.75	2,667	25	6.33	1,580	[b] 95
3.78	2,646	30	6.78	1,475	[b] 95
3.82	2,618	30	6.92	1,445	[b] 90
3.85	2,597	25	7.20	1,389	60
3.87	2,584	25	7.27	1,376	60
3.90	2,564	25	7.54	1,326	45
4.05	2,469	15	7.70	1,299	60
4.08	2,451	15	7.87	1,271	65

See footnotes at end of table.

TABLE 1. *Observed bands*—Continued

Observed wavelength	Wave number	Intensity [a]	Observed wavelength	Wave number	Intensity [a]
Chlorobenzene—Continued					
μ	cm^{-1}	$\frac{cm^{-1}}{cm^{-1}}$	μ	cm^{-1}	$\frac{cm^{-1}}{cm^{-1}}$
8.10	1,235	55	11.08	903	[b] 80
8.26	1,211	45	11.54	867	50
8.51	1,175	75	12.05	830	65
8.90	1,124	100	13.52	740	[b] 95
9.22	1,085	[b] 90	14.25	702	[b] 85
9.36	1,068	[b] 40	14.66	682	[b] 90
9.74	1,027	100	16.22	617	60
9.98	1,002	100	21.32	469	[b] 100
10.16	984	65	23.94	418	100
			25.44	393	70
10.69	935	80	33.78	296	80
Bromobenzene					
2.09	4,785	50	6.09	1,642	70
2.13	4,695	30	6.30	1,585	[b] 95
2.21	4,525	20	6.78	1,475	[b] 100
2.29	4,367	25	6.91	1,447	[b] 95
2.35	4,255	35	7.21	1,387	75
2.40	4,167	80	7.33	1,364	60
2.44	4,098	25	7.55	1,324	85
2.73	3,663	15	7.69	1,300	60
3.13	3,195	45	7.91	1,264	75
3.22	3,105	100	8.10	1,235	60
3.27	3,058	85	8.39	1,196	60
3.31	3,021	80	8.50	1,176	80
3.36	2,976	30	8.62	1,160	80
3.40	2,941	30	9.12	1,097	85
3.54	2,825	20	9.34	1,071	[b] 95
3.57	2,801	25	9.78	1,023	[b] 95
3.76	2,660	40	9.98	1,002	[b] 90
3.79	2,639	30	10.11	989	[b] 65
3.82	2,618	35	10.37	964	60
3.87	2,584	20	11.05	905	100
3.90	2,564	35	11.50	893	50
3.97	2,519	15	12.02	832	80
4.04	2,475	15	12.31	812	60
4.18	2,392	25	13.60	735	[b] 90
4.36	2,293	25	14.68	681	[b] 95
4.44	2,252	35	15.00	667	[b] 95
4.67	2,141	25	15.94	627	60
5.08	1,969	70	16.30	614	70
5.12	1,953	80	18.36	545	15
5.28	1,894	70	20.60	485	30
5.33	1,876	80	21.81	459	100
5.48	1,824	50	22.15	452	90
5.54	1,805	75	31.87	314	90
5.76	1,736	85			
Iodobenzene					
2.11	4,739	40	5.34	1,873	80
2.15	4,651	25	5.56	1,799	80
2.32	4,310	20	5.75	1,739	80
2.42	4,132	70	6.10	1,639	75
2.46	4,065	25	6.34	1,577	[b] 100
3.14	3,185	50	6.60	1,515	45
3.23	3,096	[b] 90	6.81	1,468	[b] 100
3.29	3,040	80	6.97	1,435	[b] 90
3.32	3,012	80	7.25	1,379	70
3.38	2,959	50	7.40	1,351	50
3.42	2,924	30	7.57	1,321	90
3.48	2,874	65	7.70	1,299	55
3.52	2,841	15	7.94	1,259	80
3.55	2,817	10	8.12	1,232	50
3.57	2,801	15	8.44	1,185	70
3.61	2,770	15	8.51	1,175	65
3.65	2,740	10	8.63	1,159	70
3.72	2,688	20	8.95	1,117	25
3.75	2,667	25	9.14	1,094	65
3.78	2,646	45	9.43	1,060	[b] 100
3.82	2,618	30	9.85	1,015	[b] 90
3.85	2,597	50	10.03	997	[b] 90
3.89	2,571	30	10.16	984	90
3.93	2,545	25	10.38	963	55
4.01	2,494	15	10.87	920	60
4.07	2,457	20	11.06	904	[b] 55
4.14	2,415	10	11.57	864	25
4.37	2,288	20	11.97	835	65
4.43	2,257	25	12.66	790	40
4.63	2,160	10	13.71	729	[b] 85
4.72	2,119	15	14.17	707	90
4.83	2,070	10	14.68	681	[b] 95
4.86	2,058	10	15.31	653	[b] 95
4.96	2,016	20	16.32	613	65
5.13	1,949	80	22.32	448	[b] 100

TABLE 1. *Observed bands*—Continued

Observed wavelength	Wave number	Intensity [a]	Observed wavelength	Wave number	Intensity [a]
Orthodichlorobenzene					
μ	cm^{-1}	%	μ	cm^{-1}	%
2.17	4,608	35	5.90	1,695	70
2.41	4,149	35	6.02	1,661	40
2.44	4,098	50	6.21	1,610	90
2.62	3,817	35	[c] 6.34	1,577	95
2.65	3,775	35	6.74	1,484	[b] 25
3.25	3,077	90	6.86	1,458	[b] 55
3.53	2,833	35	6.97	1,435	[b] 45
3.69	2,710	40	7.11	1,406	95
3.85	2,597	40	7.19	1,391	75
3.91	2,558	45	7.33	1,364	85
4.17	2,398	35	7.47	1,339	40
4.23	2,364	40	[c] 7.86	1,272	85
[c] 4.38	2,283	45	[c] 7.99	1,252	100
4.41	2,268	35	8.57	1,167	100
4.55	2,198	30	8.86	1,129	[b] 55
4.62	2,164	30	9.64	1,037	[b] 70
4.73	2,114	35	[c] 9.82	1,018	[b] 30
4.84	2,066	30	10.63	941	100
4.98	2,008	35	13.38	747	[b] 85
5.13	1,949	75	13.52	739	[b] 40
5.24	1,908	85	15.18	659	[b] 100
5.31	1,883	60	20.60	485	100
5.47	1,828	60	21.56	464	90
5.58	1,792	85	22.82	438	100
5.79	1,727	50	30.85	324	100
Metadichlorobenzene					
2.15	4,651	40	[c] 6.33	1,580	100
2.29	4,367	25	[c] 6.64	1,506	95
2.39	4,184	35	6.82	1,466	100
2.40	4,167	35	6.90	1,449	95
2.45	4,082	50	7.07	1,414	100
2.51	3,984	30	7.18	1,393	100
2.57	3,891	30	7.49	1,335	85
2.64	3,788	30	7.63	1,311	60
2.83	3,534	25	7.73	1,295	95
3.02	3,311	30	7.94	1,259	90
3.17	3,155	70	[f] 8.25	1,212	85
3.22	3,106	90	8.48	1,179	60
3.24	3,086	95	8.59	1,164	95
[c] 3.48	2,874	45	8.88	1,126	100
[c] 3.51	2,849	40	8.98	1,114	100
3.64	2,747	35	9.23	1,083	100
3.70	2,703	45	9.25	1,081	100
3.74	2,674	40	9.31	1,074	100
3.86	2,591	35	[f] 9.62	1,040	55
3.96	2,525	35	9.83	1,017	60
4.08	2,451	30	10.00	1,000	100
4.16	2,404	40	10.11	989	65
4.22	2,370	35	10.32	969	85
4.30	2,326	30	10.48	954	55
4.46	2,242	30	10.74	931	45
4.55	2,198	40	[f] 11.20	893	85
4.62	2,164	30	11.51	869	100
4.68	2,137	30	12.06	829	100
4.82	2,075	25	12.77	783	100
5.08	1,968	35	12.92	774	100
5.17	1,934	80	14.86	673	100
5.23	1,912	50	15.64	639	60
5.37	1,862	80	18.25	548	30
5.58	1,792	80	18.79	532	30
[c] 5.73	1,745	85	20.46	489	45
5.97	1,675	80	23.09	433	100
5.99	1,669	75	25.19	397	100
6.13	1,631	75	27.29	366	80
Paradichlorobenzene					
2.15	4,651	35	4.22	2,370	30
2.40	4,167	30	4.26	2,347	30
2.45	4,082	35	4.34	2,304	25
2.59	3,861	30	[c] 4.39	2,278	35
2.68	3,731	30	4.50	2,222	20
3.22	3,106	55	4.57	2,188	20
[c] 3.52	2,841	35	4.70	2,128	20
3.61	2,770	30	4.95	2,020	20
3.75	2,667	30	5.12	1,953	25
3.85	2,597	25	5.28	1,894	80
3.90	2,564	30	5.43	1,842	35
4.19	2,387	30	5.65	1,770	45

See footnotes at end of table.

TABLE 1. *Observed bands*—Continued

Observed wavelength	Wave number	Intensity [a]	Observed wavelength	Wave number	Intensity [a]
Paradichlorobenzene—Continued					
μ	cm^{-1}	%	μ	cm^{-1}	%
5.68	1,760	45	9.18	1,089	100
[c] 5.72	1,748	30	9.36	1,068	65
5.90	1,695	30	9.85	1,015	100
6.01	1,664	50	9.90	1,010	90
6.08	1,645	80	10.52	951	40
[c] 6.32	1,582	70	10.69	935	40
6.77	1,477	70	12.21	819	100
6.82	1,466	100	12.75	784	70
6.89	1,451	95	13.40	746	25
7.02	1,424	85	14.59	685	20
7.16	1,397	100	15.91	628	20
7.43	1,346	45	17.92	558	80
7.77	1,287	40	18.28	547	100
7.91	1,264	50	19.08	524	45
8.18	1,222	55	20.21	495	100
8.53	1,172	55	20.67	484	45
8.94	1,118	90	24.18	414	45
9.03	1,107	90			
1,2,3-Trichlorobenzene					
2.17	4,608	25	7.83	1,277	40
2.42	4,132	25	7.90	1,266	65
2.61	3,831	25	[f] 8.22	1,216	50
3.20	3,125	40	8.38	1,193	100
3.24	3,086	45	8.52	1,174	65
3.34	2,994	25	8.63	1,159	100
3.55	2,817	20	9.19	1,088	65
3.96	2,525	25	9.53	1,049	80
4.67	2,141	20	[f] 9.63	1,038	65
5.18	1,930	50	9.91	1,009	50
5.38	1,859	45	10.21	979	40
5.60	1,786	40	10.37	964	50
5.99	1,669	50	[f] 12.70	787	100
6.72	1,488	75	12.98	770	100
6.85	1,460	80	13.63	733	90
6.97	1,435	100	14.39	695	95
7.07	1,414	100	19.42	515	65
[c] 7.27	1,376	45	20.57	486	45
7.73	1,294	40	25.06	399	45
1,2,4-Trichlorobenzene					
2.15	4,651	35	8.03	1,245	100
2.40	4,167	35	8.37	1,195	65
2.44	4,098	40	8.52	1,173	80
2.54	3,937	30	8.65	1,156	95
2.64	3,788	30	8.76	1,142	100
3.21	3,115	90	8.86	1,129	100
3.31	3,021	55	8.91	[c] 1,122	100
3.56	2,809	50	[f] 9.14	1,094	100
3.71	2,695	45	9.25	1,081	90
3.76	2,660	35	[f] 9.65	1,036	100
3.82	2,618	30	9.90	1,010	70
3.97	2,519	35	10.09	991	65
4.21	2,375	30	10.58	945	85
4.28	2,336	30	11.05	905	60
4.58	2,183	40	[f] 11.52	868	100
4.67	2,141	25	12.27	815	100
4.86	2,058	35	12.33	811	100
5.11	1,957	30	12.65	790	95
5.29	1,890	85	12.92	774	85
5.50	1,818	45	13.41	746	50
5.65	1,770	50	13.62	734	45
[c] 5.73	1,745	85	14.39	695	65
5.97	1,675	50	14.58	686	95
6.14	1,629	80	14.77	677	95
[c] 6.37	1,570	100	16.30	613	40
6.68	1,497	95	17.40	575	100
6.84	1,462	100	18.16	551	100
7.04	1,420	100	19.20	521	40
7.23	1,383	100	21.80	459	100
7.28	1,374	100	22.76	439	100
7.35	1,360	100	25.44	393	[d] 95
7.63	1,311	40	32.57	307	[d] 90
7.91	1,264	85			

TABLE 1. *Observed bands*—Continued

Observed wavelength	Wave number	Intensity [a]	Observed wavelength	Wave number	Intensity [a]
1,3,5-Trichlorobenzene					
μ	cm^{-1}	C_c	μ	cm^{-1}	C_c
2.16	4,630	25	6.77	1,477	55
2.38	4,202	25	7.04	1,420	[b] 95
2.45	4,082	25	7.16	1,397	[b] 80
2.56	3,906	25	7.24	1,381	[b] 80
3.19	3,135	55	7.77	1,287	35
3.23	3,096	70	8.19	1,221	30
3.52	2,841	35	8.43	1,180	30
3.70	2,703	25	8.74	1,144	40
3.79	2,639	30	9.13	1,095	100
4.23	2,364	40	9.46	1,057	80
4.55	2,198	30	[f] 9.66	1,035	35
5.13	1,949	40	10.05	995	30
5.27	1,898	25	11.05	905	30
5.42	1,845	20	[f] 11.77	850	100
[c] 5.74	1,742	60	12.31	812	100
[c] 5.79	1,727	65	12.55	797	100
[c] 6.21	1,610	85	13.93	718	30
[c] 6.37	1,570	[b] 100	15.10	662	95
[c] 6.46	1,548	85	23.29	429	80
1,2,3,4-Tetrachlorobenzene					
2.59	3,861	25	7.93	1,261	40
3.23	3,096	35	8.03	1,245	40
3.61	2,770	25	8.27	1,209	50
3.86	2,591	25	8.52	1,174	100
4.03	2,481	25	8.84	1,131	55
[c] 4.33	2,309	25	9.03	1,107	35
[c] 4.56	2,193	25	9.31	1,074	90
[c] 4.97	2,012	25	9.40	1,064	40
5.15	1,942	25	9.88	1,012	35
5.33	1,876	40	10.64	940	35
5.42	1,845	25	[f] 11.98	835	100
[c] 5.73	1,745	30	12.42	805	100
5.92	1,689	25	12.92	774	100
6.05	1,653	30	13.39	746	40
6.17	1,620	40	16.44	608	95
6.66	1,502	45	18.05	554	80
6.93	1,443	95	19.43	515	70
6.99	1,430	160	20.80	481	70
7.33	1,364	100			
1,2,3,5-Tetrachlorobenzene					
2.40	4,167	25	8.42	1,188	50
2.54	3,937	25	8.48	1,179	70
3.20	3,125	50	8.66	1,155	45
3.22	3,106	60	8.87	1,127	95
[c] 3.35	2,985	25	8.99	1,112	95
3.58	2,793	25	[f] 9.53	1,049	75
3.63	2,755	25	9.65	1,036	50
5.41	1,848	25	[f] 11.67	857	100
[c] 5.77	1,734	55	[f] 12.00	833	100
6.10	1,639	35	12.23	818	100
[c] 6.37	1,570	100	12.48	801	100
[c] 6.44	1,553	100	14.54	688	80
6.74	1,484	45	15.79	633	20
7.00	1,428	100	16.70	599	100
7.10	1,408	100	17.93	558	75
7.22	1,385	100	19.10	523	20
7.29	1,372	100	23.10	431	[d] 95
8.00	1,250	90	31.74	315	[d] 95
1,2,4,5-Tetrachlorobenzene					
3.23	3,096	40	9.42	1,062	100
[c] 4.32	2,288	25	10.45	957	30
5.54	1,805	25	10.56	947	35
[c] 5.74	1,742	35	[f] 11.40	877	100
6.79	1,473	80	12.08	828	40
6.95	1,439	100	[f] 12.74	785	50
7.54	1,326	90	13.13	762	35
7.81	1,280	40	15.49	646	95
8.00	1,250	55	19.63	509	80
8.13	1,230	55	22.52	444	[d] 100
8.97	1,115	100			

TABLE 1. *Observed bands*—Continued

Observed wavelength	Wave number	Intensity [a]	Observed wavelength	Wave number	Intensity [a]
Pentachlorobenzene					
μ	cm^{-1}	C_c	μ	cm^{-1}	C_c
3.21	3,115	45	8.92	1,121	60
3.25	3,077	45	9.22	1,084	100
3.63	2,755	25	9.40	1,064	40
3.90	2,564	25	9.52	1,050	40
[c] 5.79	1,727	45	10.11	989	25
6.09	1,642	30	10.31	970	30
[c] 6.32	1,582	60	10.64	940	45
[c] 6.42	1,558	95	[f] 11.60	862	100
[c] 6.53	1,531	95	12.17	822	100
6.94	1,441	65	12.54	797	35
7.15	1,399	100	14.29	700	80
7.49	1,335	100	14.70	680	100
7.70	1,299	75	17.79	562	90
8.08	1,238	50	17.92	558	80
8.17	1,224	80	19.09	524	80
8.30	1,204	80	19.36	516	25
8.57	1,167	100	36.80	272	[d] 75
Hexachlorobenzene					
[c] 7.14	1,400	30	[f] 10.75	930	25
7.42	1,347	95	13.92	718	30
7.71	1,297	65	14.37	696	85

[a] Intensities not corrected for background
[b] 0.05-mm cell.
[c] 0.40-mm cell.
[d] 1.6-mm cell.
[e] Solid in solution of CCl_4 and band partially contributed by CCl_4.
[f] Solid in solution of CS_2 and band partially contributed by CS_2.

TABLE 2. *Fundamental vibrations of monohalobenzenes in* cm^{-1}

D_{6h}		Benzene [a]	Band types	Fluorobenzene	Chlorobenzene	Bromobenzene	Iodobenzene
ν_1	A_{1g}	3,062	A_1				
ν_2	A_{1g}	992	A_1	1,019	1,002	1,002	997
ν_3	A_{2g}	[b] 1,340	B_1	(c)	(c)	(c)	(c)
ν_4	A_{2u}	671	B_2				
ν_5	B_{1u}	3,071	A_1				
ν_6	B_{1u}	[b] 1,008	A_1	807	701	668	653
ν_7	B_{2g}	995	B_2	759	740	735	729
ν_8	B_{2g}	703	B_2	684	682	681	681
ν_9	B_{2u}	[b] 1,150	B_1				
ν_{10}	B_{2u}	[b] 1,310	B_1	1,155	1,175	1,160	1,159
ν_{11}	E_{1g}	849	A_2				
			B_2	(c)	(c)	(c)	(c)
ν_{12}	E_{1u}	3,063	A_1	3,086			
			B_1	3,068			
ν_{13}	E_{1u}	1,485	A_1	1,495	1,475	1,475	1,468
			B_1	1,326	1,326	1,324	1,321
ν_{14}	E_{1u}	1,037	A_1	1,019	1,027	1,022	1,015
			B_1				
ν_{15}	E_{2g}	3,047	A_1	1,220	1,085	1,071	1,060
			B_1	3,040	3,030	3,040	3,030
ν_{16}	E_{2g}	1,585	A_1	1,592	1,580	1,585	1,577
			B_1	1,495	1,475	1,475	
ν_{17}	E_{2g}	1,178	A_1	1,155		1,160	1,159
			B_1	1,064	1,068	1,071	1,060
ν_{18}	E_{2g}	606	A_1	519	418	314	
			B_1	614	617	614	613
ν_{19}	E_{2u}	[b] 975	A_2				
			B_2	980	984	964	984
ν_{20}	E_{2u}	404	A_2	407	393		
			B_2	500	469	478	448

[a] Benzene assignments and wave numbers from R. D. Mair and D. F. Hornig, J. Chem. Phys. **17**, 1236 (1949).
[b] Partially contributed by solvent.
[c] Band lies below the range of observations.

TABLE 3. *Assignments of some of the bands of polychlorobenzene*

Orthodichlorobenzene			Metadichlorobenzene			Paradichlorobenzene			1,2,3-Trichlorobenzene			1,2,4-Trichlorobenzene		
Wave number	Identification	Intensity	Wave number	Identification	Intensity	Wave number	Identification	Intensity	Wave number	Identification	Intensity	Wave number	Identification	Intensity
cm^{-1}		$\%$	cm^{-1}		$\%$	cm^{-1}		$\%$	cm^{-1}		$\%$	cm^{-1}		$\%$
1,610	A_1 C—C	90	1,631	B_1 C—C	75	1,645	A_g C—C	75				1,629	A^1 C—C	80
[a] 1,577	B_1 C—C	95	[a] 1,580	A_1 C—C	100	[a] 1,582	B_{1g} C—C	65	1,488	A_1 C—C	75	1,570	A^1 C—C	100
1,484	B_1 C—C	100	[a] 1,506	B_1 C—C	95							1,497	A^1 C—C	95
1,458	A_1 C—C	[b] 55	1,449	A_1 C—C	95	1,451	B_{1u} C—C	90				1,462	A^1 C—C	100
1,167	A_1 C—H	95	1,164	B_1 C—H	65	1,172	A_g C—H	55				1,156	A^1 C—H	100
						1,118	B_{1u} C—H	90						
1,129	B_1 C—H	[b] 55							1,159	B_1 C—H	100			
			1,081	A_1 C—H	100				1,088	A_1 C—H	70			
1,037	A_1 C—H	[b] 75	[a] 1,040	B_1 C—H	50									
			1,000	A_1 ring	95	1,015	B_{2u} C—H	95	979	A_1 ring	35	1,010	A^1 ring	70
			969	B_2 C—H	85				964	B_2 C—H	50			
941	B_2 C—H	100	[a] 869	B_2 C—H	[b] 90	935	[c] A_u C—H	45				868	A^{11} C—H	100
			[a] 893	A_2 C—H	85							815	A^{11} C—H	100
747	B_2 C—H	[b] 85	783	B_2 C—H	[b] 100	819	B_{1u} C—H	100						
			673	B_2 C—C	[b] 85	685	B_{1g} C—C—C	10	770	B_2 C—C	100			
						628	B_{1g} C—C—C	10	733	B_2 C—C	90			
						414	A_u C—C	[d] 50						

1,3,5-Trichlorobenzene			1,2,3,4-Tetrachlorobenzene			1,2,3,5-Tetrachlorobenzene			1,2,4,5-Tetrachlorobenzene			Pentachlorobenzene		
Wave number	Identification	Intensity	Wave number	Identification	Intensity	Wave number	Identification	Intensity	Wave number	Identification	Intensity	Wave number	Identification	Intensity
cm^{-1}		$\%$	cm^{-1}		$\%$	cm^{-1}		$\%$	cm^{-1}		$\%$	cm^{-1}		$\%$
1,610	E^1 C—C	85	1,620	C—C	40	1,639	C—C	60				1,642	C—C	30
			1,502	C—C	45	1,570	C—C	100				1,558	C—C	90
1,477	E^1 C—C	50				1,484	C—C	45						
1,186	E^1 C—H	30	1,174	C—H	100				1,062	C—H	100			
995	A^1 ring	35												
850	A^{11}_2 C—H	100							[a] 877	C—H	100	[a] 862	C—H	100
662	A^{11}_2 C—C	95	805	C—H	100	[a] 833	C—H	100						

[a] Partially contributed by solvent. [b] 0.05-mm cell. [c] A_u or B_{1g}. [d] 1.6-mm cell.

The most success was possible in the case of the monohalogenated benzenes. Benzene has the symmetry D_{6h}, and thus 20 distinct vibrational frequencies are present, 10 of which are doubly degenerate. In the monohalogenated benzenes, the symmetry is reduced to C_{2v}. As a result, there are no degenerate frequencies remaining, and there are 36 distinct frequencies, although the A_2 species will be infrared inactive. A correlation between the benzene frequencies and some of the monohalogenated benzene frequencies is given in table 2. For fluorobenzene the published assignments[3] for the gas were used as a guide.

[3] D. C. Smith, E. E. Ferguson, R. L. Hudson, and J. Rud Nielsen, J. Chem. Phys. **21**, 1475 (1953).

For the more highly substituted chlorobenzenes more of the frequencies were inaccessible, and in each case only the C—C, C—H, and ring frequencies, which are more or less constant from molecule to molecule, have been designated in table 3. These assignments should be regarded as tentative, although they were made according to the procedure suggested in the paper by Randle and Whiffen.

WASHINGTON, December 4, 1956.

Journal of Research of the National Bureau of Standards Vol. 58, No. 5, May 1957 Research Paper 2759

Infrared Spectra of Chromatographically Fractionated Asphalts[1]

James E. Stewart

Undegraded and weathered specimens of three roofing asphalts were chromatographically separated into three components after removal of the asphaltenes. The infrared absorption spectra of the fractions, recorded in the 2- to 15-μ spectral region, provide information about the chemical constitution of the material, the differences among asphalts from different sources, and the changes in constitution produced by weathering.

1. Introduction

Work on the constitution of asphalt and the degradation of asphalt on weathering has been under way at the National Bureau of Standards for some time. This work has been facilitated greatly by the development of chromatographic techniques [1][2] that permit the separation of structurally similar components for chemical and physical study. One phase of this study involved the use of infrared spectroscopy in an attempt to elucidate the chemical structure of the asphalt components and to determine changes that occur in the components when the asphalts are weathered. Infrared spectroscopy [2,3] has been useful in studying the chemical structure of chromatographically fractionated petroleums of the type used as extender oils in synthetic rubber. It seemed reasonable, therefore, to apply infrared methods to the study of asphalts as well.

The purpose of this report is to present the results of a brief study of three airblown roofing asphalts of different origin. These asphalts are product 3 of asphalts I, II, and III, the properties of which were reported in detail by Greenfeld [4]. The asphalts and their components will be referred to as I, II, and III, respectively, in the following discussion. Both undegraded materials and specimens degraded by 30 months of natural weathering were examined.

2. Experimental Procedures

The asphalts were separated into four groups of components by L. R. Kleinschmidt of the NBS Floor, Roof, and Wall Covering Section. Normal pentane was used for the primary separation of the asphalts into asphaltenes and maltenes. The maltenes were fractionated further [1] into three groups of components, designated as water-white oils, dark oils, and asphaltic resins, by eluting the *n*-pentane soluble portions of the asphalts from a fuller's-earth column, with *n*-pentane, methylene chloride, and methyl ethyl ketone.

The distribution of components in the three asphalts, both before and after 30 months of exposure outdoors at the National Bureau of Standards, is given in table 1. The distribution of components changes during weathering through the conversion of certain materials into water-soluble and volatile degradation products and by the alteration of adsorption properties because of chemical reactions.

Infrared absorption spectra were obtained with a Perkin-Elmer model 21 spectrophotometer, equipped with a sodium chloride prism. In order to avoid the interference of solvents it was decided to observe the material as liquid films. A cell was constructed that could be heated to about 60° C with a nichrome heater to facilitate loading the viscous asphaltic-resin fraction. Close control of temperature was not required because of the insensitivity of the absorption by these materials to temperature changes. The windows were separated by a lead spacer 0.05 mm thick, cut away at the top and bottom. A slot was cut in the top of one window. Samples were introduced into the slot and permitted to run into the cell, sometimes with the aid of suction applied at the bottom of the cell. After a spectrum was recorded, the sample was removed by suction and the cell rinsed with solvent. To assure constancy of the cell thickness, it was not disassembled during the series of measurements.

In addition, the spectra of the asphaltenes were obtained by suspending the material in potassium iodide pellets and in mineral oil. The use of

TABLE 1. *Analyses of asphalts*

Type	I	II	III
Unweathered material, stored 30 months in covered container			
	wt %	wt %	wt %
Asphaltenes	41.2	41.0	39.2
Water-white oils	27.7	25.5	23.6
Dark oils	17.5	20.5	21.8
Asphaltic resins	8.8	10.3	10.8
Weathered, 30 months[a]			
Asphaltenes	41.6	42.0	43.6
Water-white oils	18.7	20.1	19.1
Dark oils	8.5	14.6	14.6
Asphaltic resins	9.0	9.4	8.5
Weight loss	19.7	11.7	11.5

[a] Percentage distribution of components based on the weights of the original coatings, which were 0.02 in. in thickness and 12 in.^{2} in area.

[1] This work was supported jointly by the Asphalt Roofing Industry Bureau and the National Bureau of Standards.

[2] Figures in brackets indicate the literature references at the end of this paper.

potassium iodide provided spectra that were free from losses by scatter, in contrast with those obtained by using potassium bromide. However, because of adsorbed water, alkali halide pellets absorb in the 3μ region where O—H groups are observed. The use of mineral-oil suspensions permits observations in this important region.

3. Infrared Spectra

The value of infrared spectroscopy in studies like the present one arises from the fact that certain functional groups absorb infrared radiation in fairly narrow regions of wavelength, relatively independent of other functional groups in the molecule. Hence, in a mixture of many different compounds, common structural groups can often be determined. For example, all of the asphalt fractions absorb near 3.40, 3.49, 6.82, and 7.2 μ because of the stretching and angle-deformation vibrations of the CH_2 and CH_3 groups of alkanes. On the other hand, many functional groups have no characteristic absorption or absorb so weakly that they cannot be detected. C—S and S—S groups are of this nature. Furthermore, chemically different functional groups ofter have similar vibations and therefore absorb at a common wavelength. Conjugated carbon chains and aromatic rings, for example, have bands at 6.25 μ. In the analysis of the fractions that follows, liberal use has been made of the standard reference books in chemical infrared analysis; in particular, the book of Bellamy [5] has been invaluable.

3.1. Water-White Oils

The water-white oil fractions (fig. 1) are seen to be predominantly saturated aliphatics, with a slight aromatic content producing a ring vibration at 6.25 μ. Very likely the aromatic content is largely of a paradisubstituted nature leading to the absorption band at 12.2 μ. From the relative intensities of the 6.25- and 12.2-μ aromatic bands from sample to sample, it appears that samples II and III have about the same aromatic content, whereas sample I is more aromatic by a factor of about 2 or 3. An idea of the mean chain length, and thus of branching, is obtained by observation of the intensities of the C—H band at 13.8 μ and the shoulder found on the short wavelength side of this band. In general, the longer chains absorb at longer wavelengths than the shorter chains. Simple III shows evidence of slightly more branching than sample II, and sample I is considerably more branched. This observation is verified by the intensities of the CH_3 bands at 7.24 μ, the more highly branched samples showing stronger CH_3 absorption.

The presence of cycloparaffins in hydrocarbon mixtures is believed [2] to result in increased absorption in the rather broad region centered at about 10.2 μ. Hence, sample III is slightly more cycloparaffinic in nature than II, and sample I is much more cycloparaffinic.

The water-white oil separated from a weathered sample II is almost identical to the unweathered sample, except for a slight decrease in intensity of

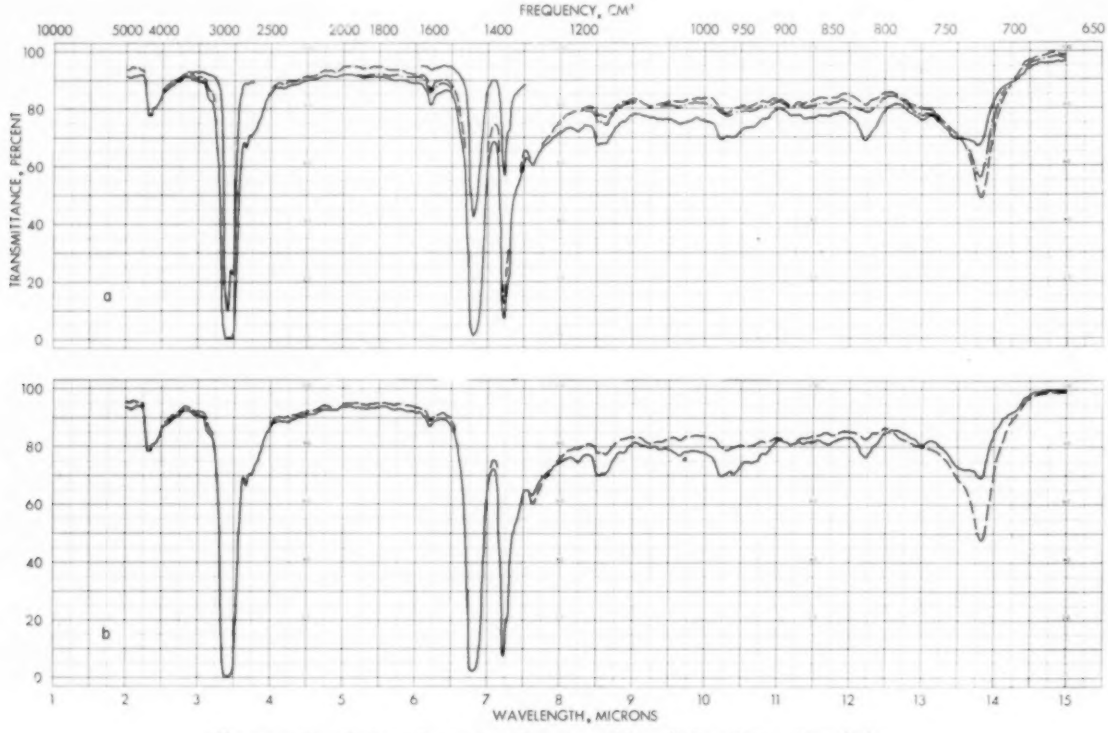

FIGURE 1. *Infrared spectra of water-white oil fractions of asphalts.*

a, Unweathered; b, weathered.

I, _____; II, _____ _____; III, _____ . _____

the aromatic bands and perhaps a slight reduction in branching. Sample III displays, in addition to reduced aromaticity, a more pronounced reduction in branching as well as reduced absorption in the cycloparaffin region. After weathering, the water-white oils from asphalts III and II are nearly identical, with the former being very slightly less branched. The aromatic and cycloparaffin absorption of sample I is reduced after weathering, but the branching seems to be unaltered.

The relatively greater loss of cycloparaffin and branched aliphatic components during weathering is in agreement with the greater reactivity of such compounds. Furthermore, sample I, which is richest in these compounds, loses a greater fraction of the water-white oils originally present (see table 1).

3.2. Dark Oils

The dark oils (fig. 2) are highly aromatic in nature, as shown by the bands at 6.21, 11.48, 12.24, and 13.35 μ. Substitution on the rings in various ways or fused rings produce the three-band pattern between 11 and 13.5 μ. In addition, two bands are found at 13.68 and 13.87 μ that are difficult to interpret. They are probably due in part to $-CH_2-$ chains, as in the water-white oils, because there are certainly aliphatic CH_2 and CH_3 groups present. Bands comparable in appearance to these were not found in the heavy petroleum fractions previously studied [2, 3]. These fractions contain oxygen in the form of O—H groups absorbing at 2.95 μ (this band could also be due to N—H groups), C=O groups absorbing at 5.86 μ, and perhaps C—O groups contributing to the general absorption from 8 to 10 μ. Sample I has more C=O, O—H, C—O, aromatic, and branched aliphatic groups than samples II or III. Sample III has the least absorption by C=O groups, whereas sample II has the least branching and absorption by O—H groups. Sample II has a stronger band at 6.21 μ but weaker bands at 12.24 and 13.35 μ than sample III. In none of these are the differences in the aromatic bands very great.

As expected, the dark-oil fractions separated from the weathered asphalts show increased absorption by C=O groups, indicating increases in carbonyl concentrations by factors of about 1.4 for sample II and about 2 for I and III. There are no changes in the O—H bands, and only sample I shows increased adsorption in the C—O band region. The aromaticity of the samples is not greatly changed, but may be slightly reduced by weathering. In all of the samples the pair of bands at 13.68 and 13.87 μ have been greatly accentuated. As in the case of the water-white oils, the dark oils separated from weathered asphalts II and III are nearly identical, although the dark-oil fractions from the unweathered asphalts are different.

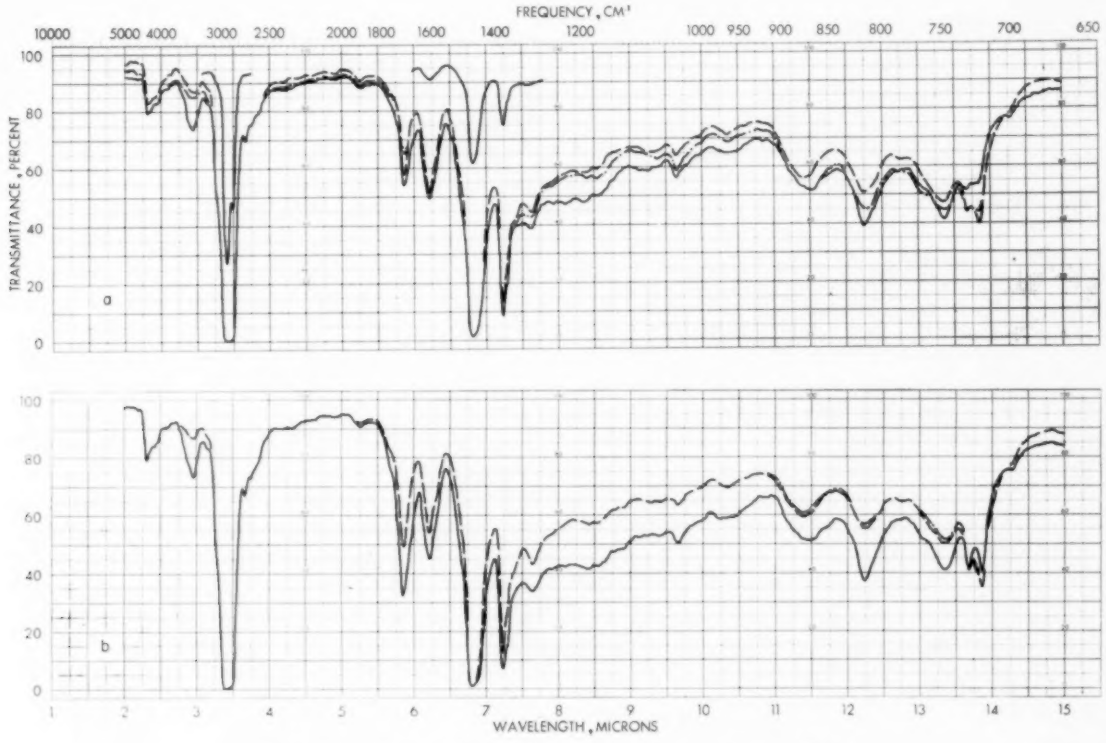

FIGURE 2. *Infrared spectra of dark-oil fractions of asphalts.*

a, Unweathered; b, weathered.

I, _____; II, _____ _____; III, _____, _____

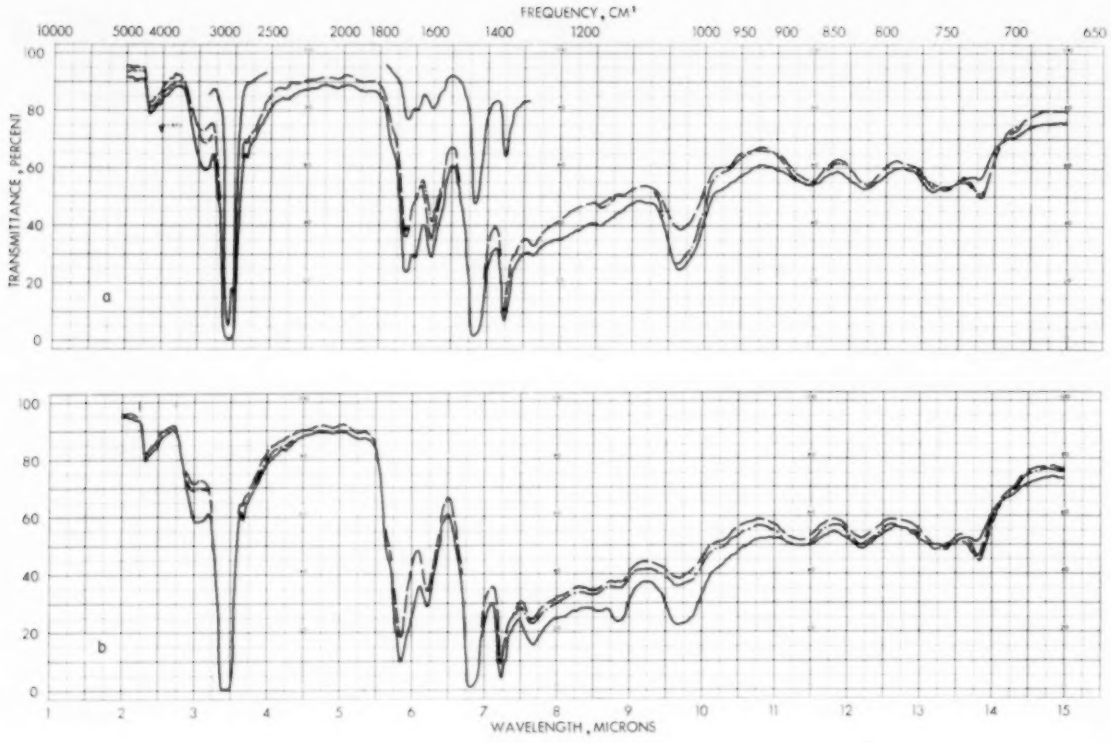

FIGURE 3. *Infrared spectra of asphaltic resin fractions of asphalts.*

a, Unweathered; b, weathered.

I, _____; II, _ _ _ _; III, _____ . _____

3.3. Asphaltic Resins

The asphaltic resin fractions (fig. 3) appear to be more aromatic [3] than the dark oils, and to contain more C=O groups. The broad absorptions near 3 μ extend to longer wavelengths than they do in the dark oil, and there is a definite absorption at 6 μ, especially noticeable in sample I, suggesting the presence of amides or amines. The strong band found in all samples at 9.62 μ is puzzling. It occurs in a region where certain C—O, S=O, and Si—O groups absorb [5]. Because the intensity of absorption by these groups is fairly large, the band at 9.62 μ does not necessarily indicate a high concentration. The band does not coincide with the band found in this region in the spectrum of fuller's earth [6] μ.

Of the three samples, material I is probably most aromatic, and contains more oxygenated groups than the others. The band at 9.62 μ is strongest in samples I and III.

The fractions obtained from weathered asphalt show increased C=O absorption, as well as stronger absorption in the C—O region. The gain in concentration of carbonyl groups measured at 5.86 μ, under the assumption of constant absorptivity of carbonyl groups, is again larger for sample I (about 2.8 times) than for samples II and III (about 1.7 and 1.8 times, respectively). The band at 9.6 μ seems to be weaker in the fractions from weathered asphalt, whereas bands at 8.8 and 7.7 μ become stronger. This is consistent with an oxidation of sulfoxides to form sulfones, for example. Once more, the near identity of the samples from weathered asphalts II and III is striking.

3.4. Asphaltenes

The spectra of the asphaltenes (fig. 4) have a washed-out appearance, that is, the contrast between background and absorption peaks is relatively low. This is often the case when rather large particles are observed in suspension, even though scatter is controlled by proper choice of suspension medium [7,8]. The spectra show evidence of aliphatic and aromatic groups and for C=O and C—O groups. However, no O—H or N—H absorption is observed. There is a little difference among the spectra of unweathered asphaltenes and even less among the weathered specimens. Weathering appears to increase somewhat the aromatic and carbonyl content of the material.

[3] This observation is based on the intensity of the band at 6.25 μ. The C—H out-of-plane vibration bands between 11 and 14 μ are weaker than those in the dark-oil fractions, suggesting that the asphaltic resins contain condensed or highly substituted aromatic ring systems. It is to be emphasized, however, that conclusions based on the assumption of invariant intensities of bands are questionable until the invariance of such bands is well established experimentally.

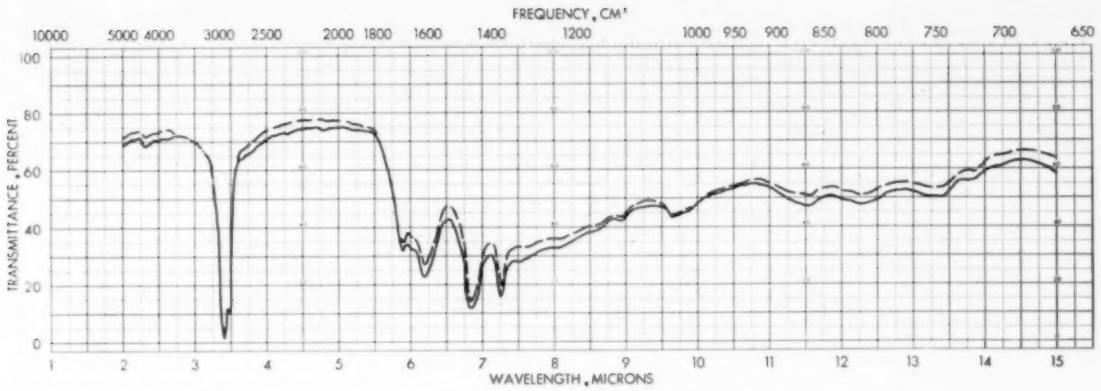

FIGURE 4. *Infrared spectra of asphaltenes separated from asphalt I.*

_____, Unweathered; _____ _____, weathered.

Samples were suspended in potassium iodide pellets, except for observation in the 2.75- to 3.25-μ region, where mineral-oil suspensions were used.

4. Discussion and Conclusion

Infrared analysis is most valuable when used in conjunction with other chemical and physical information. The discussion of the structures found in the fractions of asphalts I and II is for the most part in qualitative agreement with the elemental analyses [9] of the same or, in the case of weathered material, similar fractions.

All of the fractions of asphalt I have a higher carbon-to-hydrogen ratio than the fractions of II, except for the asphaltenes, and all the fractions of asphalt I contain more oxygen, sulfur, and nitrogen. The carbon-to-hydrogen ratio increases regularly in the order water white oils, dark oils, asphaltic resins, asphaltenes, and, although some oxygen and nitrogen are reported in the dark oils, these elements are more prevalent in the asphaltic resins and asphaltenes. The sulfur analysis, unfortunately, does not necessarily support the possible assignment of the 9.6-μ band in the asphaltic resins to S=O groups.

In general, weathering appears to reduce slightly the carbon-to-hydrogen ratio of all of the fractions and to increase the oxygen content of the dark oils, asphaltic resins, and asphaltenes.

In conclusion, the information derived from the infrared spectra of asphalt fractions can be summarized as follows:

1. The fractions from asphalt III resemble those from asphalt II, both before and after weathering.

2. Water-white oils are predominantly saturated aliphatics, with slight aromatic content. Asphalt II has less aromatic, branched aliphatic, and cycloparaffin content than I. Weathering reduces the aromatic, branched-chain, and cycloparaffin nature, particularly of asphalt I.

3. Dark oils have considerable aromatic structure and some oxygenated groups. Asphalt II has less aromatic, branched chain and oxygenated character than I. Weathering increases the carbonyl content and perhaps reduces the aromatic nature slightly, especially in asphalt I.

4. Asphaltic resins are highly aromatic with carbonyls and other oxygen groups and possibly amide, S=O, and Si—O groups; asphalt I containing more of all of these groups. Weathering increases the C=O content and changes the S or Si absorption. Again, asphalt I is most affected.

5. Asphaltenes are aromatic with C=O and C—O groups. Weathering produces some increases in aromatic and carbonyl content. There seems to be little difference among materials from different asphalts.

The author is grateful to L. R. Kleinschmidt who provided the fractionated samples and to S. H. Greenfeld for his unpublished data on physical and chemical properties of the fractions.

5. References

[1] L. R. Kleinschmidt, J. Research NBS **54**, 163 (1955) RP2577.
[2] F. J. Linnig and J. E. Stewart, J. Research NBS **59** (1957) RP2771.
[3] A. R. Glasgow, Jr., D. J. Termini, and J. E. Stewart (unpublished report).
[4] S. H. Greenfeld, Effects of mineral additives on the durability of coatings-grade roofing asphalts, NBS Building Materials and Structures Report 147 (1956).
[5] L. J. Bellamy, The infrared spectra of complex molecules, John Wiley & Sons, New York, N. Y. (1954).
[6] J. M. Hunt, M. P. Wisherd, and L. C. Bonham, Anal. Chem. **22**, 1478 (1950).
[7] M. R. Harvey, J. E. Stewart, and B. C. Achhammer, J. Research NBS **56**, 225 (1956) RP2670.
[8] J. E. Stewart, J. Research NBS **54**, 41 (1955) RP2563.
[9] S. H. Greenfeld, private communication.

WASHINGTON, November 30, 1956.

Journal of Research of the National Bureau of Standards Vol. 58, No. 5, May 1957 Research Paper 2760

Thermal Conductivity of Nitrogen from 50° to 500°C and 1 to 100 Atmospheres*

R. L. Nuttall[1] and D. C. Ginnings

A new apparatus has been constructed for measurements of the thermal conductivity of gases up to 500°C and 100-atmosphere pressure. The parallel-plate method was used with a spacing of about 0.5 millimeter between the hotplate and coldplate. A capacitance method was used to measure the effective spacing and area of the plates under the conditions of the experiment. No solid material was used between the plates. The effect of radiation was minimized by use of polished silver parts and was accounted for by experiments with the conductivity cell evacuated. Measurements on nitrogen were made at 1, 50, and 100 atmospheres, and from 50° to 500°C. It is believed that the accuracy of the results is about 0.5 percent, except at the highest gas densities.

1. Introduction

Accurate data on the thermal conductivity of gases are needed for two reasons. First, they are needed to check present theories of heat conduction in gases. Experimental measurements at very high temperatures and pressures are extremely difficult, so that theoretical means of predicting thermal conductivities in this range are needed. Second, accurate data are needed on at least one gas so that engineering data on other gases can be obtained with relatively simple apparatus by a comparison method. The present apparatus was constructed primarily to furnish very accurate data for use as standards by others making thermal-conductivity measurements on gases. Nitrogen was chosen as the first gas to be measured for several reasons. More measurements have been made on nitrogen than on any other pure gas. It is readily available in a state of high purity and is entirely suitable as a standard reference gas for use in calibrating apparatus for relative measurements.

2. Method

Measurements of thermal conductivity of gases in a steady state have been made by two general methods, radial heat flow and linear heat flow. Most measurements have been made with radial heat flow, either from a hot wire or between coaxial cylinders. In principle, these measurements are susceptible to convection errors. Elimination of these errors at the high pressures requires extremely small dimensions, which may be difficult to determine. The linear heat flow method is free from convection if the heat flow is downward. For this reason, the parallel-plate method was chosen for these measurements up to 100 atm. The spacing between the plates was made small to minimize the error caused by radial heat transfer. In addition, the small spacing reduces the possibility of convection in case the plates are not quite horizontal.

The correction for heat transfer by radiation between the hotplate and the coldplate was evaluated by an experiment with the conductivity cell evacuated. Of course, this assumes that no appreciable part of the radiation is absorbed by the gas in the conductivity experiment. In all the experiments, it was necessary to know the effective spacing between the plates. Frequently, solid spacers (of known dimensions) are used between the hotplate and coldplate. No such spacers were used in this apparatus because it was believed that the heat transfer through the contact area of the spacers and plates might be different with gas present than with the cell evacuated. The radiation correction experiment would thus be partially invalidated. The effective spacing was measured by a capacitance method under the actual conditions of the experiment. This method has several advantages over the usual method with measured spacers. First, the above-mentioned uncertainty in the effect of contact is eliminated. Second, the capacitance method automatically accounts for any change in dimensions. Third, because the direct capacitance between the hotplate and coldplate is measured, nonlinear heat flow at the circumference of the hotplate is accounted for.

The thermal conductivity, k (w cm^{-1} deg C^{-1}), for heat flow between parallel plates is given by the equation

$$k=\frac{\dot{Q}\Delta X}{\Delta t A}, \tag{1}$$

where Q is the rate of heat (watts) flowing only by conduction from the hotplate through the gas to the coldplate, Δt is the temperature difference (deg C) between the hotplate and coldplate, ΔX is the effective distance (cm) between the two plates, and A is the effective area (cm^2) of the hotplate. The factor $\Delta X/A$ may be considered as the constant of the "conductivity cell" determined by the capacitance method, so that

$$k=\frac{0.0885516\dot{Q}}{C\Delta t}, \tag{2}$$

*This work was supported in part by the National Advisory Committee for Aeronautics.

[1] Present address Argonne National Laboratory, Lemont, Ill.

where C is the direct capacitance (micromicrofarads) between the hotplate and the coldplate, assuming the material between the plates to have a dielectric constant of unity corresponding to a vacuum. With the gas between the plates, a small correction must be made for its dielectric constant. The conduction equation (2) would apply, of course, to any two surfaces, as well as to parallel plates, provided only that the temperature and electric fields are geometrically similar.

3. Experimental Procedure

3.1. Apparatus

The general assembly of the thermal-conductivity cell, the pressure vessel, and the surrounding furnace is shown in figure 1. The hotplate (H), coldplate (J), guard (F), and auxiliary guard (E) are shown schematically. The pressure vessel (G) is made of stainless steel and is sealed with a Monel gasket (D). This vessel is surrounded by a furnace (K) and furnace "neck" (C), which are made of aluminum and are equipped with electric heaters in numerous porcelain tubes in the aluminum. The furnace temperature was automatically controlled by means of a platinum resistance thermometer and bridge circuit. The furnace neck was controlled relative to the furnace by means of a thermocouple. The pressure vessel extends upward out of the furnace region so that the electric leads can be brought out of the pressure vessel in a cold region. The cooling coil (B) dissipates the heat from the furnace, so that the top is cool. The electric leads (all No. 32 gold wire) are brought up from the auxiliary guard through three Inconel tubes, which serve as electrostatic shields, as described later. There are 29 of these leads, which are brought out of the pressure vessel through a pressure seal, A. These leads go out radially between two "Kel-F" (polychlorotrifluoroethylene) disks, which are pressed together for the seal.

A number of difficulties were encountered before obtaining a successful seal at A. At first, the material Teflon (polytetrafluoroethylene) was used, but it was found to flow excessively at the high pressures necessary for the seal. The method finally used for this seal was to mold Kel-F around the gold wires at about 200° C.

The vital parts of the thermal-conductivity cell are shown in figure 2. The hotplate (M), coldplate (O), guard (E), and auxiliary guard (B) are all made of silver to minimize temperature gradients and heat transfer by radiation. The hotplate is made of three parts, silver-soldered together. The hotplate heater (L) is located between the lower parts and consists of about 55 ohms (at 25° C) of (0.05-mm diameter) platinum wire insulated with mica. Gold leads from this heater are brought out through the tempering region located at H between the upper two silver pieces of the hotplate and then to the thermal tie-down, F. The purpose of this thermal tie-down

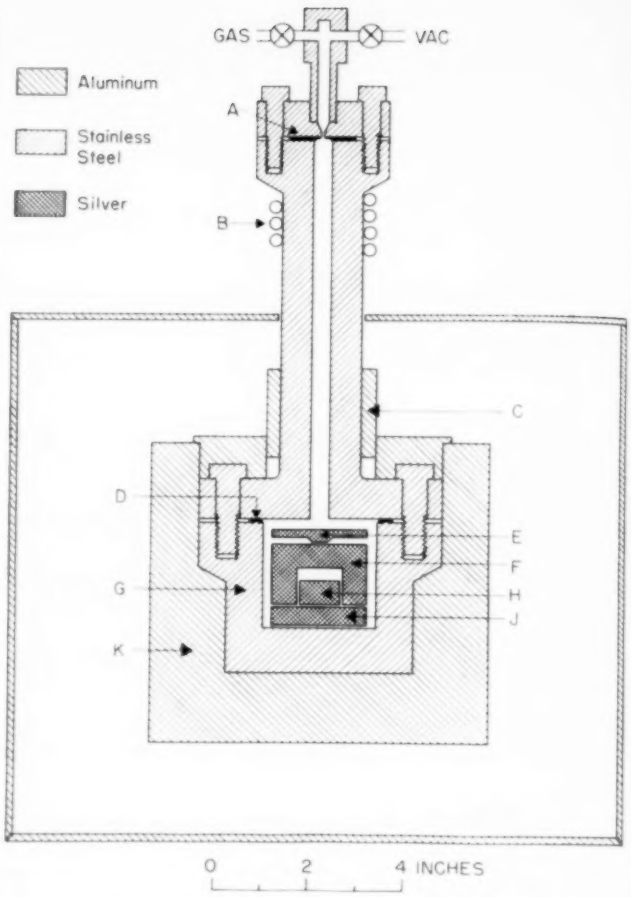

FIGURE 1. *Thermal-conductivity apparatus.*

A, Pressure seal for electric leads; B, cooling coil; C, furnace neck; D, Monel gasket; E, auxiliary guard; F, guard; G, pressure vessel; H, hotplate; J, coldplate; K, furnace.

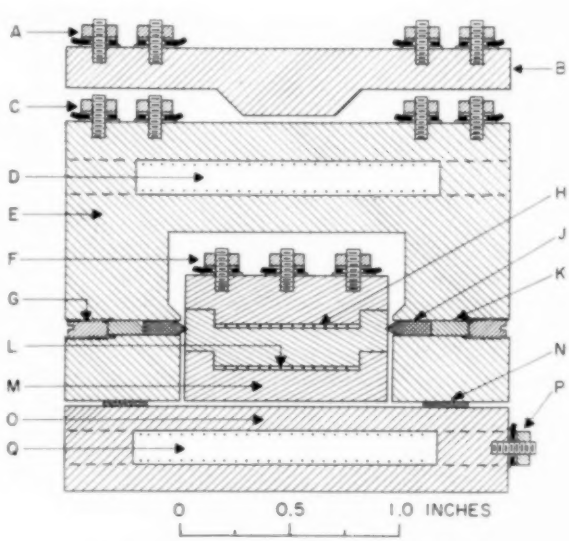

FIGURE 2. *Thermal-conductivity cell.*

A, C, F, H, P, Thermal tie-downs for electric leads; B, auxiliary guard; D, Q, platinum resistance thermometers; E, guard; G, silver screw; J, quartz supports for hotplate; K, aluminum insert; L, hotplate heater; M, hotplate; N, quartz spacers; O, coldplate.

is to bring the leads as close as possible to the temperature of the silver. This type of tie-down is used extensively throughout the apparatus and consists of a gold terminal insulated between thin mica disks and held down to the silver by a nut threaded on a machine screw. The gold terminal is spaced around the screw so that it is insulated from it.

The hotplate is supported by the guard ring at three points, using quartz supports (J), so that the bottom plane of the hotplate is in the same plane as the bottom of the guard ring. Because the coefficient of thermal expension of quartz is lower than that of silver, an aluminum insert (K) having a higher coefficient than quartz was used with the quartz for compensation. The quartz is held tightly against the hotplate by the silver screw (G) pressing against the aluminum insert. The guard (E) surrounds the hotplate, except where it is exposed to the coldplate. In the vital region near the coldplate, the guard is spaced about 0.5 mm from the hotplate. The assembly of the guard and hotplate is held about 0.5 mm from the coldplate by three quartz spacers (N) between the guard and coldplate. In this region, the silver was highly polished to reduce heat transfer by radiation. Heaters (not shown) are installed in both the guard and coldplate.

The temperatures of the guard and coldplate are measured by using the platinum resistance thermometers (D) and (Q), respectively, in conjunction with a Mueller bridge. These strain-free thermometers are not sealed. All leads (gold) from these two thermometers are thermally tied down at C and P, respectively, so that the temperatures of the platinum resistance thermometers are not affected by heat conduction along the leads. The temperature difference between the guard and hotplate is determined by means of a multiple-junction thermopile, using four No. 36 Chromel P-Alumel thermocouples in series. This thermopile has one set of electrically insulated junctions at F on the hotplate and the other set at C on the guard.

Experiments indicated the desirability of providing another thermal tie-down zone for all electric leads before they go out from C to the cold region. For this purpose, the silver auxiliary guard (B) was used with a heater built in to provide the bulk of the heat flow up along the electric leads. All three silver pieces, (B), (E), and (O), are held together by long machine screws fastened in the bottom of the surrounding pressure vessel. These four pieces are all electrically insulated from one another.

The effective operation of the thermal-conductivity apparatus depended upon the proper temperature control of the various components. For this purpose, five automatic thermoregulators were used to control the temperatures of the coldplate, guard, auxiliary guard, furnace, and the furnace neck. These thermoregulators were actuated by thermocouples or resistance thermometers (not the measuring resistance thermometers), and they consisted essentially of "chopper-amplifiers" operating saturable reactors in the heater circuits. The guard was maintained at the same temperature as that of the hotplate by means of the differential thermopile previously mentioned. This temperature control was the most important; it maintained constancy of temperature to about 0.001 deg C. The auxiliary guard was maintained at the same temperature as the guard by a single differential thermocouple. As a result of the effectiveness of the thermoregulation in the thermal-conductivity apparatus, all the observations on the thermal conductivity of nitrogen were made by one person. Both the electric power in the hotplate heater and the thermocouple readings were observed with a precision potentiometer.

A capacitance bridge was used to measure the capacitance between the hotplate and the coldplate. This bridge permitted the accurate measurement of small direct capacitances, even though relatively large capacitances exist between the "ground" and the plates. To eliminate, as far as possible, errors of measurement in capacitance, a calibrated capacitor having about the capacitance of the thermal-conductivity cell (about 10 $\mu\mu$f) was used as a reference and the measurements made by a substitution method. In this measurement, the same internal capacitance to ground was kept in the bridge circuit, so that the capacitance measurement approached very closely to the ideal comparative measurement, giving an accuracy comparable with the accuracy of the calibrated capacitor. Much care was taken to avoid significant capacitance between the leads from the hotplate and coldplate. They were effectively shielded from each other by bringing leads out through separate grounded Inconel tubes and by proper location of the leads that pass through the pressure seal.

For the measurement of the pressure of the gas in the conductivity cell, calibrated Bourdon gages were used. The requirement for accuracy on these gages was not great because the variation of thermal conductivity with pressure was much smaller than the change with temperature.

3.2. Purity of Nitrogen

The nitrogen used was extra-dry high-purity, obtained from the Linde Air Products Co., who stated that impurities did not exceed 100 ppm. Cryoscopic measurements made by G. F. Furukawa at the National Bureau of Standards with an adiabatic calorimeter showed liquid-soluble solid-insoluble impurities to be about 10 ppm. The conductivity cell was filled with this nitrogen, which had been passed through a silica-gel dryer and a filter made of glass wool.

3.3. Procedure

The general procedure was to set the furnace controls to the desired temperature, fill the conductivity cell with gas at the desired pressure, and put in a chosen electric power in the hotplate. With the coldplate automatically regulated to a constant temperature and the guard temperature automatically controlled to the temperature of the hotplate, the hot-

plate temperature became constant. After the capacitance between the two plates was measured, alternate measurements of electric power (W) and temperature difference (Δt) between the plates were made until the constancy of their values indicated that a steady state had been reached. The power in the hotplate was then changed so that similar measurements were made at three or more powers. The gas pressure was then changed and measurements were repeated for each of the pressures 0.7, 50, and 100 atm. All of these measurements were made at 50°, 100°, 200°, 300°, 400°, and 500°.

According to eq (2), the three quantities needed to determine the thermal-conductivity coefficient, k, are the rate of heat flow, $\dot{Q}$, the temperature difference, Δt, and the direct capacitance, C, between the hotplate and coldplate. Each of these quantities is discussed in detail below.

In order to obtain $\dot{Q}$ from W, the measured electric power in the hotplate, it is necessary to account for all heat flow from the hotplate other than by conduction through the gas. The possible paths of this heat flow are (1) to the surrounding guard by conduction and convection through gas, conduction through lead wires, and radiation, (2) to the coldplate by convection, and (3) to the coldplate by radiation.

Preliminary experiments were made to determine the heat-transfer coefficient between the guard and hotplate. Results of these experiments showed that an uncertainty in conductivity of less than 0.1 percent would be caused by a temperature difference between the guard and the hotplate of 0.001° C. It was found possible to control the temperature difference automatically to about this value.

The conductivity cell was designed to eliminate any convection currents. If convection does exist, it will cause an apparent change in the value of k with change in power input. At the lower gas densities, no such change was observed, and convection effects seemed absent. However, at the higher gas densities, k appeared to vary with power. The apparent k values were corrected by extrapolating to zero power input. This apparent change in k with power is believed to be due to a "chimney"-type convection resulting from gas flowing into the space between the guard and coldplate and out of the holes (not shown in fig. 2) provided for electric leads in the top of the guard. It is expected that blocking of these spaces would have eliminated this effect.

The heat transfer by radiation was accounted for by measurements with the cell evacuated. This power (W_r) transferred between two parallel plates can be expressed as

$$W_r = \epsilon A \sigma (T_2^4 - T_1^4), \tag{4}$$

where ϵ is an effective emissivity of the surfaces, A is an effective area, σ is the Stefan-Boltzmann constant, and T_1 and T_2 are the absolute temperatures. If the temperature difference, Δt, is small compared to the average temperature, $T = 0.5\ (T_2 + T_1)$, then the transfer equation can be simplified to

$$W_r = 4\ \epsilon A \sigma T^3 \Delta t = B T^3 \Delta t. \tag{5}$$

The constant B was evaluated in preliminary experiments over the entire temperature range with the conductivity cell evacuated. The gas pressure in the cell in these experiments was estimated to be less than 10^{-5} mm of mercury. During the progress of the experiments with gas, the constant B was checked periodically at temperatures of 350° C and below to test for possible changes in emissivity with time. Higher temperatures were not rechecked for reasons to be discussed later with temperature measurement.

The direct capacitance (C) between the hotplate and coldplate was measured by a substitution method using a calibrated standard and a Sylvania type 125 capacitance bridge. The precision of the bridge reading was better than the certified accuracy of the standard capacitor.

The capacitance, C, in eq (2) is that measured in vacuum. For measurements with gas in the cell, correction must be made for the dielectric constant, ϵ, of the gas. ϵ was determined by using the Clausius-Mosotti equation

$$\frac{\epsilon - 1}{\epsilon + 2} = D\rho, \tag{6}$$

where D is a constant independent of temperature for nonpolar gases, and ρ is the gas density. The value used for D was 1953×10^{-7} [1] [2] when ρ is in Amagat units [2]. Although the correction for the dielectric constant of the nitrogen may amount to 1 or 2 percent at the highest densities, it is believed that the uncertainties in k due to this correction are less than 0.01 percent.

Temperature measurements were made with the resistance thermometers in the coldplate and the guard, together with the four-junction thermopile between the guard and the hotplate. These resistance thermometers were calibrated by the NBS Temperature Measurements Section before assembly of the cell. It was found, however, that when the system was kept under high vacuum at temperatures above 400° C, the thermometer characteristics changed slightly. This was probably due to contamination of the platinum by other metals in the system. Such a change took place during the determination of radiation corrections at 500° C. Rather than dismantle the apparatus to recalibrate the thermometers, it was thought that sufficient accuracy could be retained if the two thermometers were compared in place. In this way, the temperature difference would be known more accurately than the absolute temperature. This procedure is valid only because the evaluation of the temperature *difference*, Δt, is the important factor, whereas the change in thermal conductivity with temperature is small. It is estimated that after this procedure, the accuracy of the measurement of Δt was 0.002 deg C and of average temperature T was 0.01 deg C.

[2] Figures in brackets indicate the literature references at the end of this paper.

4. Results

The results of the measurements are given in table 1. The first column gives the temperature of the experiment, which is the mean of the hotplate and coldplate temperatures. The second column gives the power (W) put into the hotplate (as measured electrically) with nitrogen in the conductivity cell. Values of power W_r, given in the third column, are based on experiments with the conductivity cell evacuated and are calculated from eq (5). These values are subtracted from the corresponding values of W to give $\dot{Q}$, as used in eq (2). Over 40 experiments were made to determine the value of B in this equation. A value of $B=4.90\times10^{-12}$ w/deg^4 in this equation was found to fit the results best. The values of B calculated from the individual vacuum experiments deviated on the average about 4 percent from the above value, and seemed to be independent of temperature. Because the *maximum* values of W_r are only 3 percent of the corresponding values of W, an error of 4 percent in B would cause a maximum error of only about 0.1 percent in conductivity k.

The values of temperature difference Δt given in column 4 are based on measurements with the two resistance thermometers and the thermopile, which was used only as a "null" indicator. Column 5 gives the values of capacitance C (as used in eq (2)) between the hotplate and coldplate as determined at the same time and under the same conditions of the conductivity experiment. These values have been corrected for the dielectric constant of the nitrogen.

The values of "apparent" thermal conductivity, k^*, given in column 6, were calculated from eq (2). These values, when corrected to even temperatures, seem to be free from error due to convection in that they are usually independent of power, except at some of the highest pressures, as mentioned earlier. Because this effect is believed to be due to a chimney-type convection, it should diminish at lower power inputs. Therefore, the values of k^* were extrapolated to zero power to give "true" conductivities, k. In the worst case, at 100-atm pressure and 50° C, the extrapolation is over a large range of values of k^*. However, it is believed that this extrapolation should introduce only a relatively small error. The results from the three experiments at different powers were fitted by the method of least squares to a linear equation in power. The maximum deviation of the observed values of k^* in this linear equation was only 0.28 percent, so that it is believed that the linear extrapolation was adequate.

At low pressures the effect of temperature discontinuity near the walls may become significant. This has been taken into account for the 0.7-atm data by use of the equation

$$k=k^*\left(1+\frac{2g}{\Delta X}\right). \tag{7}$$

TABLE 1. *Experimental results on nitrogen*

Temperature, t	Power— With nitrogen, W	Power— With vacuum, W_r	Temperature difference, Δt	Capacitance, C	Apparent conductivity, k^*
Pressure, 0.7 atm					
°C	w	w	°C	$\mu\mu f$	10^{-4} w/cm deg
51.03	0.05107	0.00027	1.647	9.786	2.790
52.75	.1039	.00056	3.332	9.789	2.804
57.85	.2630	.0015	8.306	9.797	2.846
100.13	.05895	.00042	1.664	9.975	3.122
101.87	.1202	.0009	3.371	10.049	3.120
106.68	.2927	.0022	8.117	10.017	3.165
200.09	.07569	.00088	1.686	10.450	3.737
201.50	.1387	.0016	3.101	10.455	3.744
205.02	.2981	.0035	6.614	10.463	3.769
204.86	.2971	.0035	6.615	10.435	3.767
300.48	.09072	.0148	1.704	10.80	4.293
302.17	.1818	.0030	3.404	10.82	4.299
304.25	.2972	.0049	5.534	10.85	4.312
306.64	.4308	.0072	7.991	10.83	4.336
306.56	.3719	.0066	6.891	10.85	4.326
401.02	.1064	.0026	1.706	11.17	4.822
402.65	.2177	.0053	3.484	11.18	4.829
406.43	.4732	.0116	7.539	11.20	4.841
501.60	.1311	.0040	1.776	11.71	5.408
502.93	.2369	.0073	3.205	11.71	5.416
506.46	.5248	.0164	7.045	11.77	5.430
Pressure, 50 atm					
50.59	0.04416	0.00021	1.290	9.761	3.090
51.02	.05938	.00029	1.718	9.762	3.120
52.46	.1138	.0005	3.179	9.772	3.228
55.76	.2511	.0011	6.519	9.788	3.470
99.69	.04457	.00030	1.172	9.987	3.348
100.31	.06805	.00045	1.781	9.980	3.368
101.94	.1345	.0009	3.434	9.986	3.446
105.15	.2748	.0018	6.716	10.021	3.592
200.26	.09102	.00101	1.937	10.456	3.937
201.61	.1569	.0017	3.322	10.456	3.956
206.33	.3966	.0044	8.165	10.481	4.058
301.54	.1589	.0025	2.835	10.84	4.505
305.68	.4077	.0064	7.158	10.87	4.567
302.85	.2365	.0037	4.194	10.84	4.535
400.81	.1060	.0025	1.616	11.16	5.085
402.30	.2105	.0048	3.197	11.16	5.104
405.86	.4689	.0108	7.067	11.18	5.145
501.57	.1331	.0039	1.720	11.72	5.674
502.98	.2575	.0076	3.316	11.74	5.685
507.42	.6426	.0191	8.195	11.77	5.724
Pressure, 100 atm					
50.12	0.03336	0.00014	0.835	9.809	3.591
50.83	.06738	.00026	1.576	9.813	3.843
51.82	.1210	.0005	2.615	9.821	4.158
99.86	.0597	.0004	1.423	10.007	3.689
101.10	.1195	.0007	2.675	10.014	3.926
104.96	.3421	.0018	6.689	10.036	4.490
199.70	.07664	.00083	1.603	10.41	4.023
201.08	.1502	.0016	3.021	10.43	4.177
204.51	.3473	.0035	6.556	10.46	4.440
299.62	.04732	.00082	0.889	10.83	4.276
300.79	.1150	.0019	2.048	10.83	4.516
302.76	.2366	.0038	4.079	10.84	4.662
305.30	.4068	.0065	6.811	10.84	4.802
400.79	.1059	.0024	1.570	11.17	5.231
402.68	.2468	.0055	3.641	11.19	5.244
405.56	.4650	.0104	6.778	11.20	5.303
501.21	.1342	.0039	1.698	11.69	5.816
502.66	.2612	.0075	3.290	11.70	5.836
506.68	.6218	.0180	7.727	11.75	5.890

The "temperature-jump distance", g, is related to the "accommodation coefficient", a, by the relation [16]:

$$g=\frac{2-a}{a}(2\pi RT)^{0.5}\frac{k}{(\gamma+1)C_v P} \quad (8)$$

in which R is the gas constant, T the absolute temperature, k the thermal conductivity, C_v the constant-volume specific heat, γ the specific-heat ratio, and P the pressure of the gas. Values of a for nitrogen on silver vary from about 0.8 at room temperature to 0.4 at 800° C [6]. The value of 0.5 was chosen as the most probable for the temperature range of these experiments.

Values of observed conductivity k, corrected to even temperatures, are listed in column 2 of table 2. In order to facilitate interpolation of the results between the observed points, empirical equations were derived to give conductivity as a function of temperature at each of the three pressures. These equations are as follows:

$$k=1.059\eta\left(C_v+\frac{9}{4}R\right) \quad \text{(pressure, 0.7 atm)}, \quad (9)$$

$$10^4k=2.714+0.005897t \quad \text{(pressure, 50 atm)}, \quad (10)$$

$$10^4k=3.161+2.9317\times10^{-3}t+9.0761\times10^{-6}t^2-8.8318\times10^{-9}t^3 \quad \text{(pressure, 100 atm)} \quad (11)$$

In these equations, k is in watts cm^{-1} deg^{-1}, t is in deg C, η is viscosity (poise), C_v is heat capacity (j g^{-1} deg^{-1}), at constant volume, and R is the gas constant (8.317/28.016 j g^{-1} deg^{-1}). The values of viscosity and heat capacity used in eq (9) were obtained from NBS Circular 564 (Nov. 1955), which tabulates heat-transport properties for a number of gases. The constants of these equations were obtained by the method of least squares. Values of k given in column 3 of table 2 are calculated from these equations. Column 4 gives the deviations of the observed results from these calculated values. The results are also given in figure 3, where the circles represent observed values and the solid lines the values from the above equations.

The empirical eq (10) and (11) fit the observed values at 50- and 100-atm pressure, respectively, almost as well as would be expected from the precision of the data. The average deviation of eq (10) (which is linear in t) from the observed conductivities is only 0.1 percent, with a maximum deviation of 0.3 percent. The deviations from eq (11) are also quite small except below 200°C, where there was increased difficulty, both experimentally and in fitting the observed points with an equation. The deviations of eq (9) from the observed values seem to be larger than can be attributed to experimental errors. Equation (9) is the same semi-empirical equation proposed by Eucken [3], except for the constant factor. A factor of 1.059 was found to fit the present data, as compared to a factor of 1 originally proposed by Eucken. More recent modifications of Eucken's equation by other investigators generally have predicted a value slightly greater than 1. An alternative equation for 0.7 atm, which fits well up to 400°C, and which may be easier for use in numerical interpolation in this region, is

$$k=2.495\times10^{-4}+6.366\times10^{-7}t-1.065\times10^{-10}t^2. \quad (12)$$

TABLE 2. *Thermal conductivity of nitrogen*

Temperature	Conductivity, k		Observed minus calculated
	Observed	Calculated	
	Pressure, 0.7 atm		
°C	10^{-4} w/cm deg	10^{-4} w/cm deg	%
50	2.794	2.818	−0.9
100	3.129	3.131	−.1
200	3.750	3.727	+.6
300	4.308	4.308	.0
400	4.836	4.857	−.4
500	5.430	5.381	+.9
	Pressure, 50 atm		
50	3.003	3.009	−0.2
100	3.303	3.304	.0
200	3.905	3.893	+.3
300	4.477	4.483	−.1
400	5.075	5.073	.0
500	5.660	5.662	.0
	Pressure, 100 atm		
50	3.340	3.329	+0.3
100	3.513	3.536	−.6
200	4.060	4.040	+.5
300	4.612	4.619	−.1
400	5.218	5.221	.0
500	5.794	5.792	.0

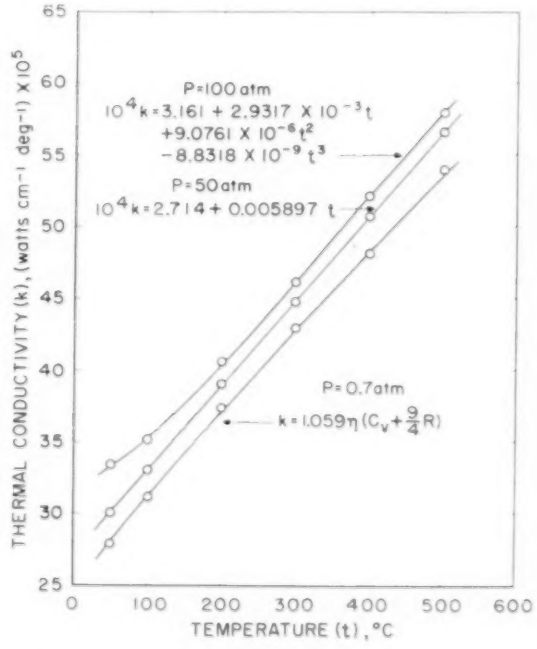
THERMAL CONDUCTIVITY (k), (watts cm⁻¹ deg⁻¹) X 10⁵
TEMPERATURE (t), °C
P=100 atm
10⁴k = 3.161 + 2.9317 X 10⁻³t
+9.0761 X 10⁻⁶t²
−8.8318 X 10⁻⁹t³
P=50 atm
10⁴k = 2.714 + 0.005897 t
P=0.7 atm
k = 1.059η(Cv + 9/4 R)

FIGURE 3. *Thermal conductivity of nitrogen.*

where k is in w cm^{-1} deg^{-1}, and t is in deg C. Although all of these equations are suitable for interpolation at their respective pressures, they may not be valid for extrapolation beyond the experimental range. Equation (9) is probably the most suitable for extrapolation to higher temperatures.

5. Discussion of Results

5.1. Accuracy

In order to estimate the accuracy of the final results, it is necessary to consider the effect of each of the terms in the conductivity equation

$$k=\frac{0.0885516Q}{C\Delta t}.$$

The constant 0.0885516 is a conversion factor to allow for the system of units. It has negligible uncertainty in its use here. Some possible sources of error in the measured capacitance, C, are the capacitance between electric leads and the relatively large capacitance to ground (the guard is grounded) of the hotplate and coldplates. The electric leads were carefully shielded to avoid significant error from this source. The effect of the ground capacitance is largely eliminated by the design of the bridge used in its measurement. Use of a substitution method that compares the conductivity-cell capacitance with that of a standard capacitor minimizes a number of possible errors. By using this method, it is believed that this comparison is accurate to better than 0.1 percent. The absolute value of the standard capacitor is certified by the NBS (with a high probability) to only 0.3 percent.

In the experiments with nitrogen, the effect of the dielectric constant of the gas must be considered. It is estimated that uncertainty in the value of the dielectric constant of nitrogen is less than 0.01 percent, giving the same uncertainty in C and k. The total uncertainty in the capacitance measurement is believed to be about 0.3 percent. This is the largest uncertainty in most of the measurements, and it is based on 1 chance in 10 that the error will be larger than 0.3 percent.

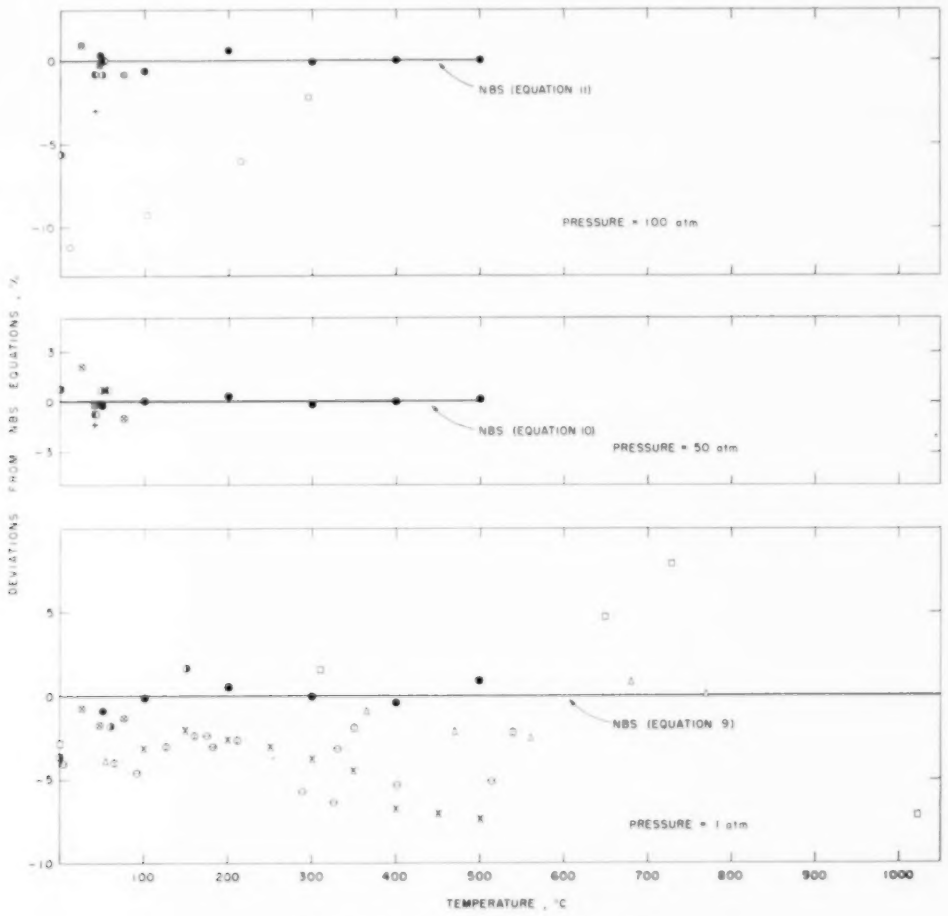

FIGURE 4. *Comparisons with others.*

●, NBS; ○, Stolyarov, Ipat'ev, and Teodorovich; ◑, Keyes; ◐, Vargaftik; ⊖, Frank; ⊕, Vargaftik and Oleschuk; ×, Schottky; △, Rothman and Bromley; ⊗, Michels and Botzen; □, Stops; +, Lenoir and Comings.

The factor $\dot{Q}$ in eq (2) is evaluated from the two powers W and W_r. The electrical measurement of W is believed to have negligible error. The uncertainty in the value of W_r determined from vacuum experiments is estimated to be less than 0.1 percent, except at the highest temperatures, where it may be as large as 0.1 to 0.2 percent. It is possible that the vacuum experiments do not account completely for all heat flow (other than $\dot{Q}$) from the hotplate during the gas experiments. This may be due to imperfect matching of the guard temperature to the hotplate temperature. It is estimated that the error from this source is less than 0.1 percent.

The measurement of Δt, which has been discussed earlier, has an estimated uncertainty of 0.002 deg C. This introduces uncertainties in the values of k of from 0.02 to 0.2 percent, depending on the magnitude of Δt. The uncertainty in the temperature scale, estimated to be about 0.01 deg C, is believed to introduce negligible error in k.

In estimating the over-all accuracy of the results, the authors believe that with most of the results, there is only 1 chance in 10 that the true conductivity values will deviate more than 0.5 percent from the observed values given in table 2. In the case of a few values at the highest pressures, it is believed that this tolerance might be increased by as much as 1 percent.

5.2. Comparison With Others

A comparison of the results of this investigation with the observed conductivity values from some other recent researches is given in figure 4. No attempt was made to include in the figure all the available data at low temperatures and low pressures, although all known high-pressure data are given. The data are plotted as deviations from eq (9), (10), and (11), which represent the NBS data for the three pressure ranges. At low pressures (approximately 1 atm), Frank [4] and Schottky [5] made measurements up to 500° C, Rothman and Bromley [6] up to 800° C, Stops [7] up to 1,020° C, Michels and Botzen [8] up to 75° C, and Vargaftik and Oleschuk [9] up to 541° C. Keyes and Sandell [10] have also made measurements up to 400° C at various pressures. Their results are not shown here because they believe their conductivity values to be too low over most of the temperature range. Later observed values of Keyes [11] up to 150° C are shown. Further measurements by Keyes [12] have been made up to about 350° C, but no observed values of conductivity have been published. At higher pressures, Michels and Botzen [8] made measurements up to 2,500 atm and 75° C, Stolyarov, Ipat'ev, and Teodorovich [13] up to 300 atm and 300° C, Vargaftik [4] up to 90 atm and 62° C, and Lenoir and Comings [15] up to 200 atm at 41° C. As in the low-pressure measurements, the results of Keyes and Sandell are not shown, although later results of Keyes are given up to 100 atm and 50° C.

6. References

[1] Handbook der Physik **12,** 517 (1927).
[2] NBS Circular 564 (November 1955).
[3] Physik Z. **2,** 1101 (1911).
[4] Z. Elektrochem. **55,** 636 (1951).
[5] Z. Elektrochem. **56,** 889 (1952).
[6] Ind. Eng. Chem. **47,** 899 (1955).
[7] Nature **164,** 966 (1949).
[8] Physica **18,** 605 (1952).
[9] Izvest. VTI **15,** #6, 7 (1946).
[10] Trans. ASME **72,** 767 (1950).
[11] Trans. ASME **73,** 597 (1951).
[12] Trans. ASME **74,** 1303 (1952).
[13] J. Phys. Chem. (U. S. S. R.) **24,** 166 (1950).
[14] Tech. Phys. U. S. S. R. **4,** 341 (1937).
[15] Chem. Eng. Progr. **47,** 228 (1951).
[16] E. H. Kennard, Kinetic theory of gases (McGraw-Hill Book Co., Inc., New York, N. Y., 1938).

Washington, December 27, 1956.

Journal of Research of the National Bureau of Standards Vol. 58, No. 5, May 1957 Research Paper 2761

Apatites Deficient in Divalent Cations

Aaron S. Posner[1] and Alvin Perloff

The preparation and results of a study of stoichiometric and divalent cation-deficient (defect) lead and calcium hydroxyapatites are reported. X-ray diffraction and index-of-refraction data show that it is possible to have divalent cations missing from "columnar" positions in the hydroxyapatite structure, with possible hydrogen bonding in proper proportion for electrical neutrality. A general formula for apatites is suggested to be $D_{10-x}M_{2x}(PO_4)_6(OH)_2$, where D represents the divalent cation (Pb^{+2}, Ca^{+2}, Mg^{+2}, etc.) and M the monovalent cation, such as Na^+ and H^+, and the upper limit of x is probably 2. It is suggested that the apatite portion of bone and tooth mineral may be some form of defect apatite.

1. Introduction

A number of finely divided calcium phosphates give the X-ray diffraction pattern of hydroxyapatite, $Ca_{10}(PO_4)_6(OH)_2$, but depart from the ideal Ca/P ratio of this mineral. (The formulas in this paper are given for unit-cell contents.) Examples are to be found in the inorganic portions of some bone and teeth, the mineral phosphorites, and the chemically precipitated synthetic apatites [1,2,3].[2] There are two conflicting explanations for a low Ca/P ratio in certain high-surface-area hydroxyapatites. The first states that an excess of phosphate ions is adsorbed on the surface of tiny crystals of stoichiometric hydroxyapatite [3,4]. The second explanation postulates a statistical absence of calcium ions from structural positions throughout the crystal [5,6].[3] In this case, electrical neutrality is probably obtained by the inclusion of protons present as hydrogen bonds between oxygens of orthophosphate groups ordinarily bonded to the missing calcium.

This paper presents data to support the latter theory and enlarges this view to include apatites containing other divalent cations, such as lead ions. These compounds, with imperfect Ca/P (or Pb/P) ratios, are referred to as defect apatites. In this usage, this crystallographic term implies that certain space-group positions normally containing divalent cations (Ca, Pb) are statistically unoccupied.

2. Adsorption Theory

Many workers have said that the large surface area of the chemically precipitated, "apparently nonstoichiometric" hydroxyapatites can accommodate excess phosphate ions neutralized by some adsorbed cation [3,4]. If this were true, it is reasonable to assume that the surface exchange of phosphorus compared to calcium would be higher than the over-all Ca/P ratio. Using radioisotopes, Weikel and Neuman [7] indicated that this was not true. The differences in chemical analysis of apatites studied could not be correlated to the surface composition. According to this work, the low Ca/P apatite did not show more phosphate surface exchange than the normal Ca/P apatite.

A few simple calculations can shed serious doubt upon the surface-adsorption theory. In the case of any apatite, to lower the divalent cation to phosphorus molar ratio from 10/6 to 9/6, there must be an adsorption of 0.67 mole of phosphate per mole of apatite [8]. Considering each tetrahedral PO_4 group as a sphere of radius 2.96 A, the effective area occupied on the apatite surface by each PO_4 group would be 27.53 A^2.

Because 1 g of apatite is about 10^{-3} mole, then 0.67×10^{-3} mole of surface phosphate ion would be needed for 1 g of this compound. Therefore, 1 g of apatite would require a surface area of 111.1 m^2 to accommodate the above amount of phosphate ($27.53\times10^{-20}\times6.02\times10^{23}\times0.67\times10^{-3}=111.1$ m^2/g). If the surface diminished below this value, the phosphate could not be adsorbed in great enough quantity to lower the Ca/P to 9/6 from 10/6. Both defect calcium hydroxyapatite and defect lead hydroxyapatite have been prepared with large enough crystal sizes to insure a maximum surface area far too small to account for the lowering of the metal to PO_4 molar ratio by adsorption of excess phosphate. This discussion has been oversimplified and does not take into account the crystal surface needed to accommodate any cations that may be associated with the adsorbed phosphate ions.

3. Preparations and Experimental Methods

A series of calcium and lead apatites, with both ideal and defect divalent cation content, were prepared. The calcium compounds prepared ranged in Ca/P weight ratio from the theoretical ratio of 2.15 down to 1.82. The two samples of lead apatite prepared had, respectively, the theoretical Pb/P ratio of 11.10 and the "nonstoichiometric" ratio of 10.03.

3.1. Calcium Apatite

The low Ca/P (1.82) (sample 6, table 1) apatite was prepared according to Arnold [9]. A liter of 0.1-molar $CaCl_2$ was mixed with about 7 liters of 0.1-molar Na_2HPO_4 and stirred for 2 days at room temperature. The solid was filtered, washed free of Cl^- and Na^+, dried at 110° C for 24 hr, and analyzed chemically.

[1] Research Associate at the National Bureau of Standards, representing the American Dental Association.
[2] Figures in brackets indicate the literature references at the end of this paper.
[3] Section 6.7 evaluates a slightly different postulate in which the ions are missing from crystal surface positions only [1].

The apatitic calcium phosphate with Ca/P ratio of 1.94 (sample 5) was prepared by the method of Dallemagne [10]. A saturated solution of $Ca(OH)_2$ was added to a solution consisting of 4 ml of 85-percent H_3PO_4 in 4 liters of water until the pink end point of phenolphthalein was visible. Filtering and drying (110° C, 24 hr) yielded a defect apatite whose molar ratio was 9 Ca to 6 P.

The other calcium compounds, which had Ca/P ratios 2.08, 2.11, and 2.15 (samples 4, 3, and 1, respectively), were all a result of the Wallaeys [11] procedure for the preparation of synthetic apatites. The method is similar to the above Dallemagne method, but after neutralization of the acid solution by $Ca(OH)_2$, the H_3PO_4 solution is boiled and neutralized at the boiling temperature by the same method. If the neutralization point is reached, the product is an apatite of theoretically correct Ca/P ratio (2.15). By falling short of the neutralization point at boiling temperatures, the lower Ca/P values of 2.11 and 2.08 were obtained.

Another method was used to obtain stoichiometric calcium hydroxyapatite (sample 2) [12]. Pure crystalline $CaHPO_4$ was prepared and hydrolyzed to hydroxyapatite with distilled water in a platinum-lined hydrothermal bomb. This method yielded larger crystals than the Wallaeys preparation.

3.2. Lead Apatites

Pure lead apatite $[Pb_{10}(PO_4)_6(OH)_2]$ (sample 7) was made by placing 8 ml of 0.5-*M* lead acetate solution in a platinum-lined hydrothermal bomb and slowly pipetting 4 ml of 0.6-*M* $(NH_4)_2HPO_4$ solution onto the first layer. Care was taken to maintain a two-layer system. The bomb was sealed and held at 300° C for 7 days, at which time the system was quenched rapidly in water. The resulting well-crystallized solid was collected by filtration, after which it was washed in water, then in acetone.

A commercial lead phosphate (Fischer Scientific L.5), which had a molar Pb-to-P ratio of 8.9 to 6 and gave the X-ray pattern of lead apatite, served as a sample of defect lead hydroxyapatite (sample 8). According to the manufacturer, it was prepared by mixing solutions of tribasic sodium phosphate and lead nitrate and decanting the supernatant liquid. The precipitate was washed with distilled water by decantation until the test for nitrate and sodium was negative. The material was then filtered and dried (110° C, 24 hr).

In all the analyses: (a) calcium was determined volumetrically by titration of the oxalate with a standard potassium permanganate solution [13], (b) phosphorus was determined colorimetrically by the heteropoly blue method [14], and (c) lead was determined gravimetrically as $PbSO_4$.

3.3. Bomb Growth

The chemically precipitated apatites are usually finely divided materials yielding X-ray diffraction patterns with broadened maxima. In two cases the apatite crystal size was increased by hydrothermal-bomb growth [15, 18].

Two grams of low Ca/P calcium apatite (sample 5) were introduced into the platinum-lined chamber of the bomb and covered with 4 ml of distilled water. The bomb was sealed with a platinum gasket and inserted into a furnace at 300° C for 7 days. The resulting solid was filtered, washed, and dried, and designated as sample 5a.

In the case of the lead sample, 0.52 g of sample 8 and 10 ml of distilled water constituted the bomb charge. The bomb was held at 300° C for 8 days; the sample was removed by filtration and designated as sample 8a.

In both cases the solid phase did not change in chemical analysis after the bomb treatment. In the case of the calcium apatite growth the bomb water showed only trace quantities of calcium and phosphate ions.

3.4. Physical Measurements

The average indices of refraction of the preparations were obtained by using oil-immersion techniques with the polarizing microscope. X-ray powder diffraction studies were carried out on a proportional-counter X-ray spectrogoniometer, using nickel-filtered copper K-radiation, taking special precautions in preparing the sample to avoid crystal orientation.

In the detailed X-ray study of the line intensities of the two lead apatite samples, a digital recorder was attached directly to the X-ray scaler and set to print out the integrated intensity every 10 sec. Because the spectrogoniometer traveled at 0.2° 2Θ per minute, a 10-sec print-out corresponded to an integration over a range of 0.033° 2Θ. The intensity of each diffraction maximum was calculated from the digital information appearing on the adding-machine tape print-out system.

4. Results

Table 1 presents the results obtained for the calcium apatites.

It is possible to calculate by the method of Lorentz and Lorenz [16] the theoretical change in average index of refraction as calcium ions are removed statistically from structural positions. Figure 1 compares the variation in average index of refraction in calcium apatite as the Ca/P is varied by missing calcium ions (data for sample 2 omitted).

Table 2 presents the results of the studies on the lead apatites. Included in the table is a comparison of the observed and calculated index of refraction for both the stoichiometric and defect materials. The Gladstone-Dale [17] method was used for these calculations.

The X-ray diffraction patterns of the calcium apatite samples were all very similar. As reported earlier [8], there is a slight tendency for the unit-cell volume to shrink as the Ca/P ratio falls. However, the relative intensities of the maxima do not change appreciably with changing calcium content. On the other hand, there are detectable differences in the relative intensities and spacings of the X-ray

TABLE 1. *Data obtained from the synthetic, calcium apatite series*

Sample	Ca/P		Average index of refraction	X-ray pattern
	Weight	Molar		
1	2.15	10.0:6.0	1.635 ±0.005	Hydroxyapatite.
2	2.15	10.0:6.0	1.645 ±0.005	Do.
3	2.11	9.8:6.0	1.625 ±0.005	Do.
4	2.08	9.7:6.0	1.615 ±0.005	Do.
5	1.94	9.0:6.0	1.600 ±0.005	Do.
5a	1.94	9.0:6.0	1.600 ±0.005	Do.
6	1.82	8.5:6.0	1.582 ±0.005	Do.

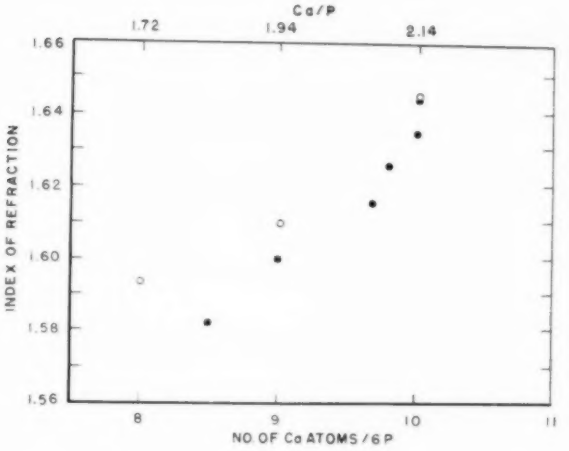

FIGURE 1. *Change in average index of refraction with Ca/P ratio.*

The open circles are the theoretical values calculated by the method of Lorentz and Lorenz [16]. The solid circles are the observed data.

TABLE 2. *Data obtained from the synthetic, lead apatite series*

Sample	Pb/P		Average index of refraction		X-ray pattern
	Weight	Molar	Observed	Calculated	
7	11.10	10.0:6.0	2.022 ±0.005	2.023	Lead apatite.
8	10.03	8.9:6.0	1.992 ±0.005	1.995	Modified lead apatite.
8a	10.03	8.9:6.0	1.992 ±0.005	1.995	Do.

patterns of normal lead apatite and defect lead apatite. The following study is based on these differences. A complete X-ray diffraction powder pattern of stoichiometric lead apatite will be published in a future section of National Bureau of Standards Circular 539, Standard X-ray diffraction powder patterns.

5. X-ray Study

5.1. Stoichiometric Lead Apatite

The powder pattern of lead apatite (table 4) was found to be in good agreement with earlier reports [18, 19]. A structural analysis of the data was performed to see if the fluorapatite parameters were suitable for lead apatite. Because so many of the X-ray maxima of this complicated structure represent the superimposition of many independent reflections, the X-ray analyses in this work were carried out by using the relative-intensity values rather than the structure factors.

The space group of apatite is $C_{6h}^2(P6_3/m)$. The atomic parameters assumed were taken from S. Naray-Szabo [20] except for the x-axis parameter of P, which was suggested by C. A. Beevers as an improved value (private communication).

TABLE 3. *Atomic parameters of the asymmetric unit of the unit cell of fluorapatite applied to lead hydroxyapatite*

Atom	Number per unit cell	Parameters in fraction of axis length		
		x	y	z
Pb I	4	0.333	0.667	0.000
Pb II	6	.250	.000	.250
OH	2	.000	.000	.250
O I	6	.333	.500	.250
O II	6	.600	.467	.250
O III	12	.333	.250	.063
P	6	[a].390	.390	.250

[a] Beevers' value; all others from Naray-Szabo [20].

Using the parameters in table 3, the structure factors, and in turn the theoretical intensities for the observed X-ray maxima, were calculated. Comparing the observed and the calculated *intensities* of the first eight reflections (table 4), one arrives at a reliability factor of 21.8 percent. This is good agreement for *intensity* (as opposed to structure factor) comparisons, and the atomic parameters of fluorapatite are acceptable for this powder diffraction study of lead apatite. The employment of the multiple-index, higher-order reflections would have added little change to the reliability factor.

TABLE 4. *Comparison of the observed and calculated X-ray diffraction intensities for the powder pattern of lead apatite*

Line	hkl	Observed intensity [a]	Calculated intensity [a]	$I_o - I_c$
1	110	270	346	−76
2	200	1,134	1,291	−157
3	111	1,226	1,734	−508
4	002	238	263	−25
5	102	1,169	1,688	−519
6	120/210	1,306	1,322	−16
7	211/121, 112	5,658	4,248	+1,410
8	300	1,510	1,483	+27

$$\text{Reliability factor } (R) = \frac{\Sigma |I_o - I_c|}{\Sigma I_o},$$

$$R = \frac{2,738}{12,511} = 0.218.$$

[a] Scale factor obtained from ratio of ΣI_o and ΣI_c. This scale factor differs from that used in table 6 for comparing I_o and I_{lo}.

5.2. Defect Lead Apatite

The four Pb I (columnar) atoms are stacked in two columns in the cell interior on the threefold rotation axes parallel to the *c*-axis. The six Pb II (hexagonal-screw) atoms are found associated with the hydroxyl ions, which are located on the hexagonal-screw axes parallel to the *c*-axis. Figure 2 diagrams a projection of the atoms of lead apatite upon the basal (001) plane. Figure 3 is the same projection with only the lead atoms shown.

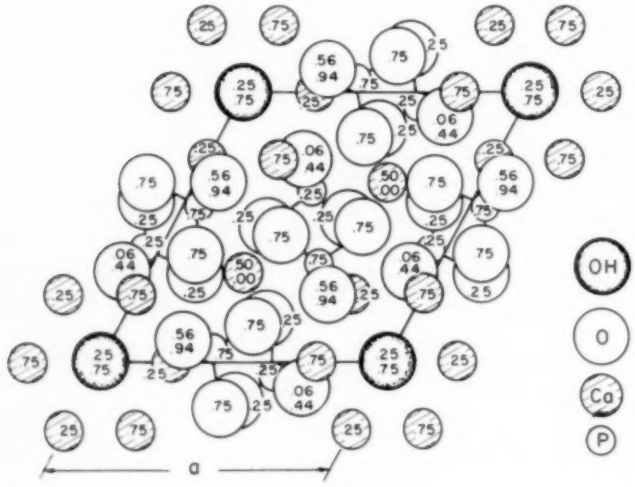

FIGURE 2. *Projection down the c-axis onto the 001 plane of the hydroxyapatite structure.*

[1] The values within the atoms represent the height in the c-axis direction in fractions of this axis. The lead ions in lead apatite appear at same positions as the calcium ions in hydroxyapatite.

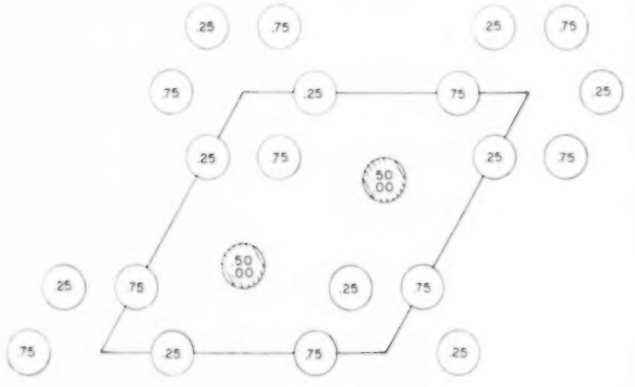

FIGURE 3. *Same projection of hydroxyapatite as figure 2, showing only the divalent cations* (Pb, Ca, *etc.*).

The molar Pb-to-P ratio in the sample studied was 8.9 to 6, but for simplicity of calculation, it was assumed to be 9 to 6, with one lead ion missing per unit cell. This cation may be absent in three different ways: (a) missing statistically from all possible cation positions; (b) 1 of the 4 Pb I atoms may be missing statistically; or (c) 1 of the 6 Pb II atoms may be missing statistically. There is also the possibility that a specific cation is missing in each unit cell, but the lack of X-ray evidence of a superlattice made this improbable, and the possibility was ignored. Because the above parameters were found acceptable for lead apatite, the structure factors for reflections out to $\sin\Theta/\lambda=0.471$ ($\lambda=1.5405$) were calculated for the above possible arrangements and for ideal lead apatite.

Table 5 lists the observed and calculated [4] intensities for the first 23 reflections of the defect apatite. As can be seen, the over-all reliability factors for the four possibilities are all reasonable. This is not surprising because the majority of the reflections are little changed by a missing lead ion. Table 6 summarizes the difference between observed and calculated intensity values of these eight most strongly affected reflections. There is no question that case (b), in which one of the four Pb I atoms is missing per unit cell (table 6, last column), is the best match.

6. Discussion

6.1. Lead Apatite

The X-ray data obtained from defect lead apatite indicates that the cation is missing statistically from the Pb1 structural position (fig. 3). Thus, in the case of a "$Pb_9:P_6$" apatite, 1 of 4 cations located on the trigonal axes (i. e., Pb1) is missing per unit cell, with the defect statistically distributed through the 4 positions.

This corroborates the index-of-refraction data for lead apatite given in table 2. The observed drop in index of refraction is as expected, with one lead atom missing from the structure. Index-of-refraction data alone can merely suggest a missing cation per unit cell. The X-ray data identifies the exact nature of the defect structure. Recall that the problem was simplified by assuming one Pb ion missing per unit cell. Actually, the chemical analysis of the nonstoichiometric apatite indicated that there was a defect of 1.1 lead atoms per unit cell. This emphasizes the point that statistical absences of cations in such a structure need not be in discrete numbers. This is well illustrated by the calcium apatite series.

6.2. Calcium Apatite

The index-of-refraction data (fig. 1) show that the calcium series parallels the lead apatite case. As more cations are removed, the observed index drops. It is not surprising that the X-ray patterns of stoichiometric and all the nonstoichiometric calcium

[4] Calculated for the above three cases, (a), (b), and (c), as well as for the case where all 10 ions are present.

TABLE 5. *Comparison of the observed X-ray powder data on defect lead apatite with the calculated intensities for the four possible cases*

Line	hkl	[a]I_o	[b]I_{10}	$\lvert I_{10}-I_o\rvert$	[c]I_9^{st}	$\lvert I_9^{st}-I_o\rvert$	[d]$I_9^{1/6}$	$\lvert I_9^{1/6}-I_o\rvert$	[e]$I_9^{1/4}$	$\lvert I_9^{1/4}-I_o\rvert$
1	110	1.7	9.7	8.0	9.1	7.4	18.3	16.6	1.6	0.1
2	200	41.7	52.2	10.5	50.9	9.2	56.1	14.4	49.1	7.4
3	111	69.6	72.9	3.3	68.4	1.2	58.1	11.5	91.7	22.1
4	002, 201	26.1	14.1	12.0	15.3	10.8	9.2	16.9	29.7	3.6
5	102	87.2	106.7	19.5	105.1	17.9	114.9	27.7	101.6	14.4
6	210, 120, 211	111.5	96.3	15.2	94.6	16.9	103.6	7.9	91.3	20.2
7	121, 112	585.8	364.0	221.8	362.8	223.0	387.9	197.9	368.8	217.0
8	300	154.4	142.1	12.3	143.6	10.8	165.1	10.7	127.7	26.7
9	202	2.1	5.0	2.9	6.2	4.1	12.4	10.3	1.1	1.0
10	301	1.8	0.3	1.5	0.3	1.5	0.3	1.5	0.3	1.5
11	220	2.3	8.8	6.5	8.4	6.1	16.4	14.1	1.7	0.6
12	212, 122, 103	2.5	2.6	0.1	3.2	0.7	7.0	4.5	4.7	2.2
13	310, 130	8.1	8.6	.5	10.6	2.5	9.4	1.3	17.1	9.0
14	221	1.0	0.8	.1	1.1	0.1	1.2	0.2	1.1	0.1
15	311, 131, 302	14.2	19.4	5.2	19.2	5.0	34.7	20.5	6.5	7.7
16	113	87.6	106.7	19.1	107.7	20.1	97.4	9.3	134.3	46.7
17	203, 400	50.5	39.2	11.3	36.9	13.6	27.0	23.5	63.7	13.2
18	222, 401	221.1	375.2	154.1	379.1	158.0	284.3	63.2	220.5	0.6
19	312, 132, 320	151.1	185.4	34.3	185.3	34.2	201.7	50.6	179.6	28.5
20	230, 123, 213	311.1	314.3	3.2	318.3	7.2	306.5	4.6	370.7	59.6
21	321, 231, 303	216.3	188.5	27.8	189.5	26.8	172.0	44.3	237.2	20.9
22	410, 140	192.3	185.6	6.7	184.1	8.2	213.2	20.9	161.2	31.1
23	402	390.0	433.9	43.9	433.0	43.0	436.1	46.1	471.4	81.4

[a] I_o = Observed relative intensity.
[b] I_{10} = Calculated relative intensity for all 10 lead ions present.
[c] I_9^{st} = Calculated relative intensity for one lead ion per unit cell missing statistically from all possible positions.
[d] $I_9^{1/6}$ = Calculated relative intensity for 1 lead ion per unit cell missing statistically from the 6 hexagonal-screw positions.
[e] $I_9^{1/4}$ = Calculated relative intensity for 1 lead ion per unit cell missing statistically from the 4 columnar positions.

TABLE 6. *Abstract of table 5, showing the X-ray intensities most affected by the missing lead atoms*

X-ray line	Defect lead apatite ($I_o - I_c$)			
	I_o-I_{10}	$I_o-I_9^{st}$	$I_o-I_9^{1/6}$	$I_o-I_9^{1/4}$
1	−80	−74	−166	1
2	−105	−92	−114	−74
4	120	108	169	36
9	−29	−41	−103	10
11	−65	−61	−141	6
15	−72	−50	−205	77
17	113	136	235	−132
18	−1541	−1580	−632	6

apatites are so similar. A calculation of the effect of a missing Ca ion per unit cell indicated no measurable change. The high atomic number of lead as compared to calcium results in a greater change in the X-ray intensities when 1 in 10 atoms is missing.

It is fortunate that the missing calcium atoms do not affect the crystalline unit-cell volume appreciably. As the number of calcium atoms per unit cell declines, it is inevitable that the index of refraction falls, because the unit-cell volume is reduced only slightly. The lack of exact match between calculated and observed indices of refraction in the calcium apatite series is probably due to the inexact nature of the molecular refractivities assumed for the Lorentz-Lorenz calculation. It is important to note the parallel nature of the drop in index of the observed and theoretical apatites as the calcium content of the unit cell is reduced. It seems reasonable that a defect apatite series exists in the case of calcium with cations missing from columnar positions as in the lead compounds. Here, too, the calcium ions are probably absent statistically from the four unit-cell positions on the trigonal axes and not in any integral number per unit cell.

An earlier study [8] showed that the observed density of a calcium-defect hydroxyapatite (with Ca/P=9/6) was 2.89, as opposed to 3.13 for pure hydroxyapatite. This is the value predicted by assuming the missing calcium mechanism. It serves to corroborate the index-of-refraction data presented above.

6.3 Hydrogen Bonds

Electrical neutrality in these low-cation apatites can be achieved by the inclusion of hydrogen ions as hydrogen bonds in the proper proportion. It is not reasonable to place two protons in a lattice position previously occupied by a lead or calcium ion. The hydrogen probably enters into the structure as a hydrogen bond between the oxygens of adjacent orthophosphate tetrahedra. It is not possible to prove this hypothesis with the present X-ray data. Future single-crystal studies with X-ray and neutron diffraction will be needed to further establish this suggested mechanism of achieving neutrality.

One can envision these apatites with missing cations as hybrids between the acid and basic orthophosphate structures. In the calcium series the structure of hydroxyapatite is quite different from $CaHPO_4$ or $CaHPO_4{\cdot}2H_2O$ [21,22], and it is unlikely that a continuous solid-solution series exists between apatite and either of the latter compounds. There must be a lower limit to the amount of missing cation in the nonstoichiometric series for, as the Ca/P atomic ratio approaches unity, there will be alterations in the crystal structure. In the synthetic calcium apatite system, the lowest Ca/P ratio reported to date is 8/6 [9,23,24]. Whether this is the limit or not is unknown at this writing. All attempts to precipitate apatites with Ca/P ratios lower than 8/6 by the authors and others [9,24] have resulted in the formation of an acid phosphate phase.

6.4. Evidence for Hydrogen Bonds

An interesting series of experiments [25, 26] has given some experimental evidence for the presence of hydrogen in defect calcium apatite. The calcium uptake from saturated $Ca(OH)_2$ solution by finely divided "low-calcium" apatites was observed by chemical analysis of the solid and conductivity measurements in the solution. Higher temperatures resulted in an increased calcium uptake, and the amount of calcium *chemically* bound (i. e., Ca not removed by washing) always brought the Ca/P of the solid to 10/6, the ratio for pure apatite.[5] In all cases the conductivity of the $Ca(OH)_2$ solution dropped further than the Ca loss would require. It is feasible that the hydrogen leaving the apatite when calcium returns to the empty cation position (either by diffusion or recrystallization) will form poorly ionized H_2O, thus altering the conductivity expected by only considering the Ca loss. Neuman [27] confirms this by showing a lowering of the *p*H in solution when calcium is added to "basic calcium phosphates" (another term for low-calcium apatites). He reports this to be due to the release of H_3O^+ as the calcium ions return to the defect sites (see section 6.7).

[5] Samples dried at room temperature gave 10.5/6 as the final chemically bound Ca/P ratio.

6.5. Nomenclature

In light of the probable hydrogen bonding it is not completely correct to refer to these compounds as nonstoichiometric hydroxyapatites. The more precise term *defect apatite* is thus employed.

As in other complicated series of compounds, the hydroxyapatite "family" is best characterized by a general formula. This might be $D_{10-x}M_{2x}(PO_4)_6(OH)_2$, where D represents the divalent cation (Ca^{++}, Pb^{++}, Sr^{++}) and M the monovalent cation (Na^+, H^+, etc.). In the case of the defect lead apatite given above, the formula becomes $Pb_{8.9}H_{2.2}(PO_4)_6(OH)_2$. A sodium substituted apatite would have the general formula $D_{10-x}Na_xH_x(PO_4)_6(OH)_2$, where Na can occupy the divalent cation positions in the lattice with hydrogen bonding effecting electrical neutrality. This paper does not deal with possible isomorphous substitutions for phosphate and hydroxyl ions.

6.6. "Octocalcium Phosphate"

Arnold [9] suggested a mechanism to explain the calcium-deficient hydroxyapatites that he prepared. He postulated that as many as 2 of the 4 columnar calcium ions per unit cell could be missing to form octocalcium phosphate, an apatite with a Ca/P ratio of 8/6. To achieve this stoichiometry and maintain the structural symmetry of apatite, Arnold proposed that all the hydroxyl groups are missing, whereas the calciums (missing at the same columnar *c*-level) are replaced by water, and that hydrogen ions are in some way associated with the columnar calciums that are present. His theory allows for a series ranging between this low-calcium apatite and pure apatite. He suggests that octocalcium phosphate is an infinite two-dimensional complex, $Ca_4H(PO_4)_3{\cdot}3H_2O$, with sheets held together by hydrogen bonds between the oxygens in the PO_4 groups and the oxygens of the water molecules. As more columnar calcium is taken up, Arnold feels that hydrogen would be randomly eliminated, resulting in ionic bonding between the sheets.

Even though Arnold's viewpoint superficially resembles the theory of defect apatites presented in this paper, it is actually quite different. He recognized the need for an explanation of low-calcium apatites, but his mechanism must be rejected on a few simple grounds. First, it seems unlikely that the apatite structure will hold together with the hydroxyl ions missing. Granting that such a structure were possible, the removal of the OH^- ions from their special positions would result in measurable changes in the relative intensity of many of the X-ray diffraction maxima. In addition, the mechanism of water substitution for columnar calcium between the "sheets" would certainly result in expanded unit-cell constants. Such changes in the apatite X-ray patterns of these low-calcium materials have not been demonstrated. Arnold [24] and Engström [25] reported certain low-angle, "nonapatite" X-ray maxima in the study of octocalcium phosphate that

could not be fully explained. Segerman (private communication) observed similar low-angle X-ray reflections in studying dental calculus. He suggested they may be due to an *ordered* loss of calcium ions in the columnar position, resulting in an apatite superlattice. If this can be clearly demonstrated, it will add further proof to the existence of calcium-deficient hydroxyapatites. In addition, such a mechanism may provide the structural link between the hydrogen-containing orthophosphates and the basic orthophosphates.

Besides the lack of X-ray diffraction corroboration, Arnold's theory does not correctly predict the observed index-of-refraction data. If missing calcium ions are supplanted by water, the index of refraction of low-calcium apatites will not drop as observed (fig. 1). Thus, Arnold's hypothesis, although provocative, is felt to be incorrect.

6.7. Calcified Tissue

The major phase of the inorganic portion of bone and teeth is generally accepted to be a low Ca/P form of hydroxyapatite [1]. Neuman and Neuman [1], in a very thorough review article on the mineral portion of bone, offer a concept to explain this lack of stoichiometry in bone apatite. Adopting Arnold's view that water can replace calcium in the apatite structure (see section 6.6), they postulate missing calcium ions supplanted by hydronium ions (H_3O^+) on the surface of the tiny apatite crystals in bone. Because the surface in bone-apatite crystals represents such a large proportion of the solid, the average Ca/P of the material is thereby lowered. Like the Arnold theory, this view of nonstoichiometry in bone apatite is open to question on the basis of index of refraction and X-ray diffraction results (section 6.2).

The theory of Neuman and Neuman depends entirely upon a small crystal size in the same way as the phosphate-adsorption theory discussed in section 2. In contradiction to this, it is possible to prepare lead defect and calcium defect apatites with low specific areas (section 3.3). According to Neuman and Neuman, the particle size of a bone-apatite crystal will dictate the Ca/P stoichiometry. In the results reported above (section 3.4), there is no correlation between crystal size (from X-ray diffraction line broadening) and Ca/P ratio.

Surface-exchange experiments on a calcium defect apatite (Ca/P=9/6) showed that about 5 percent of the total calcium was found on the crystal surface [27]. Because 10 percent of the total calcium ions were postulated to be missing from *surface* positions, 15 percent of all the calcium *positions* in the crystal would have to be on the surface. Such a crystal would require a specific surface of about 200 m^2, or at least three times the value reported for the above defect apatite with 5 percent of exchangeable calcium [27].

Bone-apatite crystals range in size from about 25 A to about 1,500 A, with an average diameter of about 200 to 300 A [28]. The surface-substitution mechanism could only explain the calcium defects in the 25- to 100-A region because larger crystals cannot furnish the surface needed for this postulated effect. It seems improbable that the defects should exist only on the surface for smaller crystals and be distributed throughout the material for larger crystals.

It is probable that the apatites in bone and tooth mineral are isostructural with the synthetic, low-calcium apatites described in this paper. It is further suggested that these biological apatites can take up calcium (and other ions that can isomorphously substitute for calcium) from the body fluids and release hydrogen ions previously found as hydrogen bonds in the solid. The differences in stoichiometry found in various specimens of bone and tooth salt may be related to changes effected by exposure to serum containing ions (Ca^{++}, Mg^{++}, Sr^{++}, Sn^{++}, etc.) that react with defect apatites.

7. Summary

Methods of preparation of both stoichiometric and defect lead and calcium hydroxyapatites are discussed.

X-ray diffraction data are given to verify the use of the fluorapatite parameters for lead apatite in structure-factor calculations.

The existence of defect lead hydroxyapatite and calcium hydroxyapatite is supported with X-ray diffraction and index-of-refraction data. An analysis of the X-ray data for cation-defective lead apatite indicates the lead ions to be missing statistically from the "columnar" positions.

With divalent cations missing from positions in the unit cell, the electrical neutrality of apatite is postulated to be obtained by hydrogen bonding between oxygens of the orthophosphates surrounding the defects.

A general formula for apatites of this type is suggested to be $D_{10-x}M_{2x}(PO_4)_6(OH)_2$, where D is the divalent cation (Pb^{+2}, Ca^{+2}, Mg^{+2}, etc.) and M is the monovalent cation (H^+ and Na^+). The upper limit of x is unknown but present results suggest that this value is about 2.

It is quite probable that the apatite portion of bone and tooth mineral is identical to the synthetic, defect apatites described herein.

8. References

[1] W. F. Neuman and M. W. Neuman, Chem. Revs. **53,** 1 (1953).
[2] A. S. Posner, M. J. Dallemagne, and C. Fabry, J. Physiol. (Paris) **46,** 325 (1954).
[3] S. B. Hendricks and W. L. Hill, Proc. Nat. Acad. Sci. U. S. **36,** 731 (1950).
[4] W. F. Bale, M. L. LeFevre, and H. C. Hodge, Naturwess. **24,** 636 (1936).
[5] A. S. Posner, Proc. Int. Union Pure and Appl. Chem., Inorganic Section, Münster (1954).
[6] A. S. Posner, C. Fabry, and M. J. Dallemagne, Biochim. et Biophys. Acta **15,** 304 (1954).
[7] J. H. Weikel, and W. F. Neuman, U. S. Atomic Energy Report UR 228 (1952).
[8] A. S. Posner and S. R. Stephenson, J. Dental Research **31,** 371 (1952).

[9] P. W. Arnold, Trans. Faraday Soc. **46,** 1061 (1950).
[10] M. J. Dallemagne, J. Physiol. (Paris) **43,** 425 (1951).
[11] R. Wallaeys, Thesis, Univ. Paris (1952).
[12] A. Perloff and A. S. Posner, Science **124,** 583 (1956).
[13] F. F. Tisdall and B. J. Kramer, J. Biol. Chem. **48,** 1 (1921).
[14] D. F. Boltz and M. J. Mellon, Anal. Chem. **19,** 873 (1947).
[15] G. W. Morey and E. Ingerson, Am. Mineralogist **22,** 1121 (1937).
[16] H. A. Lorentz, Wiedem. Ann. **9,** 641 (1880); L. Lorenz, Wiedem. Ann. **9, 70** (1880).
[17] J. H. Gladstone and T. P. Dale, Roy. Soc. (London) Phil. Trans. **153,** 337 (1863).
[18] R. Klement, Z. anorg. u. allgem. Chem. **237,** 161 (1938).
[19] M. Müller, Helv. Chim. Acta **30,** 2069 (1947).
[20] S. Naray-Szabo, Z. Krist. **75,** 387 (1930).
[21] G. MacLennen and C. A. Beevers, Acta Cryst. **8, 579** (1955).
[22] C. A. Beevers and B. Raistrick, Nature **173,** 542 (1954).
[23] R. Warington, J. Chem. Soc. **19,** 296 (1866).
[24] D. Carlström, Acta Radiol. Suppl. 121 (1955).
[25] C. Fabry, Biochim. et Biophys. Acta **14,** 401 (1954).
[26] C. Fabry, J. Physiol. (Paris) **46,** 361 (1954).
[27] W. F. Neuman, U. S. Atomic Energy Report UR 238 (1953).
[28] M. L. Watson and R. A. Robinson, Anat. Record **114,** 383 (1952).

WASHINGTON, December 27, 1956.

U. S. GOVERNMENT PRINTING OFFICE: 1957

Recent Publications of the National Bureau of Standards

Journal of Research of the National Bureau of Standards, Volume **58**, No. 3, March 1957 (RP2742 to 2748 incl.), 60 cents. Annual subscription $4.00.

Technical News Bulletin, Volume **41**, No. 3, March 1957. 10 cents. Annual subscription $1.00.

Basic Radio Propagation Predictions for June 1957. Three months in advance. CRPL–D 151. Issued March 1957. 10 cents. Annual subscription $1.00.

Research Papers

Journal of Research, Volume 58, No. 3, March 1957. 60 cents.

RP2742. Relative dimensional stabilities of a selected series of stainless-steel decimeter bars. Benjamin L. Page.

RP2743. Thermal quenching in alpha- and gamma-excited fluorescent solutions. H. H. Seliger and C. A. Ziegler.

RP2744. Two-parameter gloss methods. I. Nimeroff.

RP2745. Glassy state transitions of poly-(chlorotrifluoroethylene), poly-(vinylidene fluoride), and their copolymers. L. Mandelkern, G. M. Martin, and F. A. Quinn, Jr.

RP2746. Measurement of the corrosion rate of iron by polarization techniques. W. J. Schwerdtfeger.

RP2747. Numerical computation of the transfinite diameter of two collinear line segments. Philip Davis.

RP2748. Influence of crystallographic orientation on the corrosion rate of aluminum in acids and alkalies. Theodore H. Orem.

Publications in Other Journals

A direct approach to the problem of stability in the numerical solution of partial differential equations. John Todd. Commun. on Pure and Appl. Math. (Inst. of Methematical Sciences, New York University, N. Y.) **9**, No. 3, 597–612 (Aug. 1956).

A panoramic X-ray dental machine. Donald C. Hudson, Colonel, John W. Kumpula, and George Dickson. Armed Forces Medical J. (U. S. Government Printing Office, Washington 25, D. C.) **8**, No. 1, 46–55 (Jan. 1957).

Australite (Meteoric) glass. Donald Hubbard, Elizabeth M. Krumrine, and Ralph Stair. Trans. Am. Geophys. Union. (American Geophysical Union, 1530 P St., N. W., Washington 5, D. C.) **37**, No. 6, 767–778 (Dec. 1956).

Determination of resin content of glass fiber-polyester laminates containing calcium carbonate filler. S. D. Toner. Anal. Chem. (American Chemical Society, 1155 16th St., N. W., Washington 6, D. C.) **28**, 1109–1112 (July 1956).

High frequency induced electroluminescence in zinc sulfide. G. G. Harman and R. L. Raybold. Phys. Rev. (American Institute of Physics, 57 E. 55th St., New York 22, N. Y.) **104**, No. 6, 1498 (Dec. 1956).

In vitro production of experimental enamel caries. A. F. Forziati, F. L. Losee, W. W. Pigman, W. H. Jennings, M. E. Lawson, Jr. J. Am. Dental Assoc. (222 E. Superior St., Chicago 11, Ill.) **53**, 655–661 (Dec. 1956).

Infrared spectrum of hydrogen sulfide. Harry C. Allen, Jr., and Earle K. Plyer. J. Chem. Phys. (American Institute of Physics, 57 E. 55th St., New York 22, N. Y.) **25**, No. 6, 1132–1136 (Dec. 1956).

On the relaxation of vibrational non-equilibrium distributions. III. The effect of radiative transitions on the relaxation behavior. Kurt E. Shuler and Robert J. Rubin. J. Chem. Phys. (American Institute of Physics, 57 E. 55th St., New York 22, N. Y.) **26**, 137 (1957).

Photoconductivity and photovoltaic effect in intermetallic compounds. H. P. R. Frederikse and R. F. Blunt. Photoconductivity Conference at Atlantic City. (John Wiley & Sons, Inc., New York, N. Y.) 414–426 (1956).

Radiative electron capture in cesium-131. D. D. Hoppes and R. W. Hayward. Phys. Rev. (American Institute of Physics, 57 E. 55th St., New York 22, N. Y.) **104**, No. 2, 368–369 (Oct. 1956).

Radiative orbital electron capture in vanadium-49. R. W. Hayward and D. D. Hoppes. Phys. Rev. (American Institute of Physics, 57 E. 55th St., New York 22, N. Y.) **104**, No. 1, 183–185 (Oct. 1956).

Slit function effects in the direct measurement of absorption line half-widths and intensities. Henry J. Kostkowski and Arnold M. Bass. J. Opt. Soc. Amer. (American Institute of Physics, 57 E. 55th St., New York, 22, N. Y.) **46**, No. 12, 1060–1064 (Dec. 1956).

Some physical properties of gallium-copper-tin alloys. Denton L. Smith, Harold J. Caul, and William T. Sweeney. J. Amer. Dental Assoc. (222 E. Superior St., Chicago 11, Ill.) **53**, 677–685 (Dec. 1956).

Spectroscopic observations on pentaborane-air flames and explosions. W. G. Berl, E. L. Gayhart, H. L. Olsen, H. P. Broida, and K. E. Shuler. J. Chem. Phys. (American Institute of Physics, 57 E. 55th St., New York 22, N. Y.) **25**, No. 4, 797 (Oct. 1956).

Spectrum of the C_2 molecule between 3600 Å and 4300 Å. Norman H. Kiess and Herbert P. Broida. Can. J. Phys. (National Research Council, Ottawa, Canada) **34**, 1471–1479. (1956).

The Government's bookstore. Lewis T. Milliken. The Capital Chemist. (The Chemical Society of Washington, Washington, D. C.) **7**, No. 1, 10–15 (Jan. 1957).

Mathematics.—Unimodular matrices of order 2 that commute. Karl Goldberg. J. Wash. Acad. Sci. (U. S. National Museum, Washington 25, D. C.) **46**, No. 11 (Nov. 1956).

Les recherches sur la structure des polymeres au National Bureau of Standards. Norman Bekkedahl. Revue generale du Caoutchouc. (Societe d'editions Techniques Coloniales, 42, rue Schaffer, Paris 16, France) **33**, 1129 (1956).

The nature, cause and effect of porosity in electrodeposits. II. Radiographic detection of porosity in electrodeposits. F. Ogburn and M. Hilkert. Annual Tech. Proc. Amer. Electroplaters' Soc. (Amer. Electroplaters' Soc., 445 Broad Street, Newark 2, N. J.) 256 (1956).

Accelerating effect of amines on polymerization of methyl methacrylate. G. M. Brauer, Ruth M. Davenport, and William C. Hansen. Modern Plastics. (Modern Plastics, Inc., 575 Madison Avenue, New York 22, N. Y.) **34**, No. 3, 153 (Nov. 1956).

Absorption of gases and vapors on glass spheres. II. Two-dimensional condensation of oxygen. J. L. Shereshefsky and C. E. Weir. J. Phys. Chem. (American Chemical Society, 1155 16th St., NW., Washington 6, D. C.) **60**, 1162 (1956).

Bremsstrahlung polarization measurements for 1.0-Mev electrons. J. W. Motz. Phys. Rev. (American Inst. of Physics, 57 E. 55th St., New York 22, N. Y.) **104**, No. 3, 557–562 (Nov. 1956).

Compressibility of binary alkaline-earth borate glasses at high pressures. Charles E. Weir and Leo Shartsis. J. Am. Chem. Soc. (American Chemical Society, 1155 16th St. NW., Washington 6, D. C.) **39**, No. 9, 319–322 (Sept. 1956).

Dental materials and instruments 1951–55. G. C. Paffenbarger, D. D. S. Intern. Dental J. (A. Stjthoff—Publishers, The Hague, Holland) **6**, No. 3, 299–322 (Sept. 1956).

Publications for which a price is indicated are available only from the Superintendent of Documents, U. S. Government Printing Office, Washington 25, D. C. (foreign postage, one-fourth additional, except where otherwise stated). Reprints from outside journals and the NBS Journal of Research may often be obtained directly from the authors.

UNITED STATES
GOVERNMENT PRINTING OFFICE
DIVISION OF PUBLIC DOCUMENTS
WASHINGTON 25, D. C.

OFFICIAL BUSINESS

PENALTY FOR PRIVATE USE TO AVOID
PAYMENT OF POSTAGE, $300
(GPO)

Journal of Research of the National Bureau of Standards Vol. 58, No. 5 May 1957

Contents

	Page
Frequency conversion with nonlinear reactance. Chester H. Page. RP2755	227
Amplitude and phase of the low-frequency ground wave near a coastline. James R. Wait. RP2756	237
Vessels for the storage and transport of liquid hydrogen. B. W. Birmingham, E. H. Brown, C. R. Class, and A. F. Schmidt. RP2757	243
Infrared spectra of polychlorobenzenes. Earle K. Plyler, Harry C. Allen, Jr., and E. D. Tidwell. RP2758	255
Infrared spectra of chromatographically fractionated asphalts. James E. Stewart. RP2759	265
Thermal conductivity of nitrogen from 50° to 500° C and 1 to 100 atmospheres. R. L. Nuttall and D. C. Ginnings. RP2760	271
Apatites deficient in divalent cations. Aaron S. Posner and Alvin Perloff. RP2761	279

[A list of recent NBS publications is given on page 3 of the cover.]

For sale by the Superintendent of Documents, U. S. Government Printing Office, Washington 25, D. C. Price 60 cents (single copy). Subscription price: $4.00 a year, $1.25 additional for foreign mailing.

UNITED STATES GOVERNMENT PRINTING OFFICE, WASHINGTON : 1957